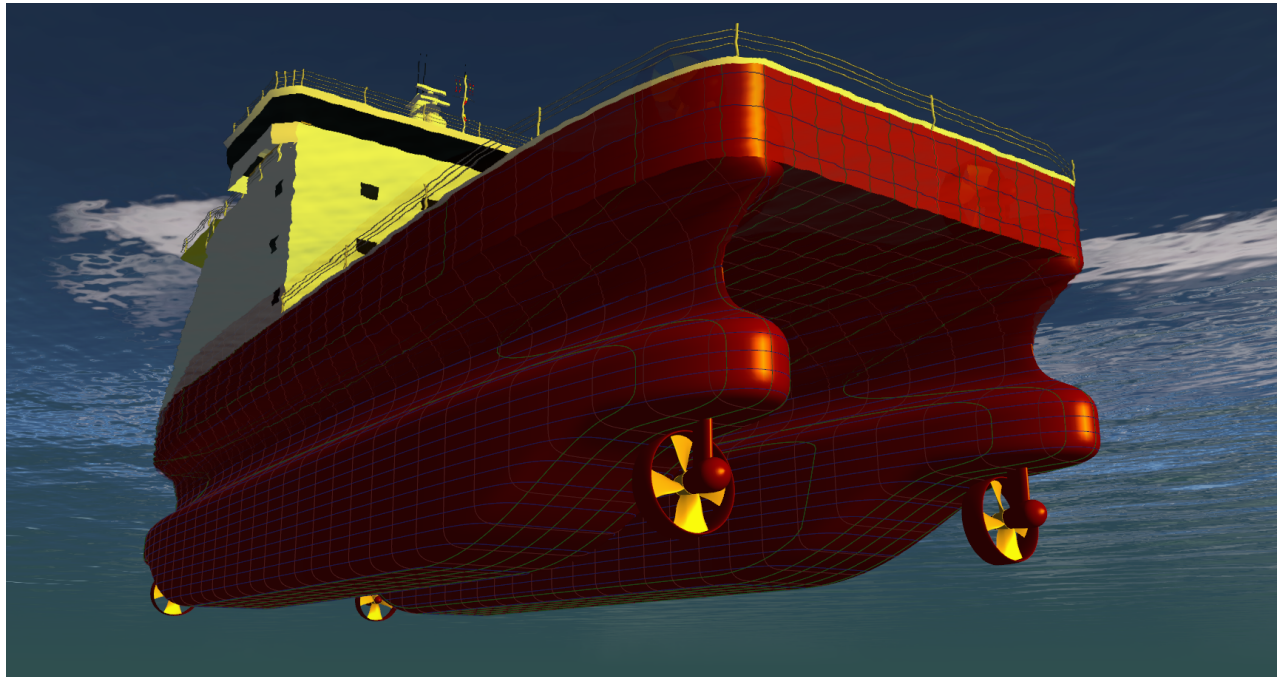




CHALMERS
UNIVERSITY OF TECHNOLOGY



SWATH SOV Hull Concept and Optimisation for Seakeeping

Parametric modelling, motions evaluation, hull optimisation
and comparison to SOV monohulls

Paulo Macedo

Naval Architecture and Ocean Engineering International Master Programme

Department of Mechanics and Maritime Sciences
CHALMERS UNIVERSITY OF TECHNOLOGY
Gothenburg, Sweden 2018

MASTER'S THESIS 2018:77

SWATH SOV Hull Concept and Optimisation for Seakeeping

Parametric modelling, motions evaluation, hull optimisation
and comparison to SOV monohulls

PAULO MACEDO



CHALMERS
UNIVERSITY OF TECHNOLOGY

Department of Mechanics and Maritime Sciences
CHALMERS UNIVERSITY OF TECHNOLOGY
Gothenburg, Sweden 2018

SWATH SOV Hull Concept and Optimisation for Seakeeping
Parametric modelling, motions evaluation, hull optimisation
and comparison to SOV monohulls

© PAULO MACEDO, 2018.

Supervisor: Dr Stefan Harries, Friendship-Systems AG
Examiner: Dr Rickard Bensow, Department of Mechanics and Maritime Sciences

Master's Thesis 2018:77
Department of Mechanics and Maritime Sciences
Chalmers University of Technology
SE-412 96 Gothenburg
Telephone +46 31 772 1000

Cover Picture: Render of the SWATH SOV concept, featuring azimuth-thrusters configuration, deckhouse and sea surface.

Typeset in L^AT_EX
Printed by Chalmers Reproservice
Gothenburg, Sweden 2018

Abstract

There is a fierce competition for the European market of offshore wind OMS (Operation, Maintenance and Service), expected to a significant growth in the coming years. Shipowners are constantly pursuing lower costs, increasing efficiency and profitability of its vessels in order to endure through time in the industry.

In this thesis project, an innovative SWATH (Small Waterplane Area Twin Hull) hull form is investigated as an SOV (Service Operation Vessel) and compared to operating monohull SOVs. The hull form was idealised by members of Rolls Royce Marine Norway and inspired in semi-submersible platforms and SWATH vessels. The alternative hull claims to allow the reduction of the vessel size, currently a request from shipowners, whilst maintaining the ability to operate in rough seas.

In order to investigate this claim, guidelines given by the interested partner were followed to develop a parametric model of a SWATH hull in CAESES® and connected to NEWDRIFT+, a seakeeping calculation software. With the goal of reducing heave motions at the connection point between the vessel and the offshore wind turbine, the parametric model was optimised and compared to two different sized monohulls, designed for the same purpose. From the optimisation process, optimisation patterns towards lower heave motions were identified and an additional SWATH variant was developed. This variant was also optimised and compared, totalling four vessels evaluated in this project. The comparison evaluated seakeeping performance in different sea states, heading angles and sailing speeds by means of heave RMS (Root Mean Square) motions, RAOs (Response Amplitude Operators) of motions and forces and moments caused by added wave resistance.

Results obtained indicates that optimised SWATH hull forms have high potential to have a larger operational window than longer monohulls by heaving, rolling and pitching less when excited by waves in several different sea conditions. Notwithstanding superior seakeeping performance, SWATHs are likely to be more susceptible to wave drift forces, therefore possibly requiring higher propulsive capacity. Additionally, in-depth studies of weight placement for hydrostatic stability requirements, as well as, estimations of towing resistance and propulsion system efficiency, are essential to be evaluated as they will definitely impact the hull form, construction and operational costs. These factors were not entirely considered in this project.

The conclusions reached are definitely not enough to neither praise nor condemn the utilisation of a SWATH hull form as an SOV. On the other hand, they are the starting point for a series of future studies before it can be officially declared impracticable or the future of SOV designs.

Keywords: parametric modelling, SWATH, SOV, walk-to-work, offshore wind energy, CAESES®, NEWDRIFT+, seakeeping, optimisation, simulation-driven design.

Preface and Acknowledgements

This thesis was completed as a part of the Master Programme in Naval Architecture and Ocean Engineering at Chalmers University of Technology, Sweden. Its subject was part of an ongoing project at Rolls Royce Marine Norway for the development of service operation vessels for the offshore wind industry.

It was undertaken at Friendship Systems AG, Potsdam, Germany, developer of the software CAESES® for intelligent surface design, automated design exploration and optimisation. It was supervised by Dr Stefan Harries, one of the founders of Friendship Systems, in which I would like to express my gratitude for providing me with constant support, networking, priceless guidance and wise advice. It was examined by Dr Rickard Bensow from Chalmers University of Technology, which skillfully balanced guidance and freedom.

My interest in parametric modelling started during classes from Fabian Tillig, endured during the whole master program and continues to grow. This was the essential starting point of this thesis and my connection with all parties involved in this project. I am deeply thankful for this opportunity and to be part of the future of 3D modelling.

Special thanks I owe to Martijn de Jongh and his team at Rolls Royce Marine Norway. It was a great honour to learn from your experience and to participate in this unique venture. Involving renewable energy, innovative ideas and international cooperation, it surely provided me valuable experience for my future career.

Furthermore, I would like to thank all colleagues at Friendship Systems, especially Claus Abt, Heinrich von Zadow, Stefan Wunderlich, and Fanis Papakonstantinou for providing me with resources, support and a pleasant and sapient environment.

I would also like to thank and express my gratitude for Prof. George Zaraphonitis and his team, especially George Dafermos, that took the time to provide and patiently explain in detail the seakeeping evaluation software NEWDRIFT+.

To my classmates, now friends, and to *Föreningen Chalmers Skeppsbyggare*, I am really glad to have shared these last two years and our graduation study-trip to Asia. I am sure that our bonds will carry on through life, count on me.

Additionally, I could not be more grateful for have been given a high-class baccalaureate degree provided by the Brazilian Government, including the chance of participating in the Science Without Borders programme, an exchange year studying Offshore Technology at the University of Stavanger, Norway. It definitely broadened my life opportunities and, without it, I would not have been here.

Finally and most importantly, I would like to express my gratitude to my family, especially to my parents, Luisa Basso and Paulo Macedo. Without their invaluable encouragement and consistent support to pursue my life objectives, I would not have been able to succeed once again.

Paulo Macedo, Gothenburg, August 2018

Contents

Abstract	v
Preface and Acknowledgements	vii
Contents	ix
List of Abbreviations	xi
List of Variables	xiii
List of Figures	xv
List of Tables	xvii
1 Introduction	1
1.1 Offshore Wind and Service Vessels	1
1.2 The Research Problem	2
1.3 Design Objective	3
1.4 Motivation	3
1.5 Limitations and Delimitations	4
1.6 Parties Involved	5
2 Basic Concepts	7
2.1 Offshore Wind Energy	7
2.2 Offshore Wind Service Vessels	8
2.3 SWATH Vessels	11
2.4 Geometric Modelling	14
2.5 Ship Motions at Sea	16
2.5.1 Ocean Waves Description	16
2.5.1.1 Linear Wave Theory in Deep Waters	17
2.5.1.2 Sea Wave Spectrum	18
2.5.2 Ship Motions in Waves	20
2.5.2.1 Equations of Motion	21
2.5.2.2 Responses to Harmonic Loads	23
2.5.2.3 Derived Responses	23
2.6 Seakeeping Evaluation with NEWDRIFT+	24
2.6.1 Calculation Methodology	25
2.6.2 Input Data	25
2.6.3 Output Data	26
3 Methodology	27
3.1 Rolls Royce Marine SOVs Design	27
3.1.1 82m SOV monohull	28
3.1.2 62m SOV monohull	29
3.2 Concept Design	29
3.3 Parametric Modelling of a SWATH SOV	30
3.3.1 Parallel Midbody	31
3.3.2 Bulb	32
3.3.3 Transition	33

3.3.4	Design Waterline	33
3.3.5	Displacement Adjustment	34
3.4	NEWDRIFT+ Mesh Creation	36
3.5	Sea States Selection	38
3.6	Body-Fixed Point for Evaluation	39
3.7	Simulation Set-Up	40
3.8	Optimisation Procedure	41
3.8.1	Single Variable Investigation	41
3.8.2	Multi-Variable Optimisation	42
3.8.3	Small Impact Variables Investigation	44
3.8.4	Fine Tuning Algorithms	45
3.9	Further Design Investigation	46
3.10	Post-Processing	47
4	Results and Comparison	49
4.1	Optimised SWATHs	50
4.2	Heave RMS	52
4.2.1	Sea States	52
4.2.2	Heading Angle	53
4.2.3	Speed Investigation	54
4.3	Response Amplitude Operators	55
4.4	Body Excitement by Forces and Moments	59
4.5	Identified Optimisation Patterns	62
5	Conclusions	63
	References	69
	Appendix	I
A -	Additional Figures	I
B -	Additional Tables	III
C -	NEWDRIFT+ Input Files	V

List of Abbreviations

Abbreviation	–	Description
3D	–	Tri-Dimensional
ASCII	–	American Standard Code for Information Interchange
CAD	–	Computer-Aided Design
CFD	–	Computational Fluid Dynamics
CO ₂	–	Carbon Dioxide
CSS	–	Compact Semi-Submersible
CTV	–	Crew Transfer Vessel
DC	–	Direct Current
DNV-GL	–	<i>Det Norske Veritas - Germanischer Lloyd</i>
DP	–	Dynamic Positioning
DP2	–	Dynamic Positioning Class 2
DWL	–	Design Waterline
EU	–	European Union
FPP	–	Forward Perpendicular
HOLISHIP	–	HOLIstic optimisation of SHIP design and operation for life cycle
JONSWAP	–	Joint North Sea Wave Project
LCB	–	Longitudinal Centre of Buoyancy
LOA	–	Length Overall
LWL	–	Waterline Length
MARIN	–	Maritime Research Institute Netherlands
NTUA	–	National Technical University of Athens
OMS	–	Operation Maintenance and Service
O&M	–	Operation and Maintenance
PM	–	Parallel Midbody
RAO	–	Response Amplitude Operator
RMS	–	Root Mean Squared
RRM	–	Rolls Royce Marine
RSM	–	Response Surface Method
STB	–	Safe Transfer Boat
SOV	–	Service Operation Vessel
SWATH	–	Small Waterplane Area Twin Hull
USV	–	Autonomous Surface Vessel
UT	–	Ulstein Trading

This page was intentionally left blank.

List of Variables

Variable	[unit]	Description
α_{POD}	°	Thruster base inclination angle
ζ	m	Wave surface elevation
η	–	Motional degree of freedom
η_T	–	Efficiency of a wind turbine
λ	m	Wavelength
∇	m ³	Displacement of a underwater body
∇_{diff}	–	Displacement difference error function
∇_t	m ³	Displacement targeted
ρ_{air}	kg/m ³	Density of the air
ρ_w	kg/m ³	Density of the water
φ	rad	Phase of a wave system
ω	rad/s	Wave angular frequency
a	m	Amplitude of a wave ($H/2$)
a_c	kg	Added mass coefficient
A_R	m ²	Rotor swept area
B	m	Breadth
b_c	kg/s	Damping coefficient
B_{PM}	%	Width of the parallel midbody
BB_{EXT}	%	Bulb extension size
c_c	kg/s ²	Spring stiffness coefficient
d	m	Water depth
D_{POD}	m	Base diameter of the azimuth thruster
E	m ² /Hz	Variance density spectrum
f	Hz	Frequency interval
F_0	N	Force amplitude for a harmonic load
g	m/s ²	Earths gravity acceleration, 9.81 m/s ²
\overline{GM}_T	m	Transverse metacentric height
\overline{GM}_{T0}	m	Transverse initial metacentric height
h	–	h^{th} order moment index
H	m	Wave height
\overline{H}	m	Mean wave height
H_{IN}	%	Height of the inner flat of side
H_{m0}	m	Significant wave height from a wave spectrum
H_{POD}	m	Thruster clearance height from keel
H_S	m	Significant wave height
I	m ⁴	Moments of inertia
k	rad/m	Wave number
\overline{KB}	m	Vertical centre of buoyancy
\overline{KM}_T	m	Limiting vertical centre of gravity

List of Variables

Variable	[unit]	Description
L_{DWL}	m	Length of constant waterline width
L_{PM}	%	Length of the parallel midbody
m	kg	Mass
m_h	–	Spectral moment of h^{th} order
n	–	Number of harmonic wave components
N	–	Number of waves recorded
p	Pa	Acting pressure on a particle
P_T	W	Power generated by a wind turbine
P_W	W	Power available in the wind
r	–	Rank number of a wave
R_B	m	Rotor blade radius
T_0	s	Period between wave zero-crossings
\bar{T}_0	s	Mean zero-crossing wave period
T_C	s	Period between wave crests
T_D	m	Design draught
T_P	s	Peak period of spectrum energy
$T(\omega)$	m/N	Transfer function in the frequency domain
u	m/s	Particle velocity in the x axis
U_W	m/s	Undisturbed wind speed at the rotor centre
v	–	Frequency index
w	m/s	Particle velocity in the z axis
W_{DWL}	m	Maximum width at design waterline
W_s	m ²	Hull wetted surface area
\hat{x}	m	Amplitude of an harmonic displacement
x_G	m	Longitudinal coordinate of the centre of gravity
xFP	m	Length between perpendiculars
xPB_{SHIFT}	m	x shift of the thruster base centre
y_G	m	Lateral coordinate of the centre of gravity
$yFPP_{SHIFT}$	%	Y shift of the forward perpendicular point
yH_{SHIFT}	°	Y shift of the upper inner width
z	m	Depth
z_G	m	Vertical coordinate of the centre of gravity
$\underline{\mathbf{F}}_e$	–	Vector of forces and moments from a wave excitation
$\underline{\mathbf{F}}_r$	–	Vector of forces and moments from hydrodynamic reactions
$\underline{\mathbf{F}}_{rs}$	–	Vector of forces and moments from a mooring system
$\underline{\mathbf{F}}$	–	Vector of acting forces and moments
$\underline{\mathbf{r}}$	–	Vector of coordinates of a point
$\underline{\xi}$	–	Vector of translational motion of a point
$\underline{\Omega}$	–	Vector of rotational motion of a point
\mathbf{A}	–	Hydrodynamic mass (added mass) matrix
\mathbf{B}	–	Hydrodynamic damping matrix
\mathbf{C}	–	Hydrostatic stiffness matrix
\mathbf{M}	–	Generalised inertia matrix

List of Figures

1.1	Annual and cumulative wind power installation and forecast under WindEurope’s low scenario (WindEurope (2017)).	2
2.1	Average water depth and distance to the shore of bottom-fixed offshore wind farms, organised by development status. The size of the bubble indicates the overall capacity of the site (WindEurope, 2018).	8
2.2	Integrated service logistics proposed by Siemens Gamesa (2018).	9
2.3	Exceedance probabilities for wind farms located in the German Bight region. Adapted from Aukland (2017).	10
2.4	CTV vs walk-to-work vessel days 2014-2016 (left) and walk-to-work by distance to OMS port (right). Adapted from Aukland (2017).	11
2.5	Ultrafast USV concept design (Brizzolara, Bovio, Federici, & Vernengo, 2011).	12
2.6	FKAB 50m offshore wind farm service vessel (FKAB, 2018).	13
2.7	Windkeeper 5m model at MARIN test basin (MARIN, 2018).	13
2.8	Compact Semi-Submersible developed by VARD. Adapted from VARD Marine (2018).	14
2.9	Qualitative assessment of available geometric modelling techniques (Abt & Harries, 2007).	15
2.10	Typical wave record at a fixed point, with definitions of terms.	16
2.11	The (ir)regular character of the waves for spectra with different widths. Adapted from Holthuijsen (2007).	19
2.12	Motional degrees of freedom (Bergdahl, 2009).	20
2.13	Calculation chain of ship motions. Adapted from Bergdahl (2009).	21
3.1	Edda Passat, UT 540 WP design by Rolls Royce Marine (Østensjø Rederi, 2018).	28
3.2	The shorter version of the UT 540 WP design (Rolls Royce Marine, 2018).	29
3.3	Initial sketch of the SWATH hull provided by Rolls Royce Marine especially for this project.	30
3.4	Main design variables of the parallel midbody.	32
3.5	Main design variables of the bulb.	33
3.6	The transition between the parallel midbody and the bulb.	33
3.7	Variables introduced in the design waterline parametrisation.	34
3.8	A slender demi-hull design variant with high inner height.	35
3.9	A wider demi-hull design variant with low inner height.	36
3.10	Meshing of the modelled surfaces to NEWDRIFT+.	37
3.11	Map of offshore wind farms and connecting power cables in the German Bight. By Maximilian Dörrbecker (2018) via Wikimedia Commons.	38
3.12	Positioning of the body-fixed point for seakeeping evaluation. Adapted from Rolls Royce Marine (2018).	40
3.13	NEWDRIFT+ connection window in CAESSES®.	41
3.14	Optimisation structure followed in this project.	42

3.15	Small variations of L_{PM} and the resulting heave RMS motion.	42
3.16	Sobol quasi-random homogeneous filling of the design domain, base for generation of the response surface.	43
3.17	Final iterations of the Dakota algorithm, converging to the final solution.	44
3.18	Iteration process of the TSearch algorithm, converging to the final solution.	45
3.19	Symmetric demi-hull SWATH hull variant.	46
4.1	Optimised asymmetric demi-hull SWATH variant.	51
4.2	Heave RMS development with sea state for the 4 compared vessels. . .	52
4.3	Heave RMS development with heading angle for 4 compared vessels in sea state 7 ($H_S = 3.25\text{m}$ and $T_P = 8.5\text{s}$).	54
4.4	Heave RMS development with speed for 4 compared vessels in sea state 7 ($H_S = 3.25\text{m}$ and $T_P = 8.5\text{s}$).	54
4.5	Heave RAO transfer function for sea state 7, 180° heading angle and 0kn sailing speed.	55
4.6	Pitch RAO transfer function for sea state 7, 180° heading angle and 0kn.	56
4.7	Heave RAO transfer function for sea state 7, 150° heading angle and 0kn sailing speed.	57
4.8	Pitch RAO transfer function for sea state 7, 150° heading angle and 0kn.	58
4.9	Roll RAO transfer function for sea state 7, 150° heading angle and 0kn.	58
4.10	Polar plots for heave RMS forces (left) and roll RMS moments (right) for sea state 7 and 0kn sailing speed.	59
4.11	Polar plot for RMS moments around y -axis (pitch) for sea state 7 and 0kn sailing speed.	60
4.12	Polar plots for surge RMS forces (left) and sway RMS forces (right) for sea state 7 and 0kn sailing speed.	61
4.13	Polar plots for resultant RMS forces (left) and yaw RMS moments (right) for sea state 7 and 0kn sailing speed.	61
A.1	Surge RAO transfer function for sea state 7, 150° heading angle and 0kn.	I
A.2	Sway RAO transfer function for sea state 7, 150° heading angle and 0kn.	I
A.3	Yaw RAO transfer function for sea state 7, 150° heading angle and 0kn.	II
A.4	A concept of the asymmetric SWATH hull with a wing connection between the demi-hulls.	II

List of Tables

2.1	Names and description of the motional degrees of freedom.	20
3.1	Design variables introduced for the main dimensions.	31
3.2	Design variables introduced in the parallel midbody design.	31
3.3	Design variables introduced in the bulb design.	32
3.4	Design variables introduced in the design waterline shape parametrisation.	34
3.5	Selected sea states based on the wave scatter diagram.	39
4.1	Optimal design variables reached for both SWATH vessels.	51
4.2	Heave RMS results for different sea states, 180° heading, 0kn speed.	53
B.1	Heave RMS results for different head angles in sea state 7 ($H_S = 3.25\text{m}$ and $T_P = 8.5\text{s}$).	III
B.2	Heave RMS results for different speeds in sea state 7 ($H_S = 3.25\text{m}$ and $T_P = 8.5\text{s}$).	III
B.3	Wave scatter diagram - modelled data at OWF Sandbank (German Bight), adapted from Brüning and Precht (2014).	IV

This page was intentionally left blank.

1 Introduction

This chapter presents a short background to the thesis subject, followed by descriptions of the research problem, the purpose and the motivation for the project, as well as the limitations faced. It is finalised with a brief presentation of the parties and persons involved.

1.1 Offshore Wind and Service Vessels

Offshore wind farms are moving further and further offshore for many different reasons. Haggett (2008) discussed what, in the first place, pushed the placement of wind turbines from onshore to offshore. The main reasons were the visual impact caused on landscapes, the scarcity of spaces with suitable wind conditions, environmental impact, conflict with other activities and public opinion.

Since then, the annual offshore installation has seen a steady increase, while onshore has been stable, with a slight decrease in the last three years, observable in Figure 1.1. To satisfy Europe's energy demand for clean energy and increase the profitability of the business, turbines have been becoming larger, seeking stronger winds and breaking engineering barriers. This can be noted by the increase in the average rated capacity of newly-installed offshore wind turbines that have been on the rise, approximately 6MW (Mega Watt) in 2017 compared to 4MW in 2012. Another milestone for the offshore industry was the completion of the first floating offshore wind farm, Hywind Scotland, mitigating the water depth limitation (WindEurope (2017)).

Independent of the location of the wind farm, all wind turbines require routine and reactive maintenance. Onshore located wind farms are rather easy to reach, while offshore wind farms introduce new challenges, requiring a well-thought cost-effective maritime logistics chain that is able to overcome weather conditions.

Currently, there are a few alternatives to the transportation of technicians and spare parts to the turbines. They are used in different logistics strategies and the most common ones are:

- CTVs (Crew Transfer Vessels), flexible transport for diverse service tasks;
- SOVs (Service Operation Vessels), floating warehouse and hub with walk-to-work turbine access;
- Helicopters, fast service response in difficult weather conditions; and
- Jack-Up Vessel, for construction and heavy component exchange.

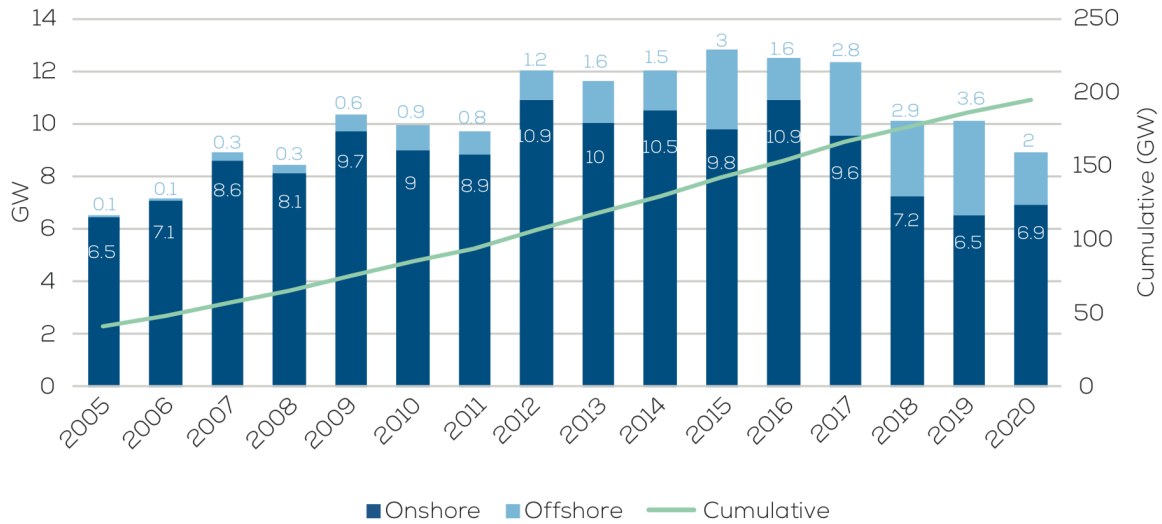


Figure 1.1: Annual and cumulative wind power installation and forecast under WindEurope’s low scenario (WindEurope (2017)).

Each of the alternatives has advantages and disadvantages. CTVs are agile, cheap and versatile, but not all can handle heavy weather, neither transport a large payload of spare parts. CTVs also have a transit window that can be considerable depending on the farm distance to shore. SOVs are larger, being an on-site living unit for up to 60 people, can carry daughter crafts, have larger operational window, provide a safe walk-to-work solution, can support multiple farms with almost zero or small transit time (if located on a nearby site), but are expensive to build and operate, compared to a CTV. Helicopters can rapidly cover any weather condition, but are expensive, carrying few technicians and limited cargo. Jack-Up vessels are expensive vessels that are utilised on construction and exchange of heavy parts, not commonly utilised for routine maintenance.

A throughout comparison between CTVs and SOVs is included in Sections 2.2, presenting the growth of usage of SOVs in the recent years and justifying further research and development of such vessels.

1.2 The Research Problem

The current issue with SOVs is that to be weatherproof, especially in the harsh conditions of the North Sea, their dimensions become inherently large in order to yield lower motions at sea. This results in large cargo and technicians capacity but also increases the building and operational cost. Shipowners, accordingly to the interested partner, are interested in weatherproof, cheaper and compact SOVs that can still carry a handful of technicians.

When decreasing the size of the vessel, seakeeping performance is largely affected and results in larger motions with wave excitation. That is the main challenge currently

posed and that has already been faced in other industries in which it is possible to get inspiration from.

1.3 Design Objective

The primary aim of this thesis project was to develop a flexible, fully-parametric Semi-Submersible/SWATH (Small Water-plane Area Twin Hull) hybrid SOV hull model that is shorter than currently operating SOVs and optimise it to heave performance.

The optimisation was focused on decreasing heave motion in order to obtain a vessel that has equivalent or even superior seaworthiness compared to an operating SOV, able to operate up to 3.5m significant wave height, about 90% of the year (in the German North Sea). This was evaluated by comparing the results to an 82m existing and operating monohull SOV, transforming the potential of the created hull to feasible numbers.

Using existing hull modelling techniques and seakeeping evaluation software, it is possible to narrow the project to three main research topics:

- *Parametric modelling*, best-practices for robust model creation and variation with a smart, and as small as possible, set of design-variables;
- *Seakeeping performance*, investigate the effects of geometry variations in the heave motion of the vessel utilising seakeeping software, identifying optimisation patterns towards superior performance; and
- *Station keeping*, evaluate wave drift forces in the SWATH and how different they are from monohulls for station keeping purposes.

1.4 Motivation

According to Puisa and Skaro (2018) the number of European SOVs are estimated to quadruple within the next ten years and the overall goal of future projects is to make offshore wind power more cost-effective.

The motivation to develop this project was to fill a potential market gap for a smaller SOV. This might be possible with an alternative hull design compared to the current option on the market, the monohull.

Some of the marine structures known for having excellent seakeeping behaviour are semi-submersibles and SWATHs. They have been successfully used for many years in the oil industry and high-speed passenger transportation.

MARIN (2018) affirmed that resonant responses can be prevented in a range of wave conditions by carefully tuning the vessel displacement and the waterline strut shape, meaning that a successful design variant is possible to be reached.

Therefore, the underlying idea behind this project was to unite the market's need for a cheaper, smaller SOV with the seakeeping characteristics of semi-submersibles and SWATHs.

1.5 Limitations and Delimitations

The limitations encountered along this project and that might have a relevant impact for future projects derived or similar to this one were:

- *Seakeeping software*, there were not many available seakeeping calculation programs that can handle the geometry in case, specially validated ones;
- NEWDRIFT+, as it is based on a linear solver, horizontal panels close to the waterline are not recommended (panels that would emerge when in a wave valley), limiting the geometry flexibility;
- *Performance quantification – heave*, most of the walk-to-work gangways manufacturers publish only the limiting significant wave height. In this project, heave evaluation in meters was used, without a direct translation and matching with products available in the market;
- *Performance quantification – Resistance*, significant effort was given in order to estimate the towing resistance of the SWATH vessel, but the geometry was not accepted by any available CFD (Computational Fluid Dynamics) software. Wave resistance coefficients could be obtained by 3D panel method solvers (Boundary Element Method), but far from interesting enough to be included in the optimisation process and in this project report; and
- *Computational power*, the system utilised for calculations was an i7-3537U @2.00 GHz, with 2 cores and 4 logical processors, equipped with 4.0GB DDR3 RAM. This was not exactly ideal for a large optimisation task with more than 1000 design variants. For this reason, the mesh utilised for calculations was reduced and the time for this project (about 5 months) did not allow a more advanced process, as a multi-objective optimisation, for example.

The boundaries set for the study, delimitations, in which might also have an impact in future projects and are worth mentioning were:

- *Geometry constrains*, imposed to the geometry in order to obtain unbiased comparisons results (length overall and displacement) may have led to unstable behaviour of the software and to the divergence of the optimisation algorithm;
- *Sea states*, only one sea state was selected for optimisation in order to simplify and shorten the optimisation process;
- *Performance quantification – DP capability*, in order to eliminate propulsion efficiency variables, as the compared vessels are completely different, DP (Dynamic Positioning) capability is compared by means of surge and sway forces, and yaw moments;

In order to keep the partner's projects confidentiality, vessel's displacement and vertical centre of gravity are not divulged in this report.

1.6 Parties Involved

The idea was an ongoing project for the future of offshore wind turbine maintenance vessels at Rolls Royce Marine Norway. The project was conducted in conjunction with Friendship Systems AG, which provided the 3D (Tri-Dimensions) modelling software CAESES® expertise and was the main hub of connection of all parties. The seakeeping software, NEWDRIFT+, was developed and provided by NTUA (National Technical University of Athens).

All involved parties, with exception of Chalmers, are members of HOLISHIP (HOListic optimisation of SHIP design and operation for life cycle), funded by the EU (European Union), where the connections were made.

The persons involved from each partner were:

- Student: Paulo Macedo;
- Friendship Systems AG Supervisor: Stefan Harries;
- Chalmers Examiner: Rickard Bensow;
- Rolls Royce Marine: Martijn de Jongh;
- Chalmers Co-supervisor: Carl-Erik Janson; and
- NTUA: George Zaphonitis and George Dafermos.

This page was intentionally left blank.

2 Basic Concepts

This chapter presents basic concepts in order to further justify this project, in order to understand what and how it was realised, and, later, be able to interpret the outcome of the analysis.

It begins with a quick overview of wind energy, explaining why the wind farms are moving further offshore and present current strategies and alternatives to offshore wind turbine OMS (Operation, Maintenance and unplanned Service). Sections with a short review of existent SWATH vessels in the market, their capabilities, and an introduction to geometric modelling techniques, advantages and disadvantages, and recommendations for each type of project follows.

The chapter also contains a section about ship motions in a seaway, including ocean waves description, ship responses to waves and transfer functions fundamental theory. Finally, the chapter is completed with a section presenting the software utilised in this project, NEWDRIFT+, including input, output and part of the theory behind it utilised in this project.

2.1 Offshore Wind Energy

The maximum power available in the wind, P_W , in Watts can be estimated by:

$$P_W = \frac{1}{2}\rho_{air}A_RU_W^3 \quad (2.1)$$

where ρ_{air} is the density of the air (1.225 kg/m³), A_R is the rotor swept area in m², and U_W the undisturbed wind speed at the rotor centre in m/s. The power output P_T of a wind turbine can, therefore, be obtained by multiplying an efficiency factor η_T , power coefficient, by P_W (Obhrai, 2014).

As it can be observed, the power output is directly proportional to the wind speed in the power of three and to the rotor area, which is πR_B^2 . So, for example, doubling the blade radius (R_B) results in a four-times increase in power output.

Obhrai (2014) concludes that major increase in the output power can only be achieved by increasing the swept area of the rotor and by placing the wind turbines on sites with higher wind speeds. This can also be interpreted as moving further offshore.

The rated capacity of offshore wind turbines has grown significantly over the past decade, focusing the harness of wind energy from sites with superior wind speeds (higher heights and further offshore) (WindEurope, 2017). This can be observed in

Figure 2.1, which clearly presents the evolution curve of future installations further from shore and in mixed water depths.

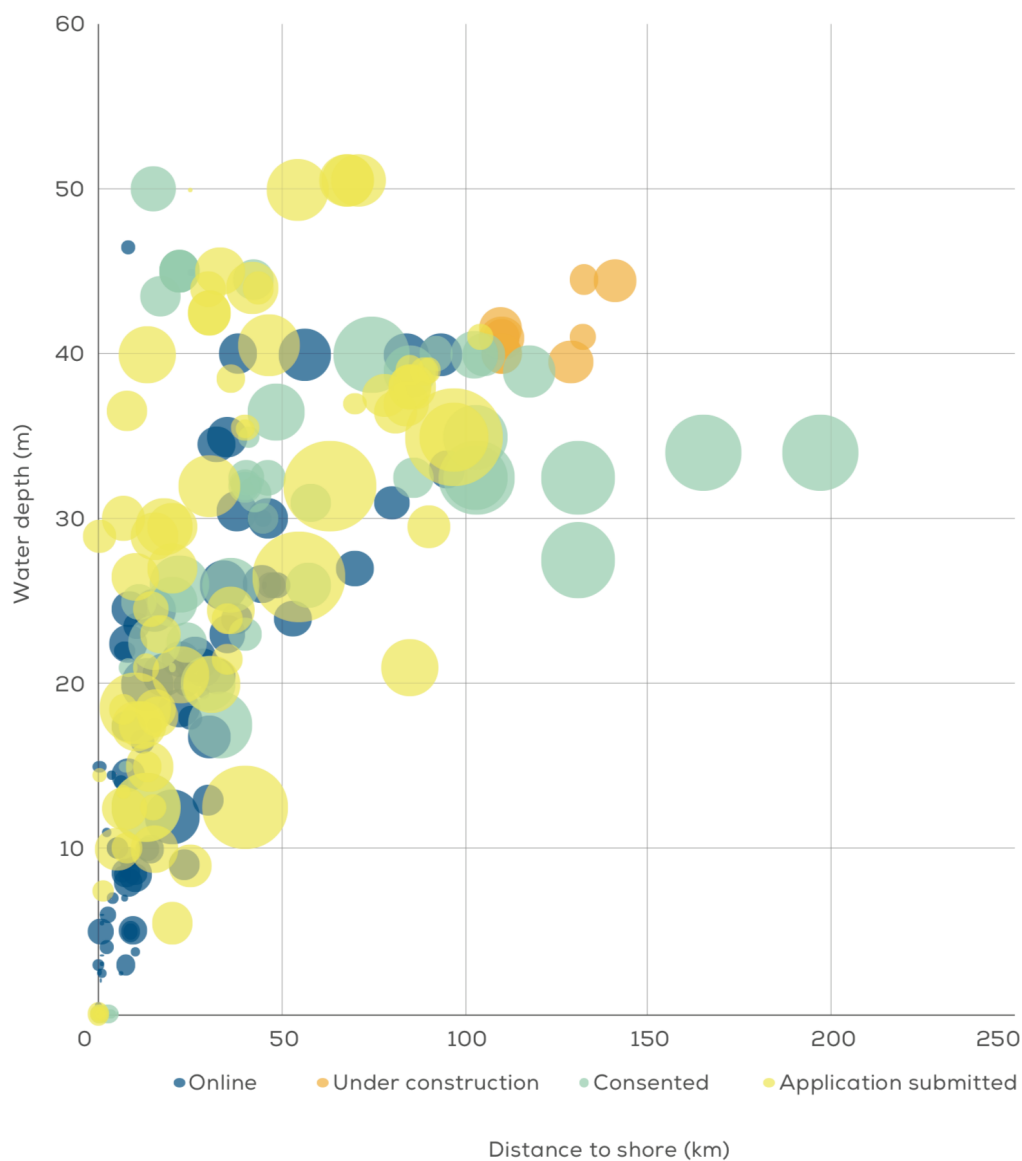


Figure 2.1: Average water depth and distance to the shore of bottom-fixed offshore wind farms, organised by development status. The size of the bubble indicates the overall capacity of the site (WindEurope, 2018).

2.2 Offshore Wind Service Vessels

A natural consequence of developing wind farms offshore is the need for suitable vessels for transportation, construction, operation, maintenance, and decommissioning (EWEA, 2011).

The placement of offshore wind farms further from shore and in more severe meteorological conditions (e.g., higher wind speeds and wave heights) has increased the challenges

of safely delivering technicians and components to the project site. Operators are addressing these challenges by rapidly incorporating next-generation OMS vessels and optimising related strategies (US Department of Energy, 2017).

Siemens Gamesa (2018) is currently investing in integrated service logistics to tackle the new challenges from wind farms located far from shore. Figure 2.2 presents the four types of vessels that compose the strategy.

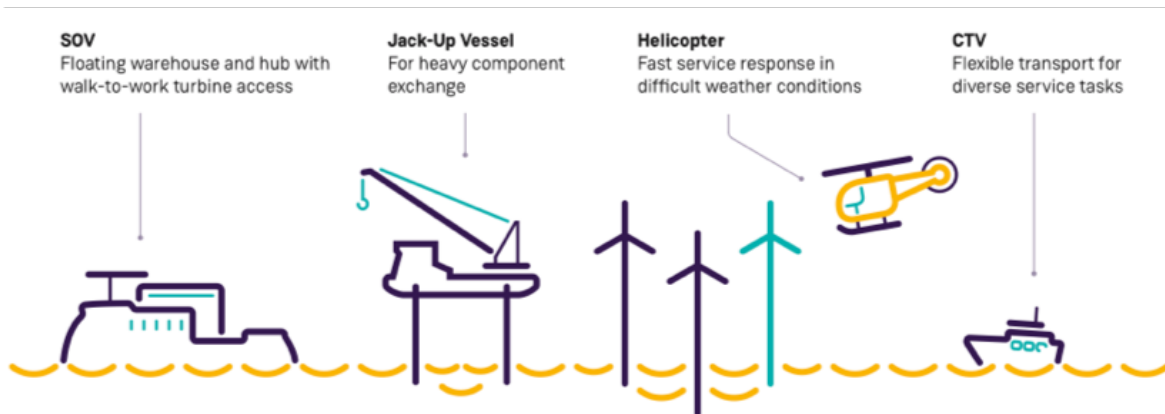


Figure 2.2: Integrated service logistics proposed by Siemens Gamesa (2018).

- *Service Operation Vessels* (SOVs) are able to stay a long period on-site, reducing significantly transport and transfer time. Innovative features make them the most effective way to service far-from-shore wind power plants, such as the deployment of daughter crafts or STBs (Safe Transfer Boats), accommodation unit, large operational window and safe walk-to-work gangways.
- *Jack-Up Vessels* are self-elevating platforms. They are mostly used for construction and complex heavy-lift tasks such as the main bearing, gearbox, and blade exchanges.
- *Helicopters* are used with other vessels for fast and wave-independent transfers directly to the top of the turbine, enabling a range of useful service tasks, including the transfer of technicians or spare parts and tools.
- *Crew Transfer Vessels* (CTVs) are used for a variety of service tasks including transfer and transport. They are multipurpose, high-speed vessels designed for wind parks closer to shore.

For projects that are a medium distance from port (nominally between 40 km and 70 km), operators are testing surface effect vessels, such as Umoe Wave Craft (a catamaran CTV with air cushions under the hull), which increases vessel speed from 20 to 35 knots and increases the limiting significant wave height (H_S) from 1.5m to 2.5m (US Department of Energy, 2017).

Grace and Lee (2017) complemented affirming that 2 or 3 hours each way in small and lightweight craft is no longer deemed a safe and economical solution. The harsher environmental conditions at 80 km or further from the coast has pushed the development of CTVs but the effectiveness and economics behind it remain limited.

Aukland (2017) presented an interesting example about transit times and disadvantages of current CTVs. The EnBW's Baltic 2 wind farm is a three hour CTV journey from Rostock, meaning six hours of a 12-hour shift would be dedicated solely to travel. If the commute could be eliminated through an SOV, technicians productivity can be increased by 100%.

For projects that are a greater distance from the port (nominally beyond 70 km), operators are using SOVs. These vessels are designed to stay on-site for extended deployments, with endurance generally exceeding 1 month. These crafts are outfitted with the capability to launch STBs and typically have motion-compensated gangways to allow for technician transfers in harsh weather. Siemens is deploying service operations vessels at four projects and estimates that its deployment of one such vessel at Westernmost Rough will cut weather-related downtime from the current levels of 40%–45% down to 10%–15% (Snieckus, 2014).

Whilst the SOV and its crew may stay at sea for a long period, transfer of wind farm engineers is typically more regular, every two weeks during operations, and is performed by CTV or helicopter. In order to minimise sea-sickness caused by the amount of time technicians spend onboard CTVs, it is possible to move the SOV closer to shore for crew exchanges (Aukland, 2017).

Another example, as shown in Figure 2.3, the station Fino 1 in the German North Sea had about 25% of days in which only SOVs and helicopters could operate due to the weather conditions (i.e. H_S was too high for a CTV with a 1.5m H_S transfer capability). If equipped with a helideck, the access to the turbines could be possible for higher sea states, encountered for 15% of the period (Aukland, 2017).

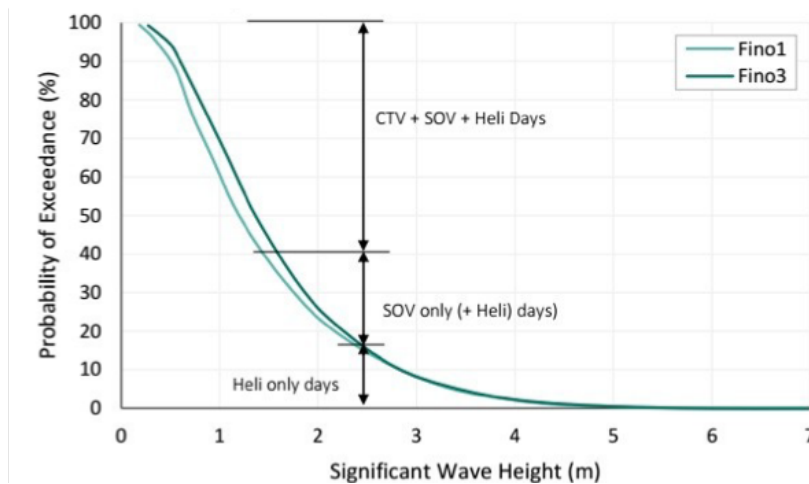


Figure 2.3: Exceedance probabilities for wind farms located in the German Bight region. Adapted from Aukland (2017).

The increasing usage of SOVs can be verified in Figure 2.4. The total of vessel days utilisation of SOVs has been on the rise even during the winter period, proving the larger operational window. CTVs, on the other hand, have been steadily oscillating due to the weather conditions of yearly seasons. Walk-to-work vessels have been on the rise even for farms that are closer than 80 km from the coastline (Aukland, 2017).

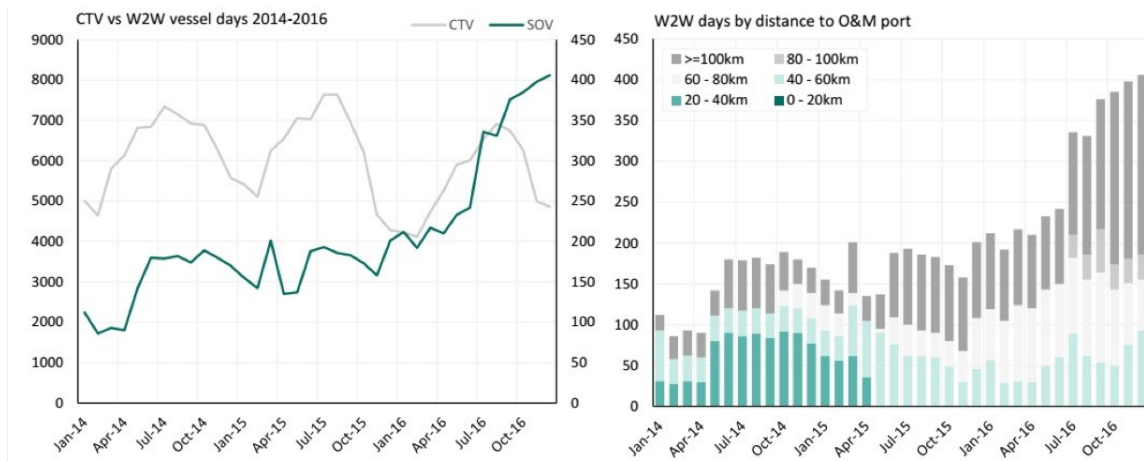


Figure 2.4: CTV vs walk-to-work vessel days 2014-2016 (left) and walk-to-work by distance to OMS port (right). Adapted from Aukland (2017).

Walk-to-work systems are becoming more common for both operations and construction activities. Along the whole year during operations, they are used in the park for routine and reactive maintenance, often combined with daughter crafts. During the construction phase they are able to assist with cable pull-in, accommodation support, substation installation support and turbine commissioning (Aukland, 2017).

Aukland (2017) also points out the downside of current SOVs and the market gap for smaller SOVs. During the summer maintenance campaign, the work-load is higher and current SOVs on the market need no additional support. However, it is possible that for the majority of the year a smaller vessel, with about 30 technicians, could suffice and be a more economical choice than a larger, only partially occupied SOV.

2.3 SWATH Vessels

Small Waterplane Area Twin Hull (SWATH) ships are a concept of vehicles with a peculiar configuration. Their hulls consist of two parts distant to each other featuring slender struts that pierce the free surface while the major part of the displacement is under the free surface, far away from the wave-induced forces (Qian, Yi, & Li, 2015).

They are known for superior seakeeping ability in relatively high sea states with respect to other conventional hulls (Brizzolara et al., 2011). Other advantages are low horsepower requirement for high speeds, ample stability, good manoeuvrability and large deck area. It also has its drawbacks, as large wetted surface (important for low speeds), sensitive to weight changes (draft/trim control required), pitch instabilities (fins required) and unique structural challenges (Papanikolaou, Zaraphonitis, & Androulakis, 1991).

Success cases of SWATH hulls include: passenger ships, as the Aegean Queen by Papanikolaou et al. (1991); research vessels such as NOAA (National Oceanic and Atmospheric Administration) Ferdinand R. Hassler (NOAA, 2015) and Planet (Schel-

lenberger, 2011); crew transfer vessels (WINDEA Offshore GmbH & Co. KG, 2017); offshore patrol vessels (Ad Hoc Marine Designs Ltd., 2013); special navy vessels, as the Sea Shadow (Lockheed Martin Skunk Works, 2018); and recently Brizzolara et al. (2011) have introduced an innovative design of a family of autonomous surface vessels (USV), Figure 2.5.

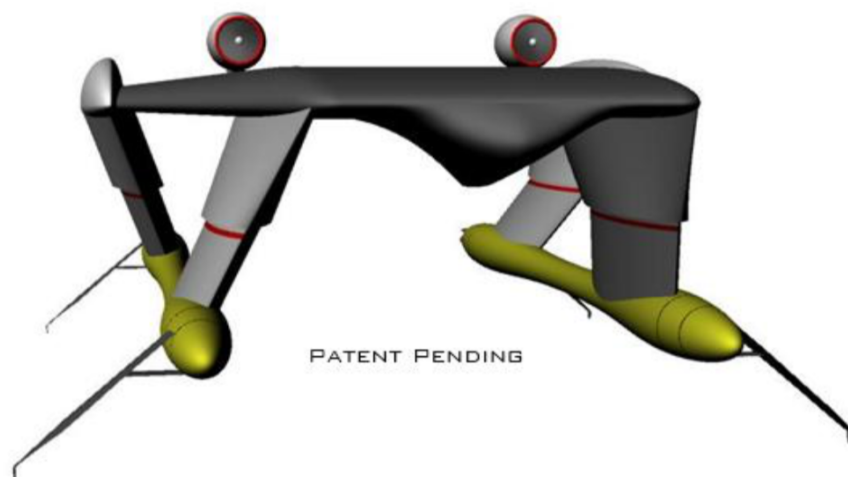


Figure 2.5: Ultrafast USV concept design (Brizzolara et al., 2011).

Besides the successful history of SWATH hulls in different industries, there is still no SWATH vessel operating as an SOV, although, there are projects under development with different approaches and purposes.

One of the available vessels available for order is currently designed by Ad Hoc Marine Designs, 41m LOA (Length Overall), having a capacity for 24 technicians in individual cabins (Ad Hoc Marine Designs Ltd., 2013). For a comparison, current operational SOVs in the range of 75-100m LOA has a capacity for 70 technicians, plus 20 crew members (Salt Ship Design, 2018).

FKAB has recently signed a contract for a 50m offshore wind farm service vessel for a Chinese shipowner. This vessel concept, equipped with a walk-to-work gangway, aims to provide maintenance service to offshore wind farms along the Chinese east coast area. In addition, the ship is equipped with DC (Direct Current) diesel-electric propulsion system and two azimuth contra-rotating thrusters, to achieve best operational function and fuel efficiency in both transit and DP2 (Dynamic Positioning Class 2) conditions. By the divulged image, Figure 2.6, it can be assumed that it is a SWATH design to be used both as a fast crew transfer and offshore wind turbine service purposes (FKAB, 2018).

Meanwhile, possibly one of the most developed project is the Windkeeper from *Compagnie Maritime CHAMBON* in partnership with *Constructions industrielles de la Méditerranée*. It was funded in 2012 and was in model test phase at MARIN (Maritime Research Institute Netherlands), Figure 2.7, in April of 2018. With main dimensions of 40m LOA, 20m breadth and a 5m draft, the goal was to develop a multi-mission SWATH ship, with high seakeeping capabilities for maintenance operations, safety, and security of offshore wind farms. In its first phase, several hull design variants



Figure 2.6: FKAB 50m offshore wind farm service vessel (FKAB, 2018).

were evaluated by linear seakeeping calculations. A final candidate was chosen to validate the design for operational conditions with model tests, including dynamic positioning capability in wind and currents. The next phase is to investigate propulsive performance (Compagnie Maritime Chambon, 2014; MARIN, 2018).



Figure 2.7: Windkeeper 5m model at MARIN test basin (MARIN, 2018).

Not far behind, VARD has been studying, developing and selling CSSs (Compact Semi-Submersibles) for various applications. It is a series of units from 65m to 100m in length with a single full-length strut per side. The compact platform integrates the motion benefits of a semi-submersible to ensure low day charter rates and increase operational flexibility. VARD has delivered a few 84m vessels for accommodation and for well intervention purposes, and has used its success to developed a 65m wind farm support vessel, Figure 2.8 (VARD Marine, 2018).



Figure 2.8: Compact Semi-Submersible developed by VARD. Adapted from VARD Marine (2018).

The 65m LOA and 28m breadth variant of the CSS evolved from several rounds of size optimisation, computational analyses and a full model testing program. The vessel's natural response to head seas, quartering seas and beam seas is a slow heaving motion. The unique hullform and its natural damping characteristics, therefore, lend itself extremely well to such an operation. Configured in a DP2 system set up like any other monohull SOV but with 4 azimuth thrusters, results in a more flexible and capable response to excursion and redundancy (Grace & Lee, 2017). The authors also discussed the regulatory challenges and advantages of such self-mobilising units, being a far more valuable asset if it can be relocated and on re-chartered with the minimum of re-certification.

2.4 Geometric Modelling

In the marine industry, many shapes need to be generated and varied during optimisation routines. To generate the geometries, several different techniques of geometric modelling are available in computer-aided design (Harries, Abt, & Hochkirch, 2004):

- *Conventional modelling* technique is built on a low-level definition of geometry. Shapes are defined by completely independent objects that do not bear any problem specific information;
- *Partially parametric modelling* has parameters that can modify geometries defined by an existing arbitrary conventional description; and
- *Fully parametric modelling* has the entire geometry described by and created by parameters that are able to capture the essence of the product to be generated or varied.

With regard to this classification, Abt and Harries (2007) organised a qualitative and subjective assessment of the techniques, presented in Figure 2.9, meant to serve as a guideline for technique selection for a task to perform.

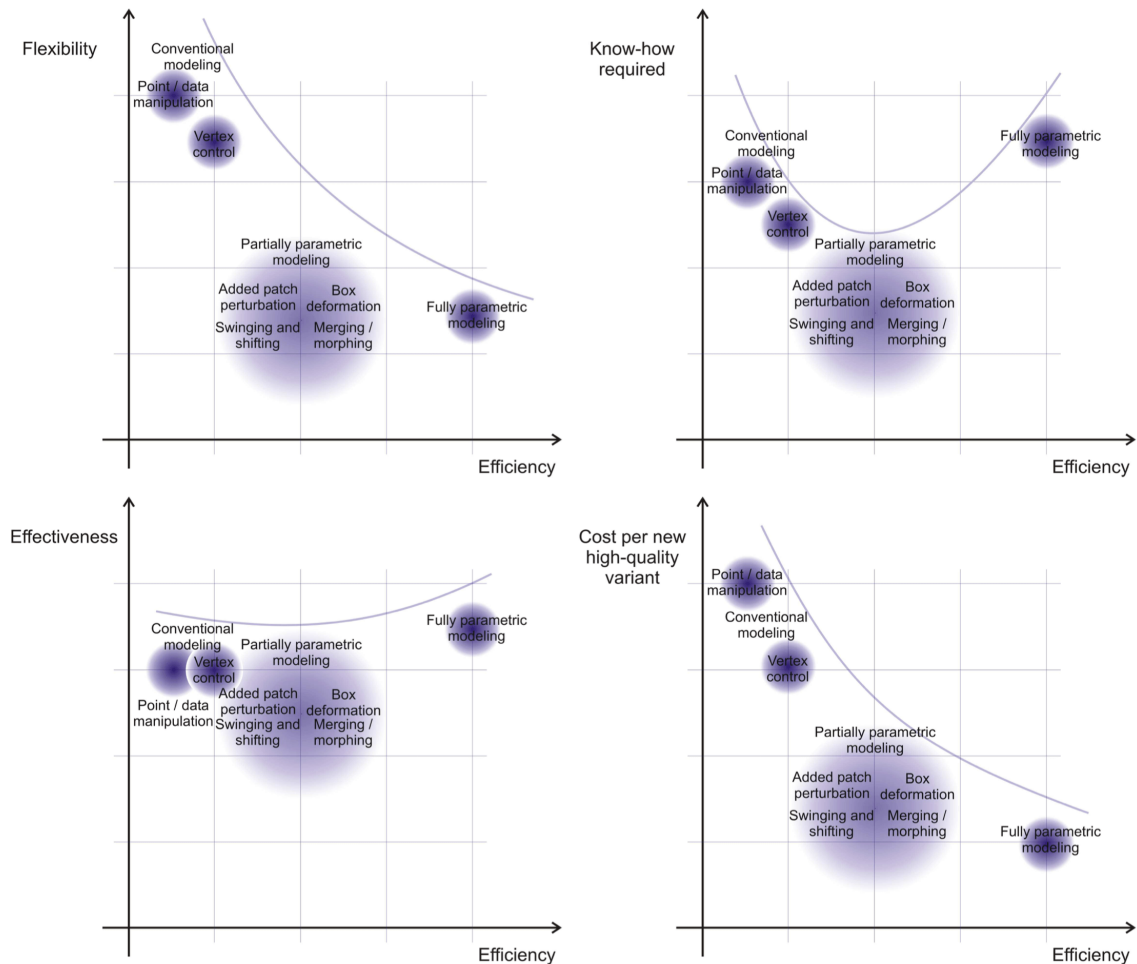


Figure 2.9: Qualitative assessment of available geometric modelling techniques (Abt & Harries, 2007).

Conventional techniques provide the highest flexibility independent of the product, but they require considerable mathematical insight and high-quality changes regarding fairness and other constraints are usually expensive (requires a lot of interactive work). Fully parametric techniques usually are very efficient, but they lack flexibility and require in-depth know-how. The initial investment to develop a fully parametric model is non-negligible, but it yields high effectiveness and low cost per high-quality variant. Partially parametric models fall in between the other mentioned techniques. Their strong point is that they call for less know-how, being relatively easy to apply (Abt & Harries, 2007).

All three models can be applied in simulation-driven design with varying effort. The choice of the technique has to be made based on the requirements and constraints of the task to be performed (Brenner, 2008).

2.5 Ship Motions at Sea

This entire section is dedicated to the sequence of topics necessary to understand the motions of a seagoing vessel.

The interactions between the vessel dynamics and several distinct hydrodynamic forces is a rather complicated phenomenon. To some extent, all ship responses are nonlinear although good predictions can be obtained with linear theories, cases when nonlinearities are small enough (Lewis, 1989).

Firstly it is necessary to study the nature of the ocean waves, understanding how observations of the sea surface elevation can be transformed into one density equation that is valid for describing all future observations under same conditions, the sea spectrum. After that, it is possible to catch a glimpse of ship motions in waves, the equations of motion, transfer functions and, finally, derived responses.

2.5.1 Ocean Waves Description

The ocean surface can be described mathematically as a random, stochastic process under short-term statistically stationary conditions (Lewis, 1989). Holthuijsen (2007) mentioned that in order to describe the chaotic appearance of ocean waves, it is reasonable to consider the free surface as a plane that smoothly moves up and down. This oscillation, at a fixed point, can be visualised in Figure 2.10.

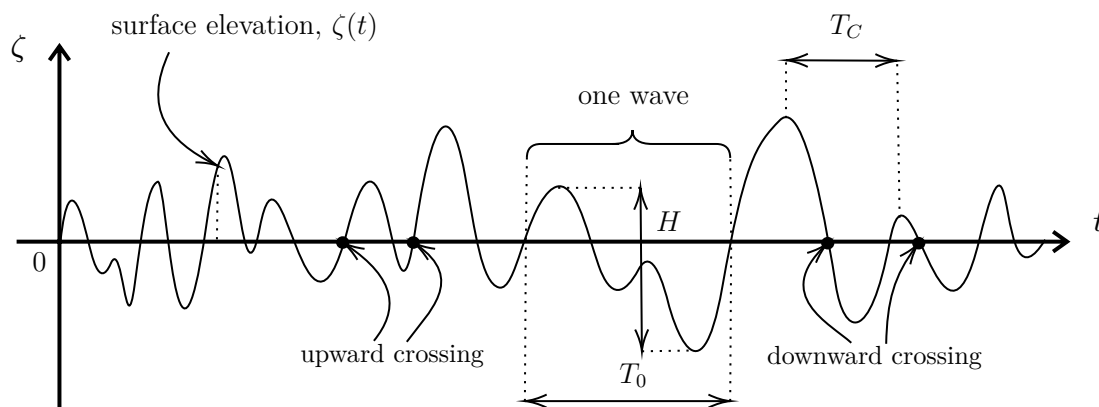


Figure 2.10: Typical wave record at a fixed point, with definitions of terms.

Figure 2.10 brings important concepts that will be necessary along the project. A wave is defined as the profile of the surface elevation between two successive downward or upward zero-crossings of the elevation. The wave height H is the vertical distance between the highest and the lowest surface elevation in a wave. The wave period is the time interval between two zero-crossings of the same type (upward or downward), therefore denoted as T_0 . Thus, a wave can only have one height and one period (Holthuijsen, 2007). Some authors might also include calculations dependent on the period between two consecutive crests, or peaks, T_C .

With these definitions, it is possible to understand the significant wave height, H_S . The significant wave height is defined as the mean of the highest one-third of the waves in the wave record, Equation 2.2, introduced by Sverdrup and Munk in 1946 in order to approximate the value of the visually estimated wave height (Holthuijsen, 2007):

$$H_S = \frac{1}{N/3} \sum_{r=1}^{N/3} H_r \quad (2.2)$$

where r is the rank number of the wave (based on wave height), and N is the number of waves in the record. A similar calculation can be made to estimate the significant wave period (which, accordingly to Holthuijsen (2007) can be approximated to the peak period of the spectrum, T_P , depending on its shape).

Other terms commonly utilised are the mean wave height, \bar{H} , the mean zero-crossing wave period, \bar{T}_0 , and the RMS (Root Mean Squared) of some definitions, $x_{RMS} = \sqrt{1/N (x_1^2 + x_2^2 + \dots + x_n^2)}$.

Further, analyses of wave records have concluded that wave elevations roughly follow a normal probability function, simplifying the application of statistics and Fourier analysis (Lewis, 1989). It is then possible to exactly reproduce that record as the sum of a large number of harmonic wave components:

$$\zeta(t) = \sum_{v=1}^n a_v \cos(2\pi f_v t + \varphi_v) \quad (2.3)$$

where n is the total number of harmonic wave components (frequencies); a_v is amplitude (half wave height); f is the frequency interval; φ_v the wave phase in radians; and v the frequency index.

2.5.1.1 Linear Wave Theory in Deep Waters

The description of random ocean waves can be achieved based on the notion of summing a large number of independent harmonic waves. This is possible with the linear theory for surface gravity waves, also known as Airy wave theory developed by George Biddell Airy in 1845. The theory describes in detail such harmonic waves and it is based on two fundamental equations and some simple boundary conditions, describing certain kinematic and dynamic aspects of the waves (Holthuijsen, 2007).

Holthuijsen (2007) continued, affirming that the approximation implies that each of these waves do not affect each other while they travel, and the main requirement for the linear theory to be applied is that the amplitude of the waves are small compared to the wavelength and the water depth (the waters are deep enough not to affect the waves).

The waveform of a harmonic progressing wave can be described by:

$$\zeta(t) = a \cos(kx - \omega t) \quad (2.4)$$

where a is the wave amplitude; k the wave number, $2\pi/\lambda$; λ the wave length; ω the angular frequency, $2\pi/T_0$; and T_0 the wave period.

Following the potential flow theory, applying the boundary conditions and derivatives, expressions for velocities, accelerations and pressure (to first order) can be obtained for water particles under the water surface,

$$u = a\omega\cos(kx - \omega t)e^{kd} \quad (2.5)$$

$$w = a\omega\sin(kx - \omega t)e^{kd} \quad (2.6)$$

$$p = a\rho_w g\cos(kx - \omega t)e^{kd} - p_g d \quad (2.7)$$

where u and w are particle velocities in the x and z directions, respectively; p the pressure acting in the particle; g the acceleration of gravity, 9.89 m/s^2 ; and d the vertical position of the particle, depth.

It is important to notice the introduction of the term e^{kd} , which exponentially minimises the effect of the wave with water depth d , often called as the Smith effect. This effect is extremely important for seakeeping characteristics of a floating body, as it presents the relation of the wave excitation forces (from particle acceleration) with the draught of a vessel (Bergdahl, 2009). As an example, a submarine is likely to feel no effect from waves during a storm, if located far enough below the water surface.

The Airy wave theory is the base for higher-order theories that are utilised for real steep waves, designing deck elevation of offshore structures, and wave forces on fixed structures from extremely large long period waves, for example. It also does not predict net mass transport, as the water particles move in closed orbits, while in reality, a small net mass transport in the wave direction of propagation is found. The main difference for higher-order theories is that it modifies and/or add terms to Equation 2.4 (Bergdahl, 2009).

2.5.1.2 Sea Wave Spectrum

Observations over time in a fixed point at the sea surface were essential and the starting point to the development of the wave spectrum, an equation capable of describing all possible observations that could have been made under the conditions of the actual observation (Holthuijsen, 2007).

The result of these observation series is a graph of the function $E(f)$, Equation 2.8, the variance density spectrum. The function statistically provides a complete description of the surface elevation, assuming that it can be interpreted as a Gaussian process (Holthuijsen, 2007),

$$E(f) = \lim_{\Delta f \rightarrow 0} \frac{1}{\Delta f} E \left\{ \frac{1}{2} \underline{a}^2 \right\} \quad (2.8)$$

where Δf is the frequency interval; $E \left\{ \frac{1}{2} \underline{a}^2 \right\}$ is the amplitude variance function. The underscore of \underline{a} indicates that the amplitude will be treated as a random variable.

Holthuijsen (2007) explained that the application of the *limit* function is done in order to obtain a continuous version of the spectrum, approximating the band frequency to zero. The overall appearance of the waves can be interpreted from the shape of the spectrum, narrower means more regular waves. This can be visualised in Figure 2.11.

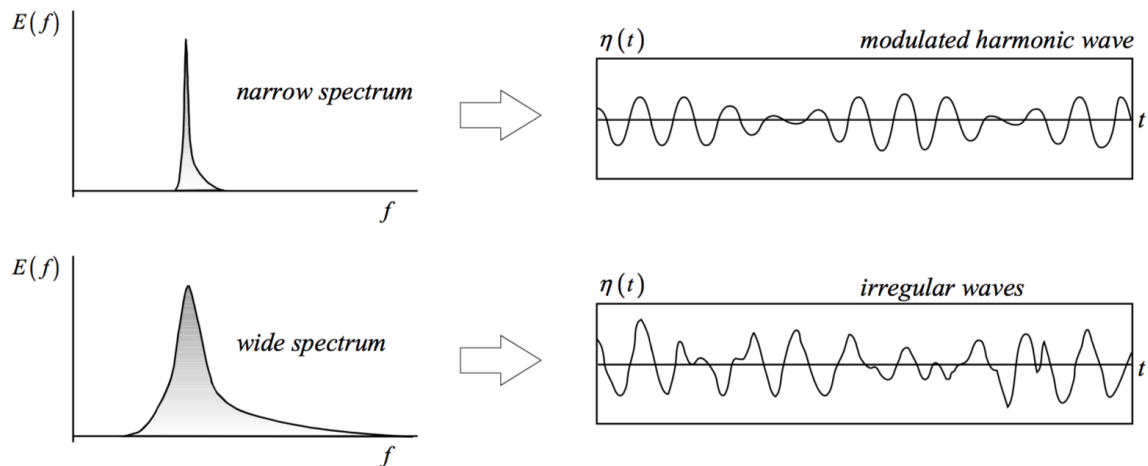


Figure 2.11: The (ir)regular character of the waves for spectra with different widths. Adapted from Holthuijsen (2007).

Alternatively, the function $E(f)$ can represent the energy spectrum if multiplied by $\rho_w g$, with ρ_w being the specific weight of the water. Therefore the spectrum graph can be referred to as the energy spectrum and it is possible to visualise how the energy is distributed along the frequency domain, as well as the location of the highest energy concentration (peak frequency, T_P) (Holthuijsen, 2007).

From a previously developed spectrum, it is possible through statistics to obtain H_S , Equation 2.9. Formulation to obtain T_P was developed by Kitano, Mase, and Kioka (2002), but it is not here presented due to its complexity. These are probably the most important wave parameters for engineers and utilised in this project.

$$H_{m0} = 4\sqrt{m_0} \quad (2.9)$$

where H_{m0} is the significant wave height obtained from a spectrum; m_0 the 0th spectral moment,

$$m_h = \int_0^\infty f^h E(f) df \quad (2.10)$$

and h is the h^{th} order moment index.

One of the most important contributions to the wave spectrum development was the JOint North Sea WAVE Project (JONSWAP; Hasselmann et al. (1973)), which is still the most widely used spectrum (Holthuijsen, 2007).

2.5.2 Ship Motions in Waves

A ship with zero or steady forward speed in an irregular short-crested sea will oscillate in six degrees of freedom, possibly amplified and out of phase with sea surface motion. In long waves, its motion will just follow the sea surface motion. For somewhat shorter waves, the motions will be opposed to the wave motion, but less amplified. The six degrees of freedom are presented in Figure 2.12 and described in Table 2.1.

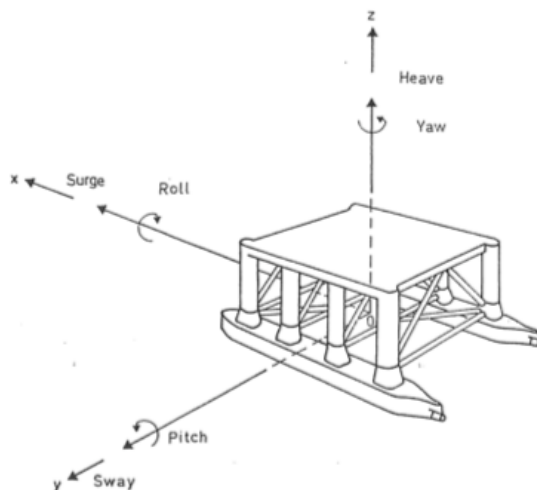


Figure 2.12: Motional degrees of freedom (Bergdahl, 2009).

Table 2.1: Names and description of the motional degrees of freedom.

Variable	Motion Name	Description
η_1	Surge	Bow-aft motion, along the x axis
η_2	Sway	Lateral motion, along the y axis
η_3	Heave	Vertical motion, along the z axis
η_4	Roll	Rotation around the x axis
η_5	Pitch	Tilting motion, rotation around the y axis
η_6	Yaw	Rotation around the z axis

In order to assess the seakeeping properties of a ship, a chain of calculations was presented by Bergdahl (2009) adapted in Figure 2.13 and has the following order:

1. Gathering of wave data, hindcasted or in-site observations;
2. Settling design-weather conditions;
3. Choosing and applying the adequate wave theory;
4. Applying an adequate method for the hydrodynamic forces and reactions of the vessel;
5. Calculate the response motions; and

6. Derive the load effects. This can be in the form of sectional forces and moments, tensions, the risk for propeller emergence, slamming and green water. For moored structures also the mooring-line tensions are derived.

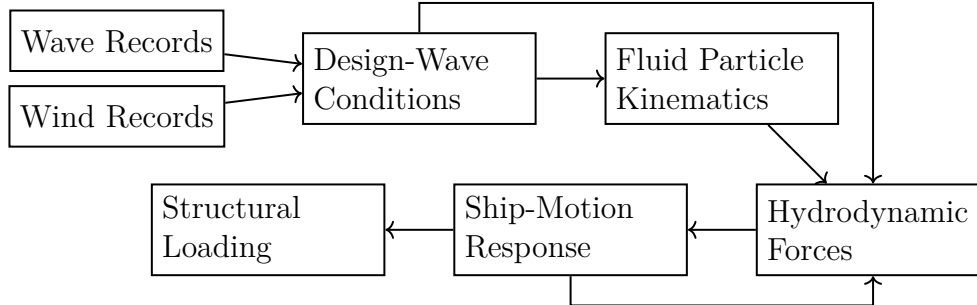


Figure 2.13: Calculation chain of ship motions. Adapted from Bergdahl (2009).

According to Bergdahl (2009) there are two fundamentally different ways to calculate wave-induced forces. One of the methods considers the structure as a whole and assess the total wave force from empirical or computed coefficients applied on water velocities and accelerations. The other method, the pressure distribution around the surface of the floating body is computed with due consideration to the water motion distorted by the structure itself, subsequently integrated around the structure. In both cases, mathematical models describing the wave properties is necessary, as presented in Section 2.5.1.

2.5.2.1 Equations of Motion

The base for the equation of motion is Newton's Second Law, force equals mass times acceleration, which affirms that an object will only accelerate if there is a net or unbalanced force acting upon it. That is the case for a floating structure in waves. The equation of motion of a floating body can be written as:

$$\mathbf{M}\ddot{\boldsymbol{\eta}} = \underline{\mathbf{F}} \quad (2.11)$$

where \mathbf{M} is a mass matrix (sometimes called generalised inertia matrix), described in Equation 2.12; $\ddot{\boldsymbol{\eta}}$ referring to the body acceleration vector, $d^2\boldsymbol{\eta}/dt^2$, with $\boldsymbol{\eta} = (\eta_1 \ \eta_2 \ \eta_3 \ \eta_4 \ \eta_5 \ \eta_6)^{\text{Tr}}$, a vector of positions in the six degrees of freedom; $\underline{\mathbf{F}} = (F_x \ F_y \ F_z \ M_x \ M_y \ M_z)^{\text{Tr}}$, the vector of forces and moments acting on the body; and "Tr" means that the vector is transposed. Furthermore,

$$\mathbf{M} = \begin{bmatrix} m & 0 & 0 & 0 & mz_G & -my_G \\ 0 & m & 0 & -mz_G & 0 & mx_G \\ 0 & 0 & m & my_G & -mx_G & 0 \\ 0 & -mz_G & my_G & I_{11} & I_{12} & I_{13} \\ mz_G & 0 & -mx_G & I_{21} & I_{22} & I_{23} \\ -my_G & mx_G & 0 & I_{31} & I_{32} & I_{33} \end{bmatrix} \quad (2.12)$$

where m is the mass of the ship; x_G , y_G and z_G the longitudinal, lateral and vertical coordinate of the centre of gravity of the structure, respectively; and I moments of

inertia defined in terms of the corresponding radii of gyration, with numbers 1 to 3 referring to axes, x , y and z , respectively (WAMIT, 2016).

The force vector $\underline{\mathbf{F}}$ can be split into the exciting forces, the reaction forces from the water and from mooring forces if any. Neglecting other exciting forces than the wave excited forces, a convenient split of the forces is:

$$\underline{\mathbf{F}} = \underline{\mathbf{F}}_e + \underline{\mathbf{F}}_r + \underline{\mathbf{F}}_{rs} \quad (2.13)$$

where $\underline{\mathbf{F}}_e$ contains the wave-excited forces; $\underline{\mathbf{F}}_r$ the hydrodynamic reaction forces from the water on the moving body in the absence of the waves; and $\underline{\mathbf{F}}_{rs}$ reaction forces from the mooring system.

The hydrodynamic reaction forces $\underline{\mathbf{F}}_r$, also known as the hydrodynamic properties of the body, is the linear approximation characterised by three properties:

1. **A** hydrodynamic mass or added mass matrix;
2. **B** hydrodynamic damping or radiation damping coefficients matrix; and
3. **C** hydrostatic stiffness matrix.

Thus, $\underline{\mathbf{F}}_r$ can be rewritten as Equation 2.14, a classic problem of mechanics of vibration:

$$\underline{\mathbf{F}}_r = -\mathbf{A}\ddot{\underline{\boldsymbol{\eta}}} - \mathbf{B}\dot{\underline{\boldsymbol{\eta}}} - \mathbf{C}\underline{\boldsymbol{\eta}} \quad (2.14)$$

A floating body with arbitrary form can exhibit hydrodynamic reactions in all degrees of freedom j caused by motion in any direction k (Bergdahl, 2009). Substituting Equations 2.13 and 2.14 into Equation 2.11, the complete expression can be obtained, Equation 2.15:

$$\underline{\mathbf{F}}_e + \underline{\mathbf{F}}_{rs} = -(\mathbf{M} + \mathbf{A})\ddot{\underline{\boldsymbol{\eta}}} - \mathbf{B}\dot{\underline{\boldsymbol{\eta}}} - \mathbf{C}\underline{\boldsymbol{\eta}} \quad (2.15)$$

where \mathbf{M} , \mathbf{A} , \mathbf{B} and \mathbf{C} are 6×6 matrices that are functions of the frequency of the wave with elements M_{jk} , A_{jk} , B_{jk} and C_{jk} ($j = 1, 2 \dots 6$, $k = 1, 2 \dots 6$), respectively.

Bergdahl (2009) mentioned that depending on the body arrangement, symmetry planes and origin of the coordinate system, in linearising the equation, many of the coefficients can be eliminated and the matrices simplified. For the detailed formulae for all coefficients, please consult Section 3 in Principles of Naval Architecture Volume III, Chapter 8, by Lewis (1989).

As an example, for a ship with lateral symmetry, Equation 2.15 can be simplified to:

$$F_x = m(\ddot{\eta}_1 + z_G \ddot{\eta}_5) \quad (\text{surge}) \quad (2.16)$$

$$F_y = m(\ddot{\eta}_2 - z_G \ddot{\eta}_4 + x_G \ddot{\eta}_6) \quad (\text{sway}) \quad (2.17)$$

$$F_z = m(\ddot{\eta}_3 - x_G \ddot{\eta}_5) \quad (\text{heave}) \quad (2.18)$$

$$M_x = I_{11} \ddot{\eta}_4 - I_{13} \ddot{\eta}_6 - m z_G \ddot{\eta}_2 \quad (\text{roll}) \quad (2.19)$$

$$M_y = I_{22}\ddot{\eta}_5 - m(z_G\ddot{\eta}_1 - x_G\ddot{\eta}_3) \quad (\text{pitch}) \quad (2.20)$$

$$M_z = I_{33}\ddot{\eta}_6 - I_{31}\ddot{\eta}_4 - mx_G\ddot{\eta}_2 \quad (\text{yaw}) \quad (2.21)$$

2.5.2.2 Responses to Harmonic Loads

A function of harmonic load $F(t) = F_0 \cos(\omega t)$, as generated by one of the harmonic wave components of the sea elevation surface, Equation 2.4, gives a response of the same harmonic type: $x(t) = \hat{x} \cos(\omega t - \varphi)$, in which F_0 is the force amplitude; $\omega = 2\pi/T$, the angular frequency; T the period; \hat{x} the amplitude of the displacement; and φ the phase lag between the force and the displacement (Bergdahl, 2009).

By solving Equation 2.14 for the given harmonic load, employing the complex notation and trigonometric expressions, Equation 2.22 can be obtained:

$$\hat{x} = \frac{F_0}{\sqrt{(c_c - (m + a_c)\omega^2)^2 + b_c^2\omega^2}} e^{-i\varphi} \quad (2.22)$$

where a_c is the added mass; b_c the damping coefficient; and c_c the spring stiffness (hydrostatic).

Interestingly, the ratio between \hat{x}/F_0 is an amplitude response function and gives the ratio between the amplitude of the harmonic response to the amplitude of the harmonic disturbance that excited it, with length/force dimensions (Bergdahl, 2009). This function is called transfer function, $T(\omega)$, or in the seakeeping case, response amplitude operator (RAO):

$$T(\omega) = \frac{\hat{x}}{F_0} = \frac{e^{-i\varphi}}{\sqrt{(c - (m + a)\omega^2)^2 + b^2\omega^2}} \quad (2.23)$$

2.5.2.3 Derived Responses

The aspects of ship response to rough seas can be, in principle, derived from the basic six modes of motion (Lewis, 1989). They include:

- Vertical and/or lateral motions, velocities and accelerations at specific points, i.e. local motions;
- Relative motions between a location in the ship and the encountered waves;
- Slamming and greenwater (non-linear);
- Yawing and broaching (non-linear);
- Added resistance and powering in waves (non-linear); and
- Wave bending moments and loads on hull and equipment (non-linear).

The motions of any point $\mathbf{r} = (x, y, z)^T$ on the body may be defined by three translations and three rotations. The translational motions, $\boldsymbol{\xi} = (\xi_1, \xi_2, \xi_3)^T$ with (ξ_1, ξ_2, ξ_3) the complex local amplitudes at x , y and z , respectively, are result from the

combined effect of rotation of the body and translation of its centre of gravity (Lewis, 1989).

For small motions (rotations $< 10^\circ$), $\underline{\xi}$ can be calculated by:

$$\underline{\xi} = \begin{bmatrix} \eta_1 \\ \eta_2 \\ \eta_3 \end{bmatrix} + \underline{\Omega} \times \underline{\mathbf{r}} \quad (2.24)$$

where $\underline{\Omega}$ is the vector of rotational motion at any point, (η_4, η_5, η_6) .

Similarly, the velocities and accelerations of any point fix to the body can be calculated by:

$$\dot{\underline{\xi}} = \begin{bmatrix} \dot{\eta}_1 \\ \dot{\eta}_2 \\ \dot{\eta}_3 \end{bmatrix} + \dot{\underline{\Omega}} \times \underline{\mathbf{r}} \quad (2.25)$$

$$\ddot{\underline{\xi}} = \begin{bmatrix} \ddot{\eta}_1 \\ \ddot{\eta}_2 \\ \ddot{\eta}_3 \end{bmatrix} + \ddot{\underline{\Omega}} \times \underline{\mathbf{r}} \quad (2.26)$$

The individual component amplitudes of $\underline{\xi}$ are given by:

$$\xi_1 = \eta_1 + z\eta_5 - y\eta_6 \quad (2.27)$$

$$\xi_2 = \eta_2 + x\eta_6 - z\eta_4 \quad (2.28)$$

$$\xi_3 = \eta_3 + y\eta_4 - x\eta_5. \quad (2.29)$$

Similar deductions can be made for the velocities and accelerations, $\dot{\underline{\xi}}$ and $\ddot{\underline{\xi}}$, respectively.

2.6 Seakeeping Evaluation with NEWDRIFT+

The Ship Design Laboratory of the National Technical University of Athens (NTUA-SDL) provided the seakeeping linear code NEWDRIFT+ for this project. The program development started in the early 80's by A. Papanikolaou and was since then continuously updated by himself and G. Zaraphonitis to improve its efficiency (Liu, Papanikolaou, & Zaraphonitis, 2001). The code, made in Fortran, is known for its robustness, arbitrary geometry support, agreement and validation to experimental data (Liu & Papanikolaou, 2015, 2016a, 2016b, 2017; Liu, Papanikolaou, & Zaraphonitis, 2011; Liu, Shang, Papanikolaou, & Bolbot, 2016; Papanikolaou & Schellin, 1992).

NEWDRIFT+ is a 6 degrees of freedom, tri-dimensional frequency domain panel code for seakeeping and wave-induced loads, including drift deviations, forces and moments of floating structures, including multi-body arrangements operating in zero or nonzero forward speed, finite or infinite water depth and being excited by sinusoidal linear waves of arbitrary frequency and heading. The consideration of a natural seaway excitation is enabled through a spectral analysis post-processor, given the sea state characteristics (Liu et al., 2001).

This section comprises the calculation methodology utilised in this project, the far field method, input data required for the calculation and output data obtained from NEWDRIFT+.

2.6.1 Calculation Methodology

Liu et al. (2011) mentioned that there are several methods to calculate the added resistance of a vessel, mainly divided into two categories: near-field and far-field methods. Far-field methods are based on considerations of the diffracted and radiated wave energy and momentum flux at infinity, resulting in a steady added wave resistance force by the total rate of momentum change. The near-field method leads to the added wave resistance as the steady second-order force obtained by direct integration of the hydrodynamic, steady second-order pressure acting on the wetted ship surface.

In NEWDRIFT+, the added resistance problem of ships in waves can be solved following Maruo's far-field theory by Maruo (1957) and numerically implemented using velocity potentials calculated by a Time Domain Numerical Simulation method for submerged bodies by Liu, Papanikolaou, and Duan (2007) a 3D Frequency Domain Panel method by Papanikolaou and Zaraphonitis (1987) and a 3D time domain HYBRID method for bodies floating on the free surface by Liu and Papanikolaou (2011).

For the short waves range, the asymptotic formulae introduced by Faltinsen et al. (1980) and also by Kuroda et al. (2008). Liu and Papanikolaou (2016b) executed the application of the present method and also extended to oblique seas by fine-tuning the Kochin function.

A systematic validation for different hull forms (submerged and floating, slender and bulky) and varying wavelengths and speeds were conducted, and the results proved that the implemented procedure appears to be fully satisfactory, reliable and robust method for the routine added wave resistance prediction, working well for both full and fine hull forms in various wave headings and speeds (Liu & Papanikolaou, 2016b; Liu et al., 2011).

2.6.2 Input Data

The input data is separated into four files: the geometry panel mesh, which can be seamlessly obtained from or converted in CAESES®; a file containing the general parameters that determine the input selection, "InputParameters.dat", that drives the pre-processing for the use of CAESES® panels and setting the calculation methods; one containing data related to ship principal dimensions and loading condition, "Ship-dat.dat"; and the last one that contains case-relative data "Casedat.dat". All files with ".dat" extension are presented in Appendix C.

"InputParameters.dat", in order, contains: input format; panel mesh format; trim angle; draft at a reference point; tolerance identification of nodes close to the waterline;

parameters for integral calculation; and parameters for listing options and calculation selection.

"Shipdat.dat", in order, contains: geometry symmetry configuration; body outer dimensions; draft; vertical position of the coordinate system; vertical position of the buoyancy centre (can be calculated automatically); x , y and z centre of gravity coordinates; centre of flotation coordinates (can be calculated automatically); hydrostatic form coefficients (can be calculated automatically); transverse and longitudinal GM values (can be calculated automatically); radius of gyration for roll, pitch and yaw; and radius of product of inertia for roll-yaw, roll-pitch and pitch-yaw in respect to the centre of gravity.

Finally, "Casedat.dat", in order, contains: calculation configuration; calculation methodology; calculate fluid velocities and accelerations on specified points; calculate motions, velocities and accelerations in body-fixed points; identifiers for calculation of Green function, speed effects, viscosity effects on roll damping, mooring forces considerations and sectional loads calculations; water depth case; wave parameters input (JONSWAP spectrum); heading angle; vessel speed; stiffness of mooring lines and positioning devices; coordinates of fluid points to be calculated; and body-fixed points coordinates.

For detailed information consult Manual of NEWDRIFT+ V7 by Liu et al. (2001).

2.6.3 Output Data

The output data is unfortunately not graphical. It is divided into many files, with three containing the principal result information: "OUT4CAESES.csv", "RAOS.dat" and "inputdat.dat".

"OUT4CAESES.csv" probably presents the most direct results: a list with displacement motion, velocities and accelerations RMS values for the centre of gravity, the centre of the coordinate system and body-fixed points; and mean added wave resistance.

"RAOS.dat" containing important information as the points calculated in the sea spectrum and transfer function values for each point in each of the modes (1 to 6).

Finally, "inputdat.dat" contains a very long list of: geometry characteristics (i.e. buoyancy and gravity centre); environment characteristics; mesh details; some of the input settings; total wave forces and moments for each point calculated in the spectrum (both Froude-Krylov and total, including diffraction); and hydrodynamic masses \mathbf{A} , damping \mathbf{B} and hydrostatic stiffness \mathbf{C} matrices. An important file for debugging and verification that the computation is correctly set-up and running.

While the computational is undergoing, NEWDRIFT+ also prints a list of functions that are called under the calculation and errors if any.

3 Methodology

This chapter presents, almost step-by-step, how this project was conducted and how to replicate it in future projects.

It starts with a brief introduction of Rolls Royce Marine SOV design alternatives, which was the baseline for comparison against the developed SWATH concept. The following section describes an SOV SWATH, its limitations and recommendations for a successful design, including a CAD (Computer-Aided Design) sketch provided by Rolls Royce Marine.

Slightly changing the subject, a section about how the SWATH hull was fully parametric modelled and how the model was adjusted to match the monohull. This was made in order to obtain an equitable comparison. The following section is dedicated to the mesh generation for the seakeeping software, NEWDRIFT+, with hints and recommendations for any geometry. Succeeding comes sections about the sea state selection, body-fixed point for motions evaluation, the connection set-up between the geometry NEWDRIFT+ and post-processing features, and a throughout explanation about the optimisation process developed and utilised in the project.

To finalise the chapter, a section about a further SWATH design exploration is presented followed by a short section of how the results were post-processed. The post-processing phase enabled a detailed comparison between the vessels, including RAOs (Response Amplitude Operators) and DP (Dynamic Positioning) capability with graphs of forces and moments on the body in a developed seaway.

3.1 Rolls Royce Marine SOVs Design

Rolls Royce Marine is the designer for the Service Operation Vessels (SOVs) that ought to operate in the Race Bank and Hornsea offshore wind farms, United Kingdom east coast. The company already offers a range of SOVs that vary in size and accommodation capacities by using a number of different hull forms and thruster configurations (Foxwell & de Jongh, 2017).

As well as designing the vessel, Rolls-Royce supplies the diesel-electric main machinery, consisting of frequency controlled electric driven azimuth thrusters, super silent mounted transverse thrusters, DP2 dynamic positioning system, power electrical system, deck machinery, and the latest generation automation and control system (Rolls Royce Marine, 2016).

The company is also investing in research projects to improve SOVs, such as the NEXUS comprising the University of Strathclyde, Astilleros Gondan, DNV-GL, and

Global Marine Systems. NEXUS's goal is to increase performance and safety with minimised lifetime cost by 20% while reducing CO₂ emissions by 30% compared to current vessels (Puisa & Skaro, 2018).

A few other innovations are: double-ended hull design with two pairs of azimuth thrusters fore and aft; permanent magnet technology to enhance performance and efficiency; energy storage concepts and hybrid arrangements to reduce fuel consumption and emissions; and the Rolls-Royce RRM boat transfer system for boats ranging in size from 12m to 20m (Foxwell & de Jongh, 2017).

This section presents two of their SOV designs. Firstly the longer, 82m, SOV that already operates and the second presenting the new shorter design under development, which is the baseline for comparison in this project.

3.1.1 82m SOV monohull

Rolls Royce marine has currently one operating SOV delivered in February 2018 to Østensjø Rederi. The vessel, Edda Passat, is 82m long, 17m wide and has 5.3m draught, comprising 60 berths, is presented in Figure 3.1 (Østensjø Rederi, 2018).



Figure 3.1: Edda Passat, UT 540 WP design by Rolls Royce Marine (Østensjø Rederi, 2018).

Besides Edda Passat, the shipowner Østensjø Rederi has signed a contract with the yard Astilleros Gondan in Spain, to design and equip a second SOV to support wind farm operations for DONG Energy in shallow waters (Rolls Royce Marine, 2016).

The award-winning UT 540 WP was developed in close cooperation with the customer and benefits from over 40 years of UT (Ulstein Trading) ship design experience across 800 vessels. The new design for offshore wind farm support has a high focus on seakeeping capabilities, station keeping performance, improved comfort and safety on board, and reduced fuel consumption (Rolls Royce Marine, 2016).

3.1.2 62m SOV monohull

The shortened SOV version current development is aimed towards the market gap described in Sections 1.4 and 2.2. It is a shorter version of the 82m SOV presented in Section 3.1.1, measuring 62.1m LOA, 16.5m breadth and 5.6m draught, presented in Figure 3.2.

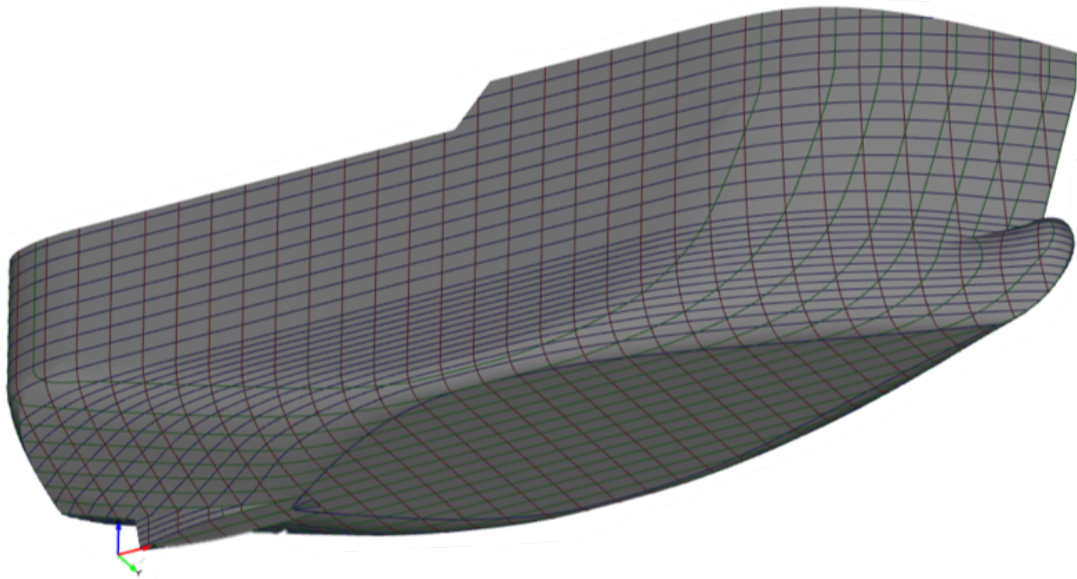


Figure 3.2: The shorter version of the UT 540 WP design (Rolls Royce Marine, 2018).

This version of the monohull was the one utilised to benchmark the performance of the developed SWATH concept. The main reasons were: to focus on the market gap for smaller SOVs, potentially cheaper and that maintain seakeeping abilities; and because was possible to match LOA and the displacement, creating a less biased comparison.

Comparing the seakeeping abilities of two vessels with similar displacement and LOA makes it easier to narrow down the reasons of different results, in this case, the hull form specifically.

3.2 Concept Design

After getting to know the current design under operation, as well as future developments, the design process of the SWATH hull could be started. The base for everything was a raw sketch provided by the interested partner, Figure 3.3.

As it can be observed in Figure 3.3, the SWATH hull is partly inspired by a catamaran and a semi-submersible structure. The sketch assumes the propulsion system consisting of azimuth thrusters under each edge of the demi-hulls. In order to

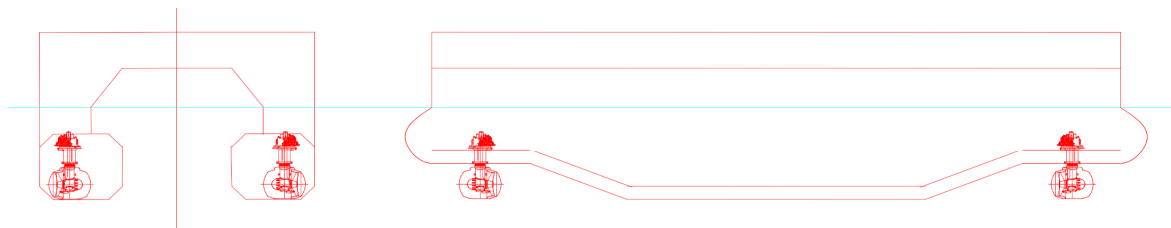


Figure 3.3: Initial sketch of the SWATH hull provided by Rolls Royce Marine especially for this project.

increase the chances of success of such an alternative hull design, a few delimitations and constraints were imposed and others suggested by the partner. These include:

- Maximal utilisation of simple geometric shapes, flat and simple curvature plating (developable surfaces, if possible);
- The most external side should be totally flat to ease construction, docking procedures and allow the deployment of smaller support vessels, such as STBs;
- Beam should be limited to 20m and draught up to 8m due to limited depth at most wind farm support harbours;
- Length should be less than operating monohull SOVs. In this case the 62.1m of the short monohull presented in Section 3.1.2 was matched; and
- The displacement is to be matched to the short monohull SOV version for all design variants.

These recommendations were used as the primary design goals, setting the bounds for most of the design variables of the model. They were also imposed to lower construction costs and ensure operational capability, satisfying shipowners' needs. It is important to mention that significant effort was given not to jeopardise the hydrodynamic performance of the vessel.

3.3 Parametric Modelling of a SWATH SOV

The fully parametric technique was selected for this project based on the lack of an initial existing design and the effectiveness of the model, for a later stage, generate design variants.

Based on the input from the concept design (Section 3.2), it was possible to start the parametrisation of the SWATH hull. Due to its symmetry in relation to planes ZX and YZ , only a quarter of the hull needed to be modelled, assuming tangency continuity at the intersection between the hull and a principal plane.

The first step was to create the main variables, presented in Table 3.1. These represent the main dimensions of the vessel and served as the reference for most of the connected elements in the parametric model.

Table 3.1: Design variables introduced for the main dimensions.

Design Variable	Lower Bound	Upper Bound	[unit]	Description
xFP	52	58	m	Length between perpendiculars
B	15	20	m	Breadth, outer beam
T_D	6	8	m	Design draught

The modelling process was divided into four main parts: the parallel midbody (PM), the bulb, the transition between the parallel midbody and the bulb, and the design waterline.

3.3.1 Parallel Midbody

The modelling of the parallel midbody introduces new design variables that are dependent on the main dimensions of the vessel.

A couple of important parameters introduced here are the inner height (H_{IN}) and the possibility of giving an angle to the inner side wall (yH_{SHIFT}). These were intuitively introduced in an attempt of changing the damping behaviour of the vessel, possibly resulting in higher heave damping.

The new design variables are presented in Table 3.2 and illustrated in Figure 3.4.

Table 3.2: Design variables introduced in the parallel midbody design.

Design Variable	Lower Bound	Upper Bound	[unit]	Description
L_{PM}	20	60	%	Length of the PM (% of xFP)
B_{PM}	0	100	%	Width of the PM (% of B)
H_{IN}	20	100	%	Height of the inner side (% of T_D)
yH_{SHIFT}	-15	15	°	Y shift of the upper inner width

It is important to notice that B_{PM} is automatically adjusted for each design variant to match the displacement of the short monohull SOV presented in Section 3.1.2. The procedure for the displacement adjustment is presented in detail in Section 3.3.5.

As it can be observed, the parallel midbody is composed of four bilges. Each of them has its own set of height and width parameters which are set to about 1m at the beginning and had their effect investigated in the final step of the optimisation (Section 3.8.3).

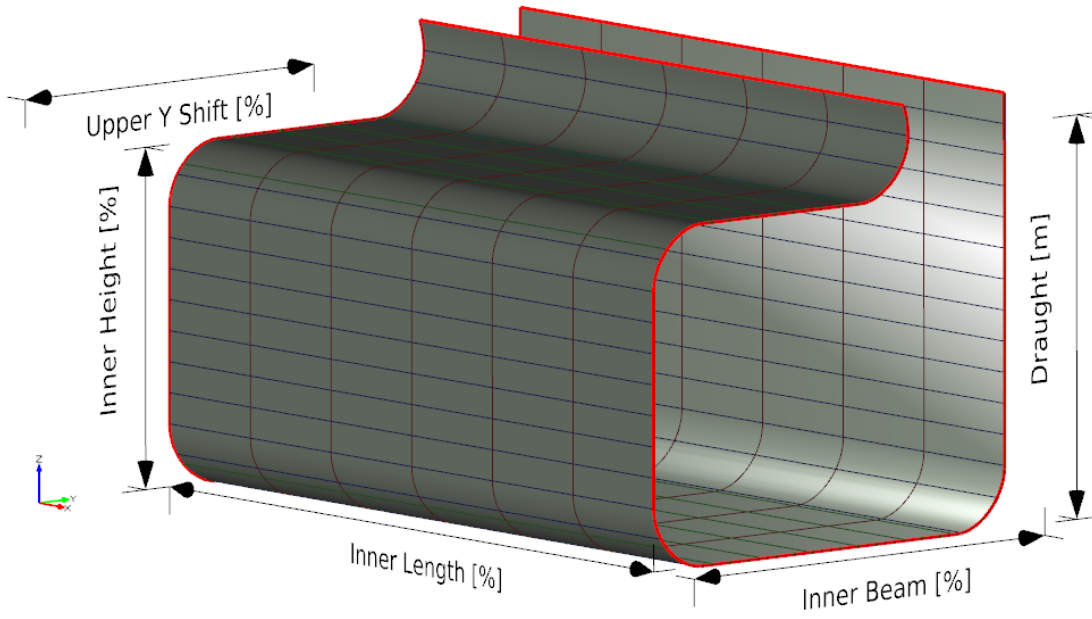


Figure 3.4: Main design variables of the parallel midbody.

3.3.2 Bulb

The modelling of the so-called "bulb" part was highly influenced by the positioning and sizes of the azimuth thrusters. The main variables introduced are the height clearance, the base diameter and base inclination angle (ZX plane). The height clearance, the thruster base diameter and the inclination were kept constant during the whole project, 3m, 2.4m and 0° , respectively. These can be further adjusted in a future iteration.

The bulb length was designed to be flexible and complement the xFP variable in order to match the LOA of the short monohull SOV, 62.1m. Another flexibility of the model is the positioning of the centre of the base of the azimuth thruster, which can be shifted from the xFP location along the x -axis. It was kept constant and equal to the thruster base diameter, 2.4m.

The set of design variables are presented in Table 3.3 and illustrated in Figure 3.5.

Table 3.3: Design variables introduced in the bulb design.

Design Variable	Lower Bound	Upper Bound	[unit]	Description
H_{POD}	2	3	m	Thruster clearance height from keel
D_{POD}	1.5	3	m	Base diameter of the azimuth thruster
α_{POD}	0	10	$^\circ$	Thruster base angle (ZX plane)
BB_{EXT}	1	1.5	%	Bulb extension (% of D_{POD})
xPB_{SHIFT}	-3	0	m	x shift of the thruster base centre

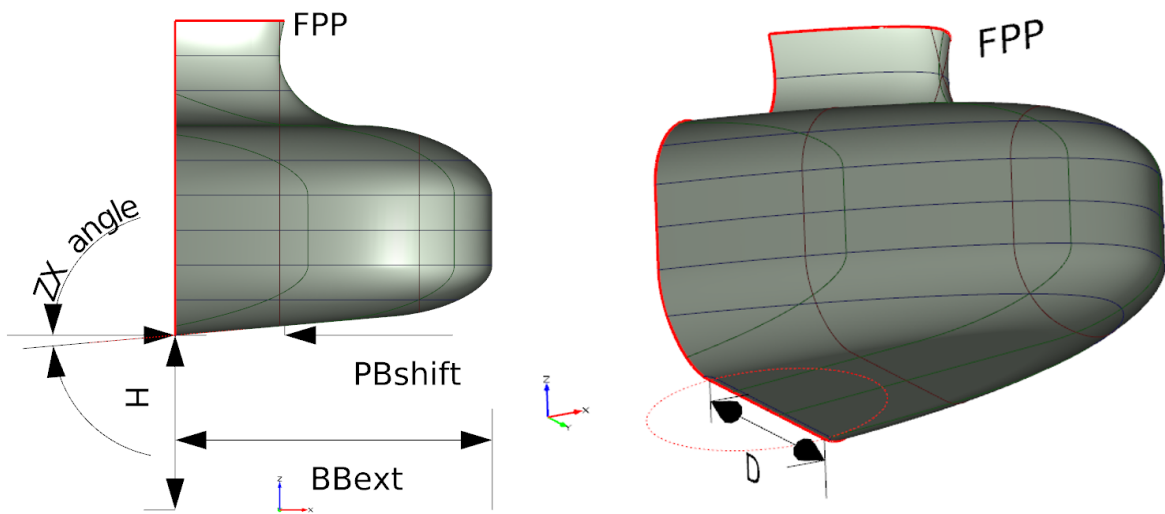


Figure 3.5: Main design variables of the bulb.

3.3.3 Transition

The transition section was designed just to ensure tangency continuity between the parallel midbody and the bulb. Only one design variable is introduced, the tangency factor, controlling the steepness of the tangency connection, which was not explored during the optimisation. The transition section can be seen in Figure 3.6.

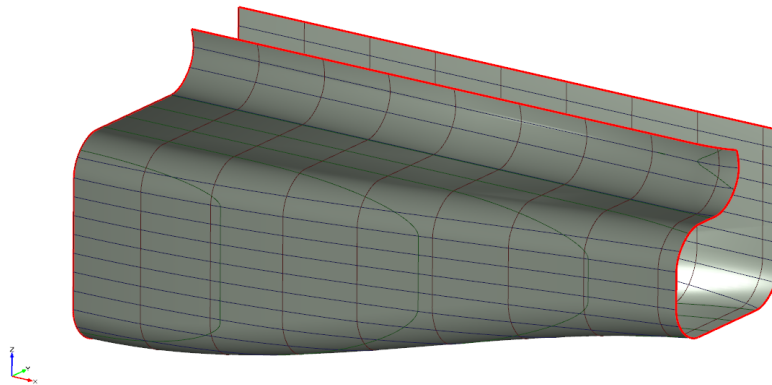


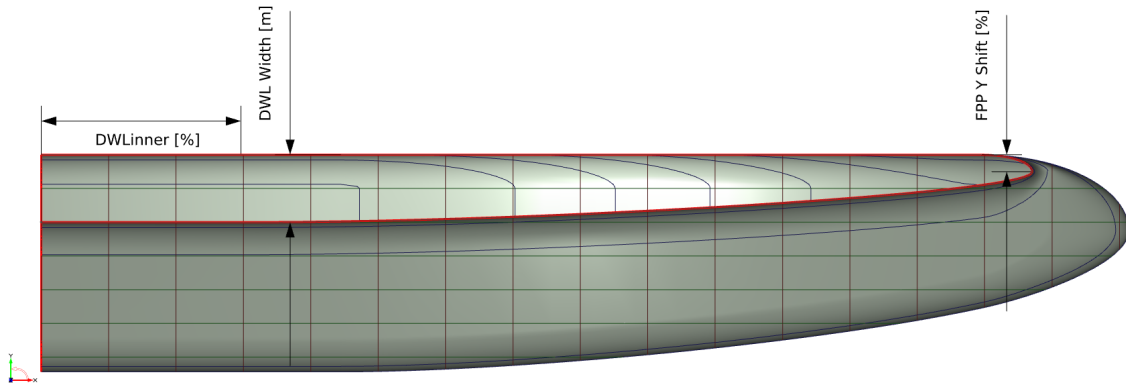
Figure 3.6: The transition between the parallel midbody and the bulb.

3.3.4 Design Waterline

The design waterline (DWL) is of great importance both for the wave resistance and for the seakeeping behaviour. Thus, it became necessary to give flexibility to the waterline shape. This was attempted by controlling the width, the length of the section with constant maximum width and the Y position of the FPP (Forward Perpendicular). The variables introduced are presented in Table 3.4 and Figure 3.7.

Table 3.4: Design variables introduced in the design waterline shape parametrisation.

Design Variable	Lower Bound	Upper Bound	[unit]	Description
W_{DWL}	2	4	m	Maximum width at DWL
L_{DWL}	20	80	m	Length of flat DWL (% of x_{FP})
$y_{FPP_{SHIFT}}$	0	50	%	Y shift of the FPP (% of W_{DWL})

**Figure 3.7:** Variables introduced in the design waterline parametrisation.

3.3.5 Displacement Adjustment

In order to keep a constant targeted displacement during all simulations, a *FBrent* design engine was executed in CAESES® for each design variant.

The algorithm uses Brent's one-dimensional minimisation algorithm to locate the minimum of the functional value within the bounds of a free variable. Basically, it applied a *Golden Section Search* whenever the objective function is "not cooperative" and switches to an iterative parabolic interpolation scheme when the function allows it. The algorithm iteratively isolates the minimum to a fractional precision of about the given tolerance (Friendship Systems AG, 2018).

Typically, as the Brent algorithm varies only one design variable, it is not used for common optimisation tasks as CFD. It is rather utilised for geometric optimisation, such as matching a target distance or displacement, as in this project.

The utilised objective function, ∇_{diff} , minimised to zero by the Brent algorithm was defined as:

$$\nabla_{diff} = (\nabla_t - \nabla)^2 \quad (3.1)$$

with ∇_t is the target displacement and ∇ is the current displacement of the geometry. ∇ can be manipulated by changing the geometry, that in this project was done by adjusting the inner beam, the width of the PM (B_{PM}).

The Brent algorithm was able to converge in less than 10 iterations for any design variant, as long as the boundaries of B_{PM} were adequate, allowing enough variation for displacement matching.

The result can be seen in Figures 3.8 and 3.9, in which each of them has a specific set of design variables, but the LOA and displacement are matched to the short SOV version of Rolls Royce Marine.

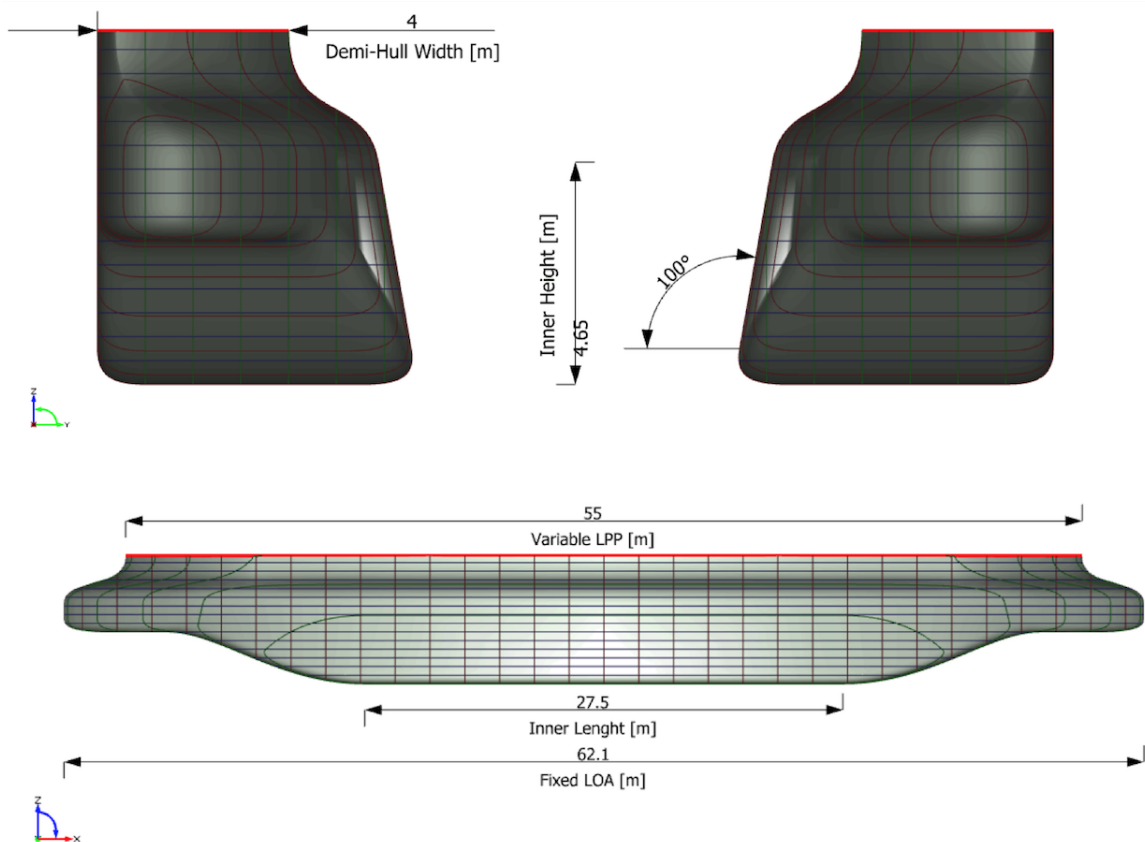


Figure 3.8: A slender demi-hull design variant with high inner height.

A similar adjustment procedure was realised with the bulb extension design variable, BB_{ext} . The LOA was matched to the short monohull SOV, described in Section 3.1.2, by elongating or shortening the bulb for all design variants. This allowed manipulation of the x_{FP} , or LWL (Waterline Length), while still keeping the minimum diameter for the pod base.

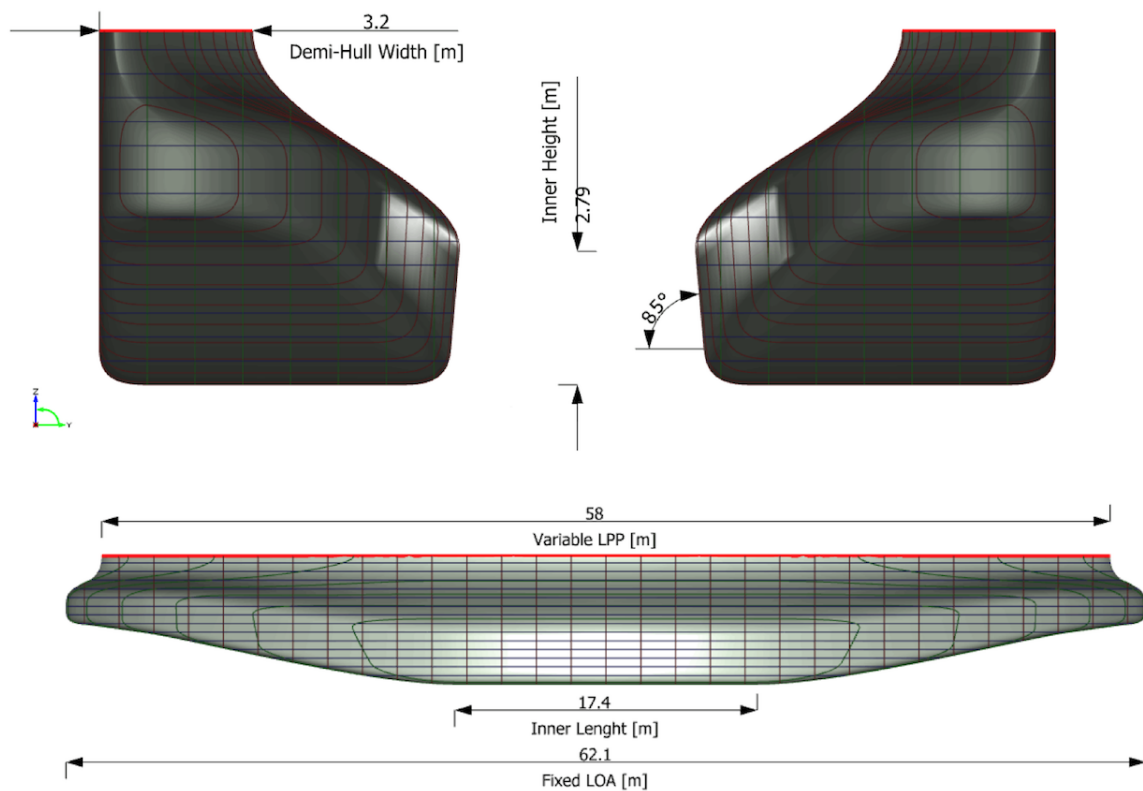


Figure 3.9: A wider demi-hull design variant with low inner height.

3.4 NEWDRIFT+ Mesh Creation

One of the required inputs for NEWDRIFT+ is the penalisation of the geometry below the waterline. CAESES® is able to generate and export mesh panels (.pan) with ease and was also used for this purpose.

A few recommendations were given by the developers in order not to significantly affect the accuracy of the results:

- Obtain, as far as possible, a uniform mesh in terms of panel sizes and aspect ratios;
- Avoid panel overlapping; and
- Obtain the nodal points on knuckle curves to fully capture hullform details.

Following these recommendations, a few different surface modelling options were investigated until finally a stable and reliable mesh was found. From this process, a few more lessons were learned:

- Avoid gaps between two or more panels and miss-aligned panel nodes. NEWDRIFT+ will execute, but when varying the geometry, even a very small variation, the results do not follow a stable pattern;

- Panels far from the water surface do not significantly impact the results. As the number of panels is limited, stretching the panels towards the waterline ensure accuracy with fewer nodes, saving computational time; and
- As NEWDRIFT+ is a based on a linear code and panels that are parallel and close to the waterline might result in convergence issues and errors during calculations, it is recommended to give a small inclination in the outer direction.

To obtain a panel mesh following all these recommendations, the only way encountered for the SWATH geometry was by modelling it as only one surface. This is by far not the most efficient way of modelling a large vessel and, in this project, impacted the overall performance for rendering and displacement adjustment (about 1 minute per design variant in the used system, described in Section 1.5).

In order to decrease computational time without losing accuracy, a mesh convergence study was realised in order to find the best cost-benefit.

It was found that NEWDRIFT+ has a limit of about 600 panels (for 180° heading angle) when using symmetry in both XY and XZ planes, the case in this project. The computational time with a mesh arrangement of 50x12 was about 7 minutes, and the heave RMS result was used as a benchmark for smaller mesh combinations. Along the process, it became clear that reducing the mesh size and stretching it towards the waterline did not significantly alter the results and drastically reduced computational time.

The final mesh utilised in the project can be visualised in Figure 3.10. It was a 38x11, with 418 panels and a 1.35 stretch factor towards the waterline. The calculation time was about 3 minutes and the result difference of 0.4cm heave RMS (0.8% difference) in comparison to the largest acceptable mesh, which took about 10 minutes.

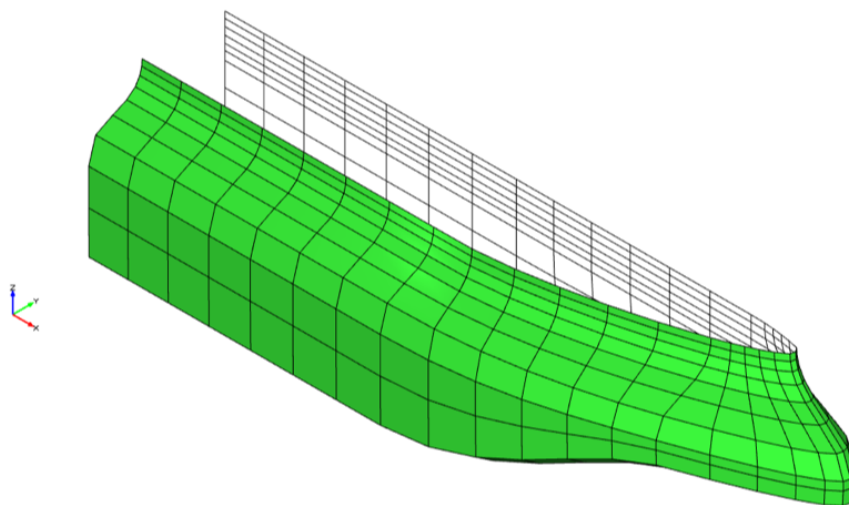


Figure 3.10: Meshing of the modelled surfaces to NEWDRIFT+.

3.5 Sea States Selection

The selection of the sea states was made based on the wave scatter diagram of the German Bight region (*Deutschen Bucht*, in German), as recommended by the involved partner. The region is located along the German coastline between The Netherlands and Denmark. As it can be seen in Figure 3.11, the region is already densely utilised for wind power generation and has many wind farms applied for and in conception, especially further away from the coastline.

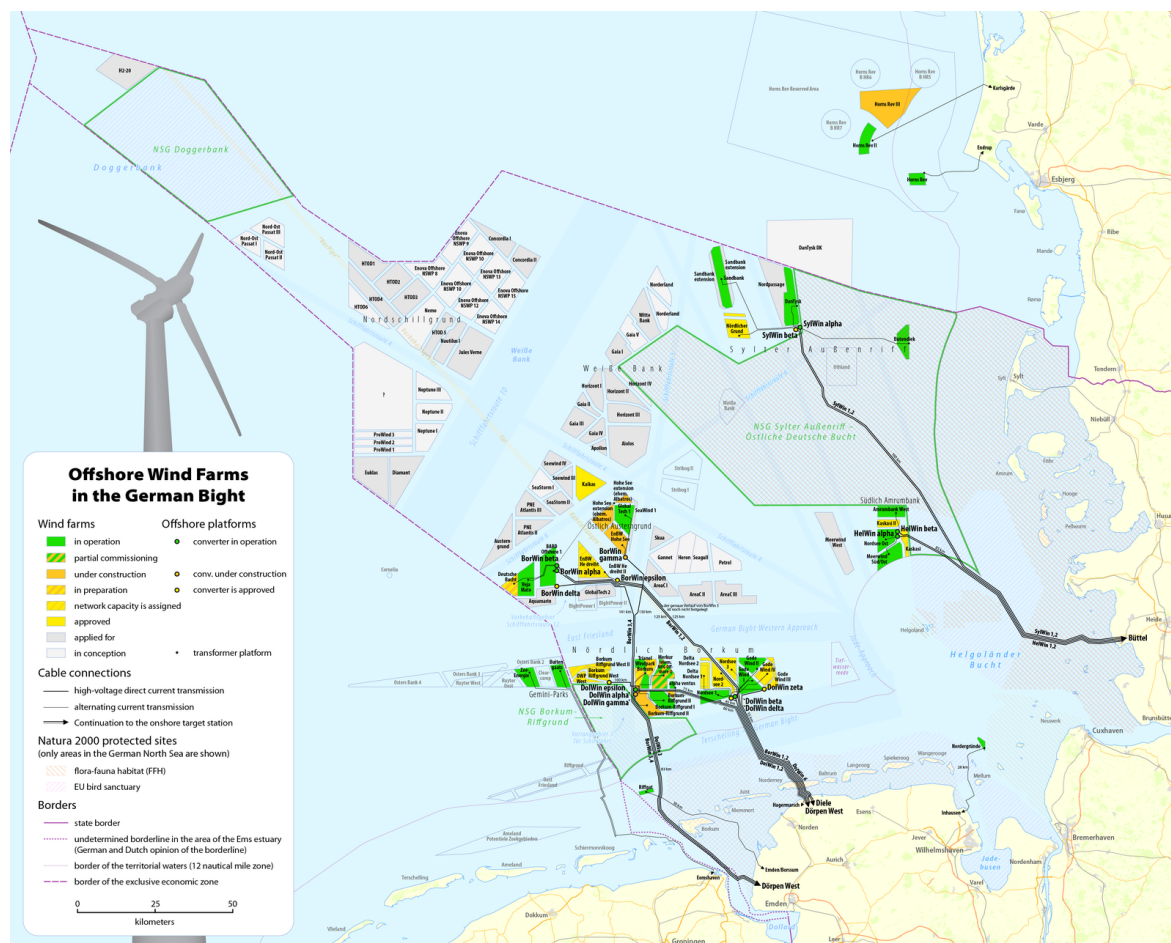


Figure 3.11: Map of offshore wind farms and connecting power cables in the German Bight. By Maximilian Dörrbecker (2018) via Wikimedia Commons.

Based on the wave scatter diagram (Table B.3 in Appendix B), 11 sea states were selected to be simulated, Table 3.5. The selection was based on the highest probability of cable concurrence for each H_S range. The wide range of significant wave height and peak period are to investigate the evolution of the vessels' responses accordingly to the sea spectrum.

The sea spectrum selected for the optimisation of the hull was sea state 7, $H_s = 3.25\text{m}$ and $T_P = 8.5\text{s}$, 180° heading angle (bow waves). Sea state 7 is the most recurrent at the verge of covering 90% of the weather window, as well as the one recommended by the involved parties.

Table 3.5: Selected sea states based on the wave scatter diagram.

Sea State	H_S [m]	T_P [s]
1	0.25	4.5
2	0.75	4.5
3	1.25	5.5
4	1.75	6.5
5	2.25	7.5
6	2.75	7.5
7	3.25	8.5
8	3.50	8.5
9	3.75	8.5
10	4.25	9.5
11	4.75	9.5

Besides the sea state input to NEWDRFT+, it requires how many points to calculate and execute the RMS calculation. The software is smart to concentrate the points around the peak of the spectrum, ensuring that the shape is correctly captured and fewer points are required, reducing computational time.

In this project, 22 points calculated in the spectrum were adequate given the limited computational power, without significant impact in the motion RMS results.

3.6 Body-Fixed Point for Evaluation

Accordingly, to information provided by Rolls Royce Marine, the tower used as the base for the walk-to-work gangway is usually positioned close to the LCB (Longitudinal Centre of Buoyancy) and midship position, minimising roll and pitch interference with heave. The gangway can be up to 30m long, depending on the manufacturer and the model, in order to keep the ship within a safe distance from the wind turbine.

Based on this information, it became agreed to evaluate, use as optimisation objective and compare against the monohull, the heave RMS displacement motion at the connection point between the edge of the gangway and the base of the wind turbine. This point, in this project, was located 5m aft of the LCB, 25m from the ship centreline ($y = 0$) and 15m above the design waterline, as can be seen in Figure 3.12. By this choice, the results were affected not only by heave and roll motions but also by pitch rotation.

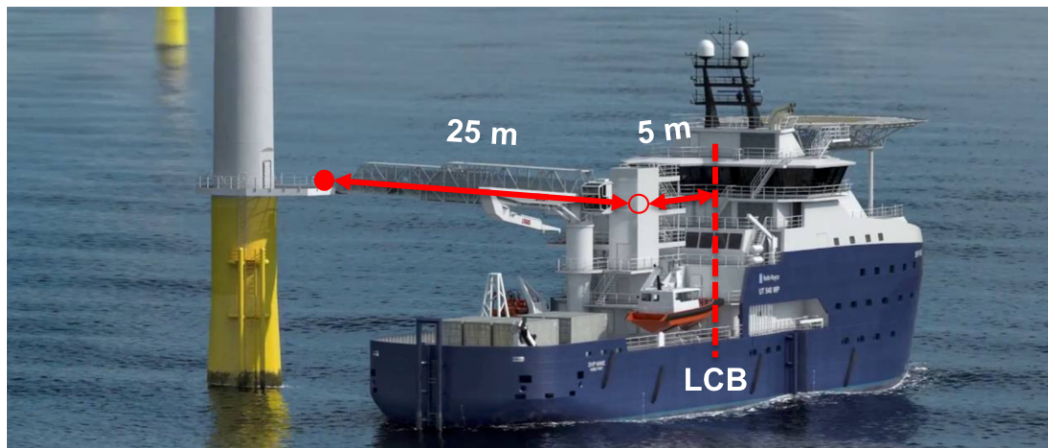


Figure 3.12: Positioning of the body-fixed point for seakeeping evaluation. Adapted from Rolls Royce Marine (2018).

3.7 Simulation Set-Up

CAESES®, besides being a parametric 3D modelling tool, also served as the connection between the geometry, the external software and the results from it. It seamlessly integrates existing simulation packages to create a closed loop (Friendship Systems AG, 2018). This extremely simplified the optimisation process, allowing automated optimisation of the developed geometry once all variables were in place.

In this project, NEWDRIFT+ was connected to the Software Connector of CAESES®, illustrated in Figure 3.13.

The "Input Geometry" contains the panel mesh from the geometry (.pan), the "Input Files" window has the three text files with commands for NEWDRIFT+ (described in Section 2.6 and exemplified in Appendix C). In the middle of the arrangement is the computation executable, "Newdrift_run", that is started automatically during the optimisation process.

The results can be separated in files like spreadsheets (OUT4CAESES.csv, for example), geometries or others, in which CAESES® can reproduce in full, or exact values that are extracted from files in ASCII (American Standard Code for Information Interchange) format ("indat.dat" file, for example).

Result files and values can be used as input to other calculations, graphs generation or any other type of post-processing.

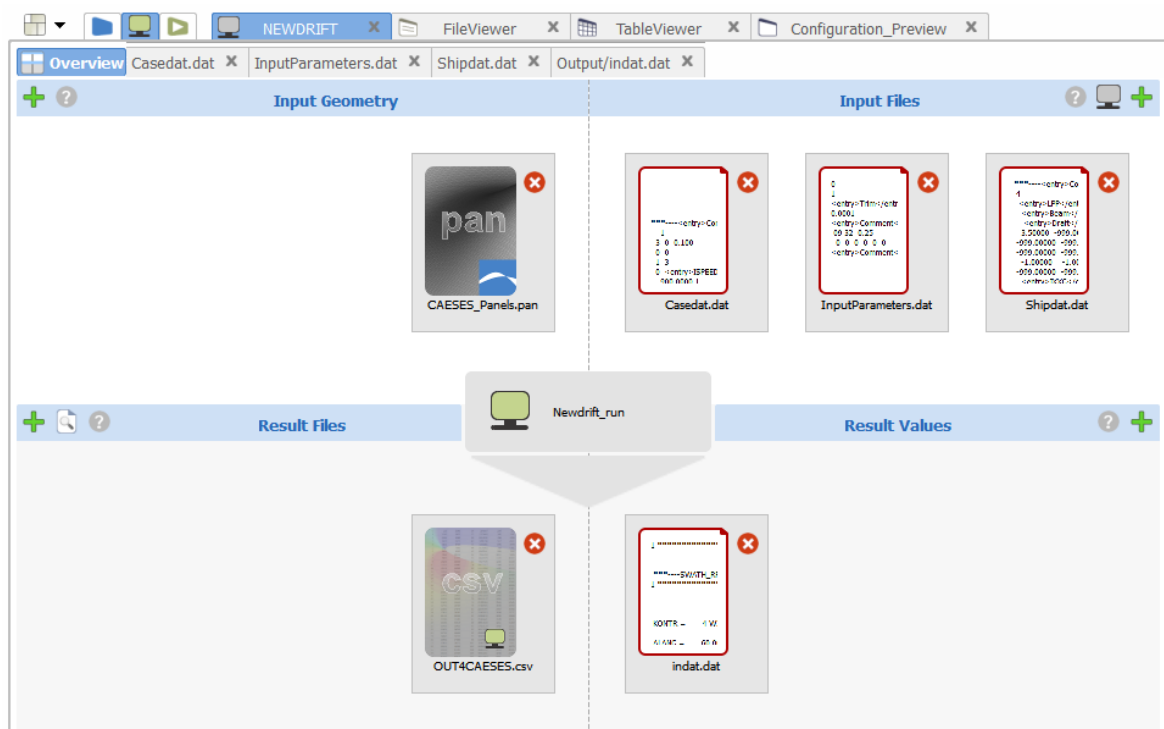


Figure 3.13: NEWDRIFT+ connection window in CAESES®.

3.8 Optimisation Procedure

After executing Sections 3.2 to 3.7, the optimisation process could be started. It was divided into three main parts: identify and eliminate unstable variables of the calculation software; identify relevant design variables and post-iteratively solve for the major optimisation; and finally, investigate the impact and optimise other design variables that have less influence on the geometry. An optional step can be added which is the final fine tuning of the already optimised design with some specific optimisation algorithms.

The whole optimisation chain, including the design loop to remove or re-insert design variables, can be better visualised in Figure 3.14. It is important to note that this process might not be adequate for other optimisation problems, especially if a different software for computations is to be used.

3.8.1 Single Variable Investigation

The first part of the optimisation was used to consolidate the seakeeping calculation set-up, investigating the stability of the results with small variations of single design variables and testing their upper and lower bounds. It also aided to identify the design variables with higher impact in the geometry and the results. The result evaluated was the heave RMS displacement in the design sea state ($H_s = 3.25\text{m}$ and $T_P = 8.5\text{ s}$).

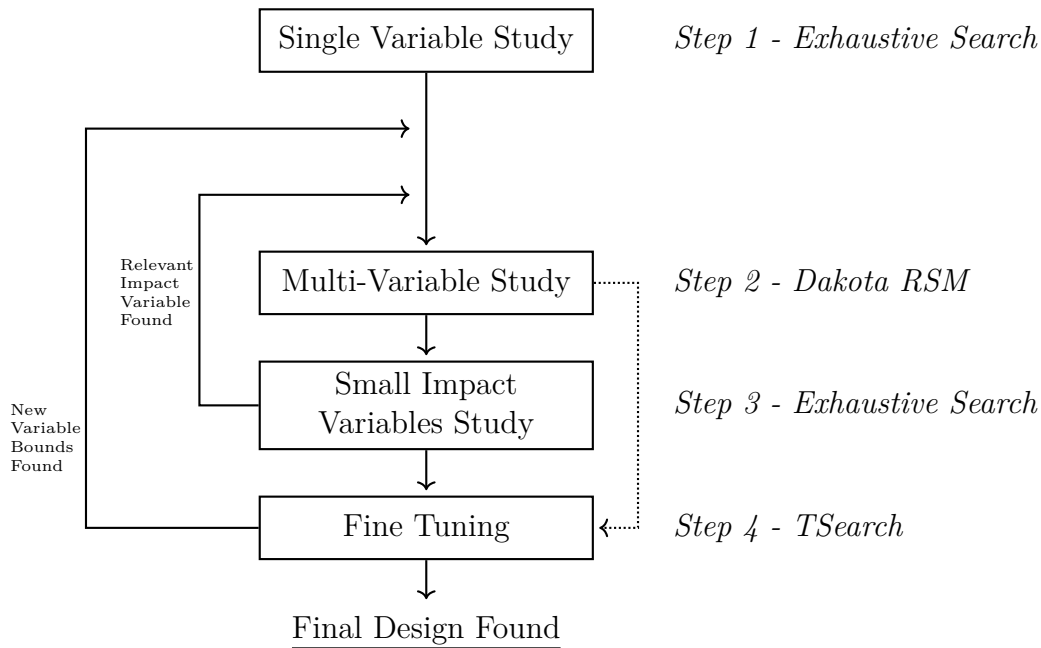


Figure 3.14: Optimisation structure followed in this project.

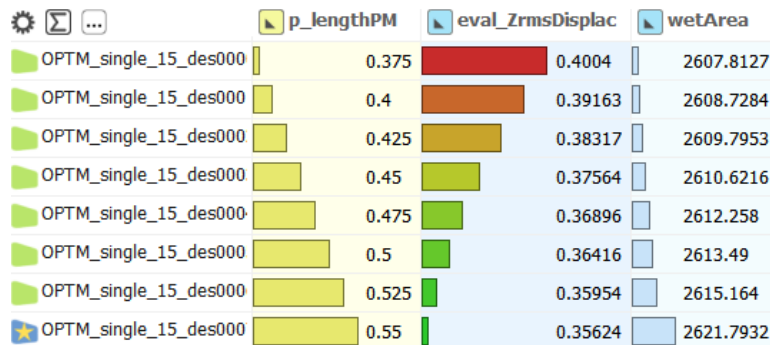


Figure 3.15: Small variations of L_{PM} and the resulting heave RMS motion.

The main single design variables evaluated were: x_{FP} , T_D , L_{PM} , H_{IN} , $y_{H_{SHIFT}}$, BB_{EXT} , W_{DWL} and L_{DWL} . One example was the investigation of L_{PM} , Figure 3.15.

This step of the process was rather time-consuming before a mesh that yielded consistent results was reached. Once the reliable mesh was developed, the one presented in Section 3.4 and Figure 3.10, NEWDRIFT+ proved to be very stable for single variable variations, allowing to proceed to the next step without further problems.

3.8.2 Multi-Variable Optimisation

For the optimisation of flow-exposed products, CAESSES® offers a set of strategies that allow for the automation of the intelligent design creation process. Design variables were linked to the variable geometry through parametric modelling and controlled by algorithms, design engines (Friendship Systems AG, 2018).

One of the advanced strategies included in CAESES® is the optimisation package, Dakota. In particular, so-called Response Surface Methods (RSM), i.e. approximation models of an expensive high-fidelity model. This method proved to be the most effective in optimising the SWATH SOV hullform.

First, it was necessary to select the design variables that most impact the sea-keeping performance found in the previous step, Section 3.8.1. The simulation was of single type objective, focusing on the optimisation of heave motions. Although the method allows it, no constraints were necessary and imposed in the set-up.

The amount of initial samples recommended is 5 times the number of design variables, but in the final run, 300 designs were generated through the Sobol (quasi-random homogeneous filling of the design domain) algorithm and used as input to the Dakota RSM method. This methodology of optimisation also allowed the calculation of multiple design variants at the same time.

With the results of the Sobol, Dakota generated the RSM and iterated the last design variants to find the best possible combination of the design variables. The process can be better understood in Figures 3.16 and 3.17.

Attribute	Active	Active	Active	Active	Objective	
Name	p_lengthPM	p_lengthDWL	a_beamInnerflareYZ	columnWidth	eval_ZrmsDisplac	wetArea
Scope	00PARAMETERS	00PARAMETERS	00PARAMETERS	00PARAMETERS	14NEWDRIFT EVAL	10HYDRO
Reference						
Lower Bound	0.20111554	0.051694783	0.0015259255	2.0044543	0.36727	2611.6109
Upper Bound	0.49994507	0.49892968	9.9791478	3.1999634	0.58148	2818.018
Feasible Designs: 100 %						
Mean Utilization Index						
Mean	0.35742007	0.28296486	4.7552738	2.6297309	0.49397437	2720.1415
Sample Standard Deviation	0.090568387	0.13162029	3.0165414	0.36247466	0.047821803	53.609091
Error-free: 100 %	100 %	100 %	100 %	100 %	100 %	100 %
OPTM_dak_18_des000i	0.26561225	0.40418847	2.4319122	2.1061317	0.5591	2775.707
OPTM_dak_18_des000j	0.30831046	0.48661112	5.2164641	3.109374	0.45631	2621.8953
OPTM_dak_18_des000k	0.41506918	0.41550656	6.0097851	2.3985893	0.51545	2738.0488
OPTM_dak_18_des000l	0.25443684	0.24802977	1.5084592	3.1364462	0.47191	2651.6501
OPTM_dak_18_des000m	0.2050207	0.44546115	9.948513	2.7937868	0.56003	2675.1786
OPTM_dak_18_des000n	0.48001373	0.060975308	7.0410825	2.3782415	0.48761	2785.1241
OPTM_dak_18_des000o	0.21271465	0.37976883	5.4246624	2.9970855	0.5181	2651.8184
OPTM_dak_18_des000p	0.21143849	0.051694783	3.9134631	2.593778	0.53977	2749.9729
OPTM_dak_18_des000q	0.32122954	0.26526604	6.647857	2.159351	0.53134	2785.5016
OPTM_dak_18_des000r	0.43731337	0.19520915	7.8436782	3.1814055	0.41321	2662.5342
OPTM_dak_18_des000s	0.40529391	0.39604861	3.6054855	2.2224985	0.52275	2763.8301
OPTM_dak_18_des000t	0.29078734	0.35751319	5.7844054	2.6592262	0.52659	2704.331
OPTM_dak_18_des000u	0.48799338	0.21517364	9.2256841	2.8061696	0.45352	2713.3318
OPTM_dak_18_des000v	0.41738256	0.14704365	2.6746393	2.7528097	0.47129	2721.8881
OPTM_dak_18_des000w	0.40286676	0.3509824	7.1970369	2.3249967	0.51676	2756.2914
OPTM_dak_18_des000x	0.33080756	0.37512255	3.0047919	2.4714972	0.52943	2728.4613
OPTM_dak_18_des000y	0.32645985	0.071130511	6.2504198	2.4441349	0.51801	2769.7281
OPTM_dak_18_des000z	0.46988019	0.31909362	5.319005	2.5257385	0.48321	2733.5619
OPTM_dak_18_des001a	0.23795251	0.30607191	3.6687683	3.1564756	0.47789	2640.3148
OPTM_dak_18_des001b	0.42909287	0.39248809	0.33308453	2.8824543	0.44452	2671.159
OPTM_dak_18_des001c	0.32460485	0.1086997	1.3492846	2.3737077	0.51912	2772.4155

Figure 3.16: Sobol quasi-random homogeneous filling of the design domain, base for generation of the response surface.

	p_lengthPM	p_lengthDWL	a_beamInnerFlareYZ	columnWidth	eval_ZrmsDisplac	wetArea
OPTM_dak_18_des013	0.49688651	0.22433595	9.8863151	3.159501	0.40245	2666.108
OPTM_dak_18_des0231	0.49288659	0.42650345	8.3410498	3.0842607	0.40153	2644.2672
OPTM_dak_18_des015	0.4293316	0.46540351	4.6340141	3.176359	0.39477	2619.5086
OPTM_dak_18_des006	0.47308473	0.34454038	5.0873121	3.166159	0.39101	2641.4698
OPTM_dak_18_des023	0.45782795	0.4629458	1.7516402	3.1379909	0.38967	2625.3113
OPTM_dak_18_des0251	0.49663076	0.44525895	0.24536882	3.198352	0.36799	2621.6813
OPTM_dak_18_des0252	0.49811396	0.43804895	0.24536882	3.198352	0.36797	2622.8373
OPTM_dak_18_des0253	0.49811396	0.43804895	0.081179235	3.198352	0.36785	2622.8837
OPTM_dak_18_des0254	0.49976196	0.43704642	0.057069613	3.198352	0.36743	2623.2066
OPTM_dak_18_des0255	0.49976196	0.43804895	0.081179235	3.198352	0.36741	2623.0473
OPTM_dak_18_des0256	0.49976196	0.43631855	0.057069613	3.1996704	0.36741	2623.129
OPTM_dak_18_des0257	0.49976196	0.43475295	0.015869625	3.1996704	0.36733	2623.3803
OPTM_dak_18_des026	0.49994507	0.43414869	0.0015259255	3.1996704	0.36733	2623.4662

Figure 3.17: Final iterations of the Dakota algorithm, converging to the final solution.

This phase of the optimisation was the most time consuming, as it was executed multiple times and in total evaluated more than 1000 design variants along the development of the project.

The final run had 7 design variables that highly impacted the results. These were: x_{FP} , T_D , L_{PM} , H_{IN} , yH_{SHIFT} , W_{DWL} and L_{DWL} . Most of them were identified in the first step of the optimisation process (3.8.1), but a couple of them were only discovered in step 3, Section 3.8.3, creating the loop of selecting relevant design variables during the optimisation process (visible in Figure 3.14).

3.8.3 Small Impact Variables Investigation

Since the beginning of the project, it was expected that some design variables would have almost no impact in the seakeeping performance. This was confirmed by a number of reasons found during the development. Firstly, because the mesh could not be fine enough to capture exact curvatures and its variations. Secondly, as mentioned in Section 3.4, the parts of the geometry far from the waterline, the lower bilge, for example, have a very low impact in the seakeeping performance.

In any case, almost all design variables were investigated in this phase (those that were not included before). Most of them resulted in no performance impact (i.e. bilge fullness, bilges height and width, transition tangency, bulb fullness), but along the process, a couple of variables, W_{DWL} and L_{DWL} , were found to be important for the evaluation and were included in the multi-variable optimisation step. These two design variables describe the shape of the waterline, which proved to be very important for the seakeeping performance.

The re-introduction of the design variables, in step 2 of the optimisation process, created a design loop that acted as a design variables selector. It was essential to execute this process in order not to miss any relevant design variable.

This step can be skipped once there are no more variables to investigate, after one execution of the final tuning, for example.

3.8.4 Fine Tuning Algorithms

After executing the multi-variable optimisation, it is still possible to further optimise a design. CAESES® offer that possibility with a few different inbuilt design engines.

One of them is part of the Dakota package, the local optimisation method. It is a gradient-free local optimisation strategy to further optimise an existing good result, the one obtained in step 2 (Section 3.8.2), for example.

Another option is the *FTSearch* design engine. The tangent search method is a reliable solver for small scaled, single-objective optimisation problems. It uses exploratory moves to detect the descent direction in the solution space, ensuring fast improvement of the results (Friendship Systems AG, 2018). This method proved to be the most efficient for fine tuning in this project, being able to reduce further 0.9cm heave RMS (about 2.5% improvement) from an already good design. An illustration of the algorithm working can be seen in Figure 3.18.

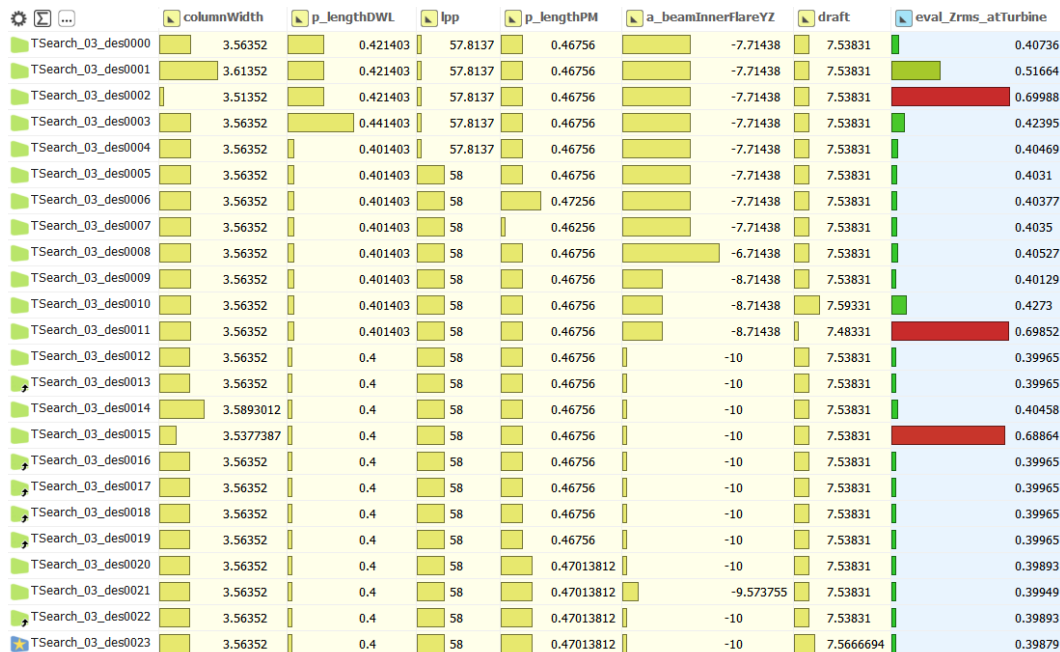


Figure 3.18: Iteration process of the TSearch algorithm, converging to the final solution.

In Figure 3.18 it is easy to identify the exploratory moves made by the algorithm in the first iterations. It is also possible to notice that some of the design variables are set to the bounds (x_{FP} and y_{SHIFT}), indicating that the RSM from the DAKOTA algorithm did not totally identify the solution. In that case, step 2 was re-executed with the newly set bounds.

It can also be seen that it took less than 25 iterations to converge to a final solution, less than one hour of computation. For these reasons, the execution of a final tuning of the design variant with specific algorithms for it is highly recommended.

3.9 Further Design Investigation

The geometry described in Sections 3.2 and 3.3 does not exactly followed the traditional SWATH hull forms. It is, with no doubt, an innovative approach to an existing type of vessel. From now on, for Chapters 4 and 5, this design will be called SWATH SOV with asymmetric demi-hull because the demi-hulls are mirrored, symmetric between each other, but asymmetric to its own demi-hull centreline.

The main challenge with the asymmetric SWATH SOV was that none of the available software for resistance calculation, in their current version (SHIPFLOW, ν -Shallo, Michlet), could handle the geometry, including SHIPFLOW Motions that could be a great tool for validation of NEWDRIFT+ results and even optimisation.

On the other hand, traditional SWATH vessels have symmetric demi-hulls in relation to its own centreline. This affirmation includes all vessels mentioned in Section 2.3, including the ones under development, with the exception of the CSS design by VARD. This triggered the question: why has everyone done it this way?

To answer the question, a further design investigation of a SWATH with symmetric demi-hulls was developed. It was rather simple to modify the existing design and the only variable completely eliminated was the yH_{SHIFT} , which was set to 0%, a totally vertical flat of side. To simplify even more, a few design variables were kept the same as the asymmetric SWATH variant, including the draught, bilge sizes and thruster sizes, eliminating variables that could prejudice the comparison. It is important to remind that LOA and displacement were also matched to the short SOV monohull version. The resulting geometry is visualised in Figure 3.19.

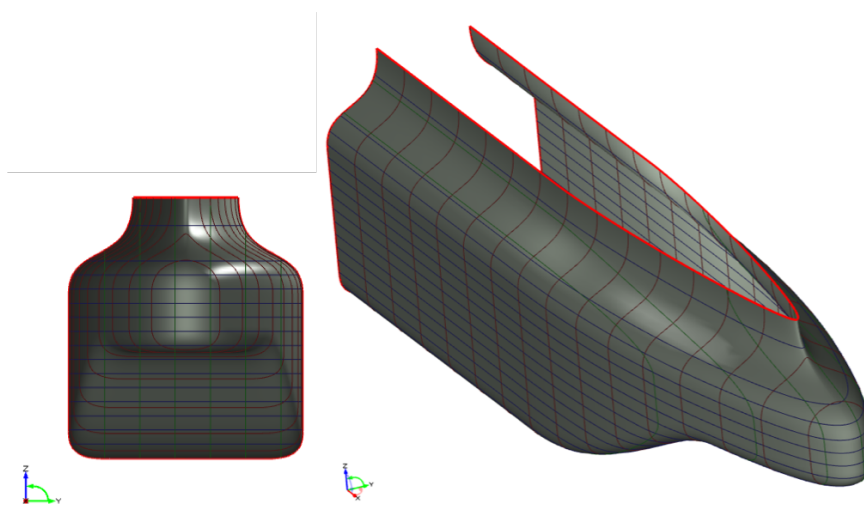


Figure 3.19: Symmetric demi-hull SWATH hull variant.

This SWATH hull form design was also optimised by the same methodology used for the asymmetric demi-hull, and compared to both monohulls and the optimised asymmetric demi-hull SWATH.

3.10 Post-Processing

Comparing the heave RMS displacement (at the connection point the gangway and the base of the wind turbine) between two vessels is a good start and possibly enough for the first design and optimisation of a SWATH SOV.

Another way of obtaining interesting insight from compared vessels is to analyse the RAO (Response Amplitude Operator) of each of them. These transfer functions translate the effect of the sea state on the vessels, allowing to find the wavelength (encounter frequency or wave frequency) that contains the largest amount of heave energy transference, for example. It was also a good optimising tool, indicating how changes in the geometry alter the transfer function and assists in finding the right optimisation direction.

Beyond that, it would be interesting to compare station keeping capabilities and requirements of such a vessel, being one of the ideas from the beginning of the project.

The problem with DP (Dynamic Positioning) capability plots is that to obtain it, it is necessary to have the propulsion system efficiency, which is available for the monohull, but is unknown for the design SWATH. For this reason, this comparison method was discarded but substituted.

In order to have a more insightful understanding of the differences between monohull and SWATH SOVs, another type of comparison based on DP polar plots was executed. It uses the output of drift forces and moments from NEWDRIFT+ to generate polar plots. These forces are F_X , F_Y , F_Z , which represent surge, sway and heave motions, respectively. The moments are M_X , M_Y , M_Z , representing rolling, pitching and yaw motions, respectively. For each heading angle (simulated in steps of 10°), the RMS of forces and moments are extracted and used to generate the polar plot. Every point calculated in the spectrum has one set of forces and moments, 22 points were utilised in this project.

It is important to notice that NEWDRIFT+ is not validated for SWATH vessels and is only validated for head and quartering seas for monohulls. For this reason, part of the results might not entirely represent the reality, although NEWDRIFT+ results presented a logically acceptable behaviour in all cases.

These three comparison possibilities, heave RMS, RAOs and body excitement forces and moments polar plots were the base for the comparison and the organisation of the results.

This page was intentionally left blank.

4 Results and Comparison

This chapter is initiated with a presentation of both optimised SWATH vessels, including the design variables and basic hydrostatics characteristics. Following are results of the seakeeping evaluation for the four compared vessels: the 82m monohull, the 62m monohull, the asymmetric demi-hull SWATH and the symmetric demi-hull SWATH.

The results are divided in three parts:

1. Heave RMS at body-fixed point (described in Section 3.6) in different environments and sailing characteristics;
2. RAOs (Response Amplitude Operators) of different motions and sailing characteristics;
3. A comparison of wave drift RMS forces and moments for sea state 7.

Finally, a section about the identified design pattern during the optimisation process towards lower heave motions. Before starting, it is important to note that a few assumptions that were made during the evaluations and a remark about seakeeping codes based on linear solvers.

- *Design Variables*, even though the built model is highly flexible in terms of shapes, a few design variables were fixed, or yet unknown, or unnecessary at this stage of the project. These were assumed to be constant for both SWATH models during the optimisation process:
 - $B = 20$ m, in order to maximise the limiting vertical centre of gravity;
 - $H_{POD} = 3$ m, approximated value for a AZ-PM 2600 Rolls-Royce permanent magnet thruster, with margin;
 - $D_{POD} = 2.4$ m, approximated value for a AZ-PM 2600 Rolls-Royce permanent magnet thruster;
 - $\alpha_{POD} = 0^\circ$, assuming that the thruster itself would be inclined, not the hull form;
 - $xPB_{SHIFT} = D_{POD}$ assuming a shift of one propeller diameter to be reasonably far from the outermost part of the vessel;
 - $yFPP_{SHIFT} = 40\%$ assuming to be a reasonable value for a slender waterline shape, but not overly sharp;
 - bilge sizes are equal for both optimised SWATH variants: lower width = 1m; lower height = 0.75m; upper width = 1m; and upper height = 1.75m (ensuring that it is located bellow wave valleys).

- *Initial \overline{GM}_T* (transverse metacentric height), \overline{GM}_{T0} , each design variant of the SWATH hulls has a different vertical centre of gravity limit, for that reason, it was set an initial \overline{GM}_T for all design variants of 1.2m (value recommended by the involved partner), including for the monohull simulations. This was realised in an attempt to remove one more "unknown" variable of the calculations, the real vertical centre of gravity of the vessels;
- *Geometry radius of gyration*, the calculation of the radius of gyration for the SWATH vessel was simplified to the values recommended by SAWE (2009), and the radius of the product of inertia was assumed to be equal to zero. This might have small impacts on the results, and should be taken into account in a future version of this project.

It is well established that seakeeping codes based on linear theory succeed extremely well for ship design purposes, such as NEWDRIFT+. But it has also been recognised that the linear model is restricted by its fundamental assumptions of small wave heights and small motion amplitudes (St. Denis, 1974). Papanikolaou (1984) elaborates, affirming that a vessel sailing in a real sea of even moderate severity moves in ways that could never be described by a linear model. For this reason, Liu and Papanikolaou (2012) developed hybrid methodologies that result in excellent agreement with model tests for monohulls and semi-submersible hull forms. These include corrections for hulls with flare at the waterline, small wave amplitudes and even the evaluation of the hull shape above the waterline. Some of these methodologies are included in NEWDRIFT+, increasing the accuracy of the linear solver for small wave lengths, for example.

In this project, unstable behaviour of the linear solver was encountered for long wave lengths at the heave RAO of the SWATH vessels. But as it was rather far from the peak of energy of the sea spectrum and the evaluated objective was the RMS of heave results, it was assumed to be of small importance and ignored for the time being.

4.1 Optimised SWATHs

First and foremost, it is important to remind that two SWATH vessels were optimised along this project. The first one, following the recommendation of the interested partner, the outer part of the hull is totally flat until the deck level. This results in an asymmetric demi-hull in relation to its own centreline. This version of the SWATH is here called "Asymmetric SWATH" even though its demi-hulls are symmetrically mirrored. The second optimised SWATH is here called "Symmetric SWATH", a variation described in Section 3.9.

Figure 4.1 presents the optimised version of the asymmetric SWATH. It can be seen that the optimal design has a short bulb, long parallel midbody, with a slightly lower an inclined inner flat of side (8.8°). The optimal design variables for both SWATH variants are presented in Table 4.1.

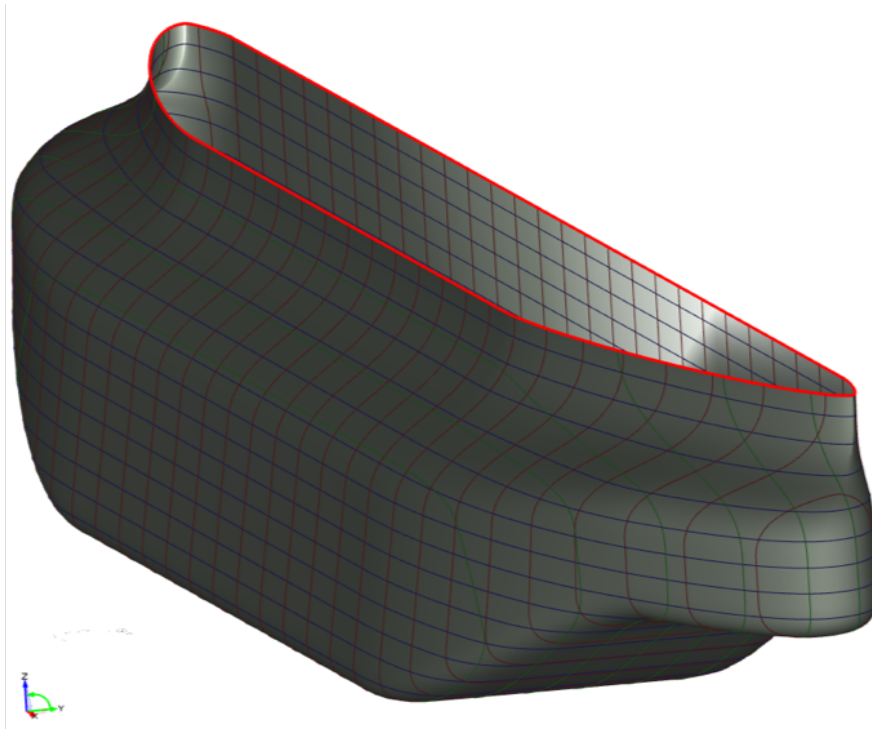


Figure 4.1: Optimised asymmetric demi-hull SWATH variant.

Table 4.1: Optimal design variables reached for both SWATH vessels.

Design Variable	Asymmetric SWATH	Symmetric SWATH	[unit]	Description
x_{FP}	56.92	55.00	m	Length between perpendiculars
T_D	7.40	7.40	m	Draught
L_{PM}	43.30	50.00	%	Length of the PM (% of x_{FP})
B_{PM}	41.74	54.98	%	Width of the PM (% of B)
H_{IN}	83.67	100	%	Height of the inner side (% of T_D)
yH_{SHIFT}	-8.81	0.00	°	Y shift of the upper inner width
BB_{EXT}	24.60	64.68	%	Bulb extension (% of D_{POD})
W_{DWL}	3.74	2.96	m	Maximum width at DWL
L_{DWL}	50.23	53.33	m	Length of flat DWL (% of x_{FP})
\overline{KB}	3.63	3.58	m	Vertical centre of buoyancy
\overline{KM}_T	9.93	6.67	m	Limiting vertical centre of gravity ($\overline{GM}_{T0} = 0$)
W_S	2375	2376	m ²	Hull wetted surface area

As it can be noted from Table 4.1, the differences are significant, except for the beam and draught, which were set equal to the optimised asymmetric SWATH, removing further design variables of the comparison.

The asymmetric variant features a smaller, shorter bulb design and inclined inner flat of side, resulting in a slightly lower vertical centre of buoyancy. It also features a wider and longer constant waterline, yielding a higher \overline{KM}_T and stability capability.

4.2 Heave RMS

This section compares the results of all four vessels (long monohull, short monohull, asymmetric SWATH and symmetric SWATH) separated into three different areas of investigation: different sea states, heading angles and sailing speeds. The main evaluated result, the design objective, was the heave RMS at the base of the wind turbine, illustrated in Figure 3.12. Note that the long monohull is 20m longer and has about 25% more displacement than the other three compared vessels.

4.2.1 Sea States

By evaluating the optimised SWATH designs against the monohulls by sea state, it was possible to recognise which sea conditions are beneficial or not. It is important to remember that the optimisation of both SWATH vessels was realised in sea state 7 ($H_S = 3.25\text{m}$ and $T_P = 8.5\text{s}$).

The results for heading angle 180° and 0kn sailing speed are presented in Table 4.2 and Figure 4.2, which provides a better visualisation of the numbers. For the markers, read the lines with squares are monohulls, triangles are asymmetric SWATH, circles are the symmetric SWATH, black filling are for similar displacement and LOA, and white filling are for different LOA and displacement (long monohull only).

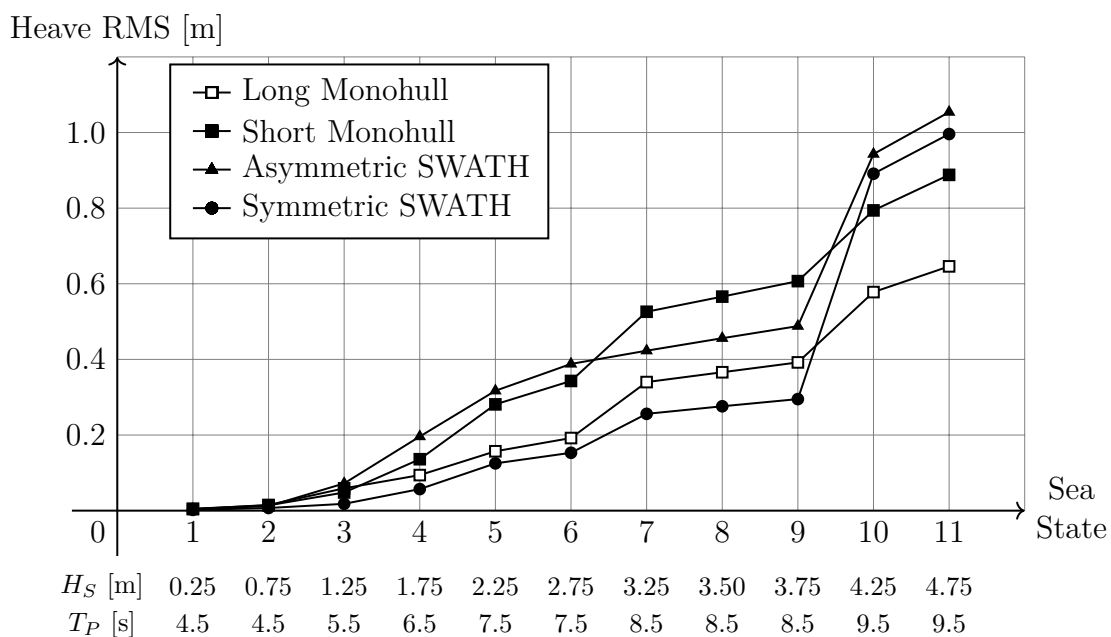


Figure 4.2: Heave RMS development with sea state for the 4 compared vessels.

Table 4.2: Heave RMS results for different sea states, 180° heading, 0kn speed.

Sea State	H_S [m]	T_P [s]	Heave RMS [m]			
			Long Monohull	Short Monohull	Asymmetric SWATH	Symmetric SWATH
1	0.25	4.5	0.004	0.005	0.004	0.002
2	0.75	4.5	0.015	0.014	0.012	0.007
3	1.25	5.5	0.059	0.048	0.072	0.018
4	1.75	6.5	0.094	0.136	0.196	0.057
5	2.25	7.5	0.157	0.281	0.317	0.125
6	2.75	7.5	0.192	0.343	0.388	0.153
7	3.25	8.5	0.340	0.526	0.423	0.256
8	3.50	8.5	0.366	0.566	0.456	0.276
9	3.75	8.5	0.392	0.607	0.488	0.295
10	4.25	9.5	0.578	0.794	0.943	0.891
11	4.75	9.5	0.646	0.888	1.054	0.996

By observing Figure 4.2, the expected difference between the monohulls can be verified, the longer and heavier one has superior seakeeping abilities than the short variant. The introduction of the SWATHs to the picture mixes the results. The first noticeable difference is that the SWATH designs are under disadvantage when T_P is over 9s. Secondly, the optimised asymmetric SWATH has superior performance compared to the short monohull, but only in when $8s < T_P < 9s$, approximately. Meanwhile, the symmetric demi-hull SWATH has superior behaviour compared to all other vessels in sea states with $T_P < 9s$. Finally, it can be seen by the slope of lines that heave RMS results, for all vessels, are mainly dependent of the peak period of the spectrum, while the significant wave height only scales the results.

4.2.2 Heading Angle

Heading angle variations were executed for all vessels in sea state 7 ($H_S = 3.25m$ and $T_P = 8.5s$). The results can be seen in Figure 4.3 and its reference numbers in Table B.1, Appendix B.

What can be observed in Figure 4.3 is that the symmetric SWATH has superior capabilities in any heading angle compared to any other vessel. The asymmetric counterpart is in a tight position being superior only in head and quartering seas to the short monohull. It is also interesting to note that the long monohull actually performs worse than the short monohull in beam seas, which could be justified for being a longer vessel.

It is important to mention that the monohulls have the lowest heave RMS motion at approximately 20° heading angle, which is not included in Figure 4.3.

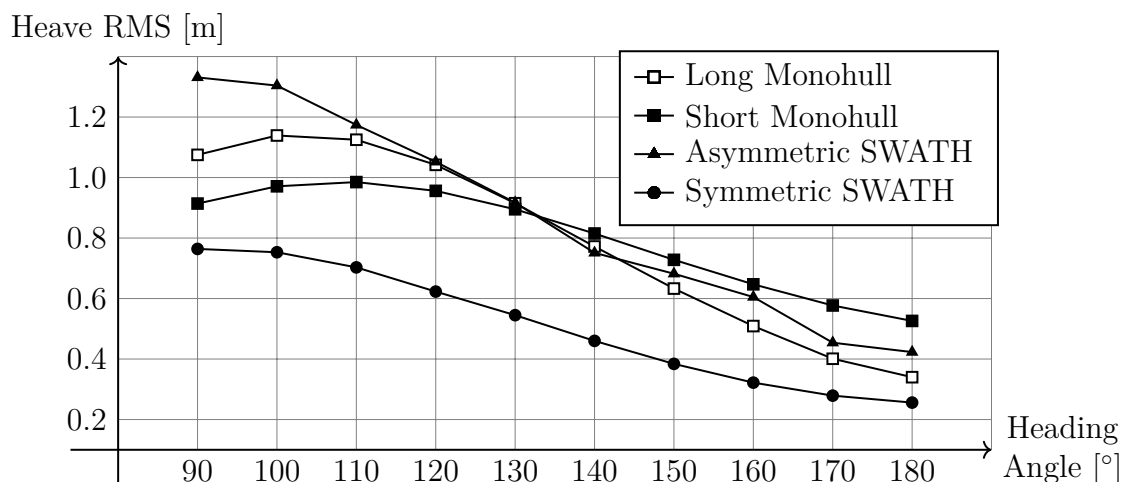


Figure 4.3: Heave RMS development with heading angle for 4 compared vessels in sea state 7 ($H_S = 3.25\text{m}$ and $T_P = 8.5\text{s}$).

4.2.3 Speed Investigation

The speed investigation was inspired by the vast utilisation of SWATH vessels as fast passenger transport, such as ferries and CTVs. The results of the investigation can be seen in Figure 4.4 and its reference values in Table B.2, Appendix B.

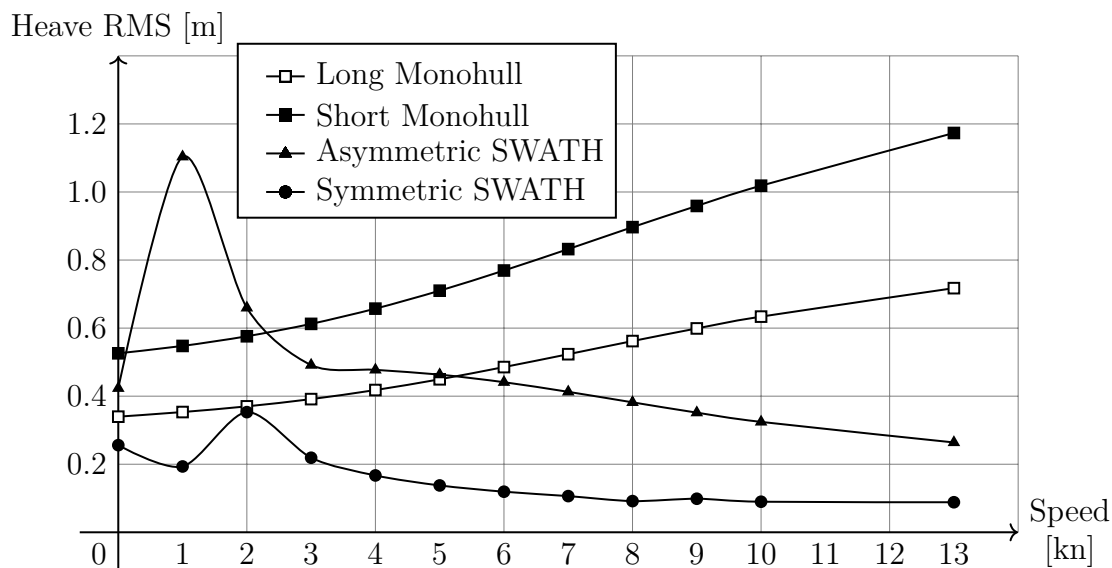


Figure 4.4: Heave RMS development with speed for 4 compared vessels in sea state 7 ($H_S = 3.25\text{m}$ and $T_P = 8.5\text{s}$).

The first observation that can be made in Figure 4.4 is that both SWATH vessels have oscillating performances in slow speeds, smaller than 3kn. This oscillation stabilises and slowly decreases heave RMS results with increasingly sailing speed. The same does not occur for monohulls. It can clearly be seen that the heave motion only increases with speed for both monohulls.

4.3 Response Amplitude Operators

Response amplitude operators (RAOs) are the source of calculation of the heave RMS. Nevertheless, it is still important to analyse the shape of it so that further insight about the behaviour in different wave conditions (length or period) in one sea state can be obtained. The results presented are for sea state 7 ($H_S = 3.25\text{m}$ and $T_P = 8.5\text{s}$) and 0kn sailing speed.

Starting with 180° heading angle, bow seas, two main RAOs can be obtained from NEWDRIFT+: heave and pitch. The solver is currently not able to calculate viscous effects for multi-body arrangements, resulting in zero roll, sway and yaw motions for 180° heading angle. For now, surge was excluded from the comparison due to its negligible coupling with heave, a discussion is presented in Section 4.4.

Figures 4.5 and 4.6 presents RAOs of the four compared vessels for heave and pitch, respectively, with the wavelength by LOA ratio in the x axis in order to adjust the long monohull length difference. For reference, having the peak wave period of about 8.5s in deep water means that the energy of the wave system is concentrated in waves with about 100m wavelength (approximately 1.2 and 1.6 λ/LOA ratio for an 82m and 62m long vessels, respectively), and higher values in the y axis represent higher motion responses.

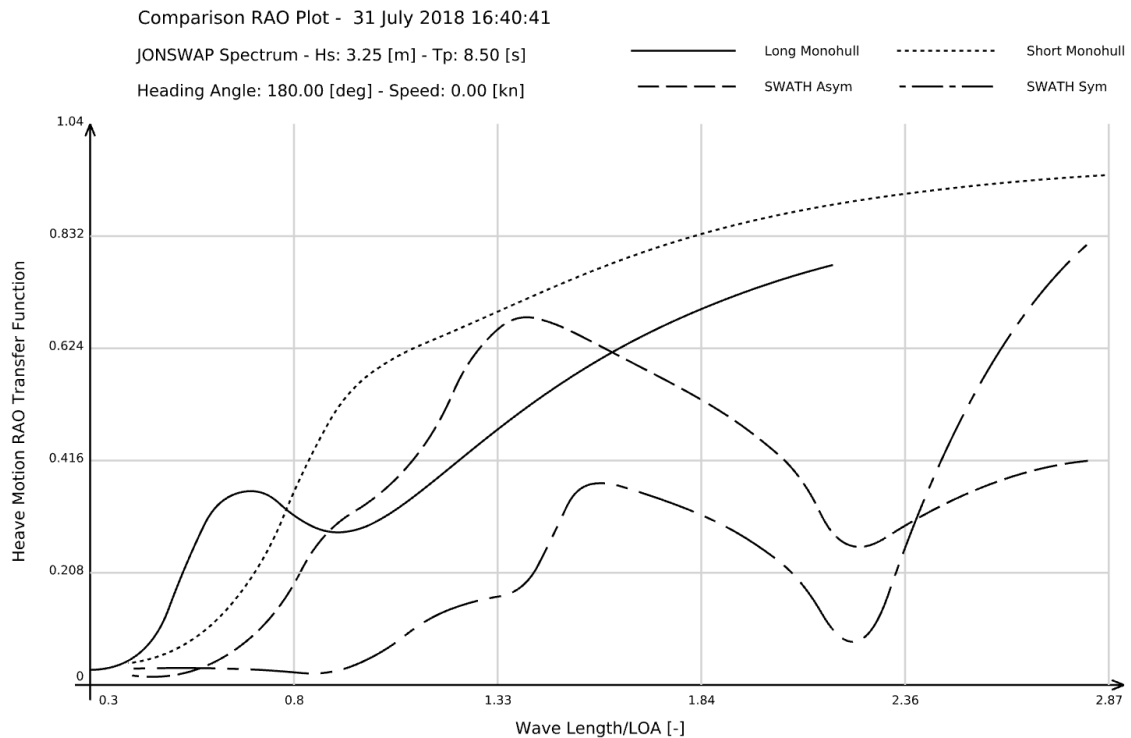


Figure 4.5: Heave RAO transfer function for sea state 7, 180° heading angle and 0kn sailing speed.

As the heave RAO is possibly the most relevant transfer function for heave motions, Figure 4.5 provides interesting observations. Initially, it is possible to notice that both monohulls are rather stable towards long wavelengths, having a small oscillation in short waves, but no real peak of intensified responses. SWATHs, in the other hand, have a rather more pronounced peak, but a very similar shape development between each other.

It is also important to notice that the symmetric SWATH has a sharp increase in heave response in long waves, above $2\lambda/\text{LOA}$ ratio. This could lead to an inferior performance in seas predominated by long swells. In spite of that, it is clear that it has lower heave responses for most of the sea state, yielding the lowest heave RMS motion of all, as seen in Table 4.2.

Meanwhile, the optimised asymmetric SWATH has a similar behaviour to the long monohull and, by far, the lowest response of all for waves with a very long period.

In the peak of energy of the spectrum (the area between 1.2 and 1.6 λ/LOA ratio), the symmetric SWATH has similar heave response amplitude compared to the long monohull, but only half of the value compared to the short monohull and two-thirds compared to the asymmetric SWATH.

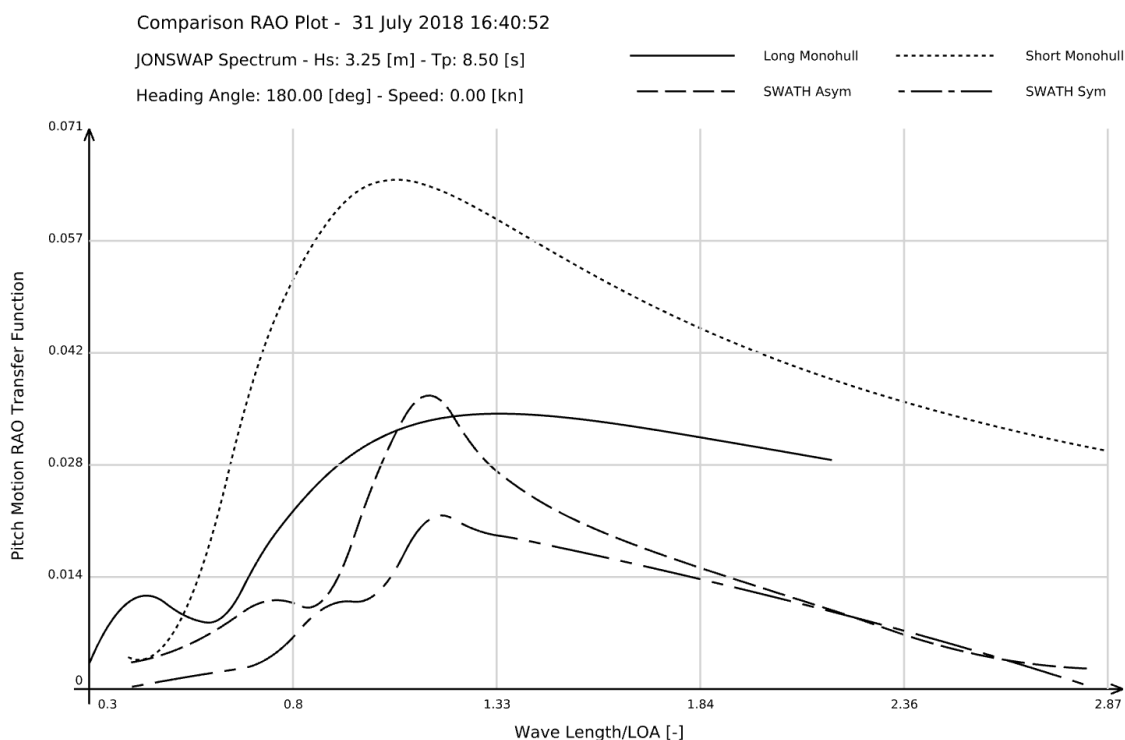


Figure 4.6: Pitch RAO transfer function for sea state 7, 180° heading angle and 0kn.

In Figure 4.6, the pitch transfer function indicates that both SWATH vessels have considerably less pitch motions, especially in waves with a long period. They again have a similar shape and development, this time with less magnitude difference between each other compared to the heave RAO. It can also be noticed that the SWATHs have

a more pronounced peak of pitch motions when the wavelength is slightly higher than the length of the vessel. On the other hand, the monohulls are rather stable, with higher pitch motions that slowly decreases with longer waves.

In its peaks, which is close to 1 λ /LOA ratio, the pitch motion of the symmetric SWATH is about a third of the short monohull, while the asymmetric and the long monohull have about half of it.

The second set of RAOs, presented in Figures 4.7, 4.8 and 4.9, are for 150° heading angle in the same sea state and 0kn speed, heave roll and pitch, respectively.

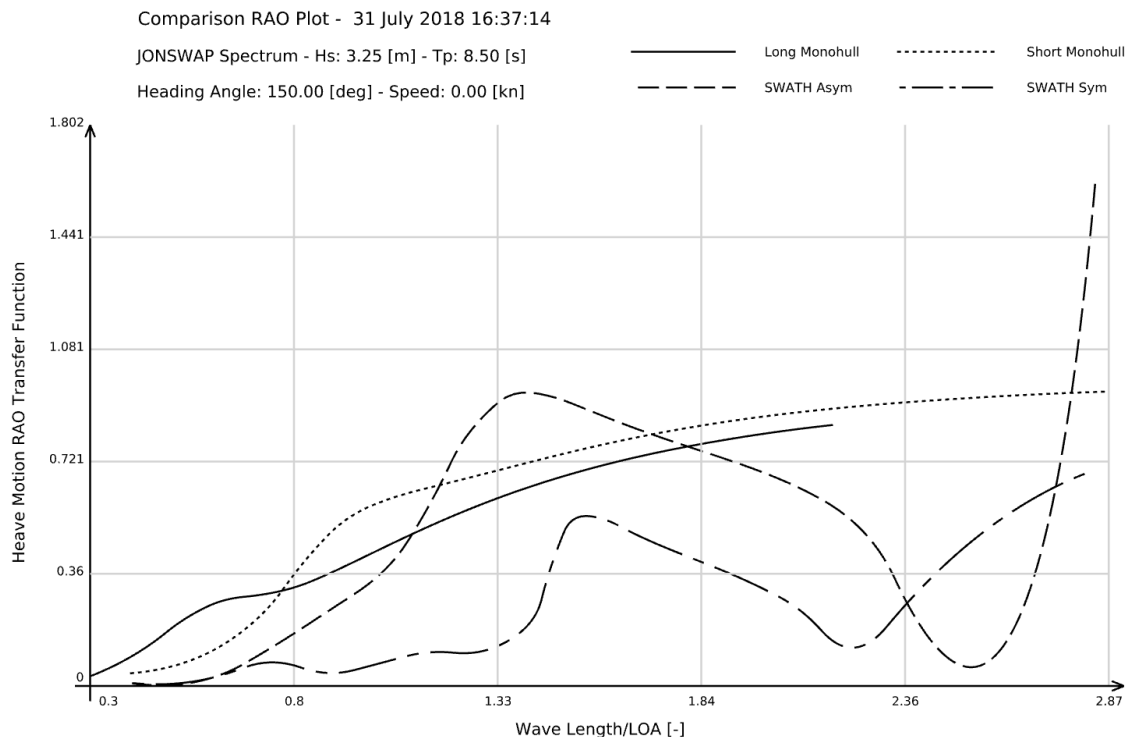


Figure 4.7: Heave RAO transfer function for sea state 7, 150° heading angle and 0kn sailing speed.

Starting with the heave RAO, Figure 4.7, similar observations can be made as for Figure 4.5. The shapes are similar, but it becomes evident that the asymmetric SWATH becomes worse than for head seas. It has increased heave motions at the energy concentration of the spectrum when compared to all other vessels, and there is a rapid growth beyond 2.4λ /LOA ratio, indicating that the solver could be presenting a strange behaviour and this area should be investigated. The symmetric variant has still the lowest motions.

The pitch RAO for 150° heading angle, Figure 4.8, has no significant difference from Figure 4.6, except that the SWATH vessels have a slightly higher peak.

Figure 4.9 introduces a new result to the comparison, a very important one as the base of the wind turbine can be located more than 20m from the vessel centreline ($y = 0$) and it will impact the loads on the walk-to-work gangway.

4 Results and Comparison

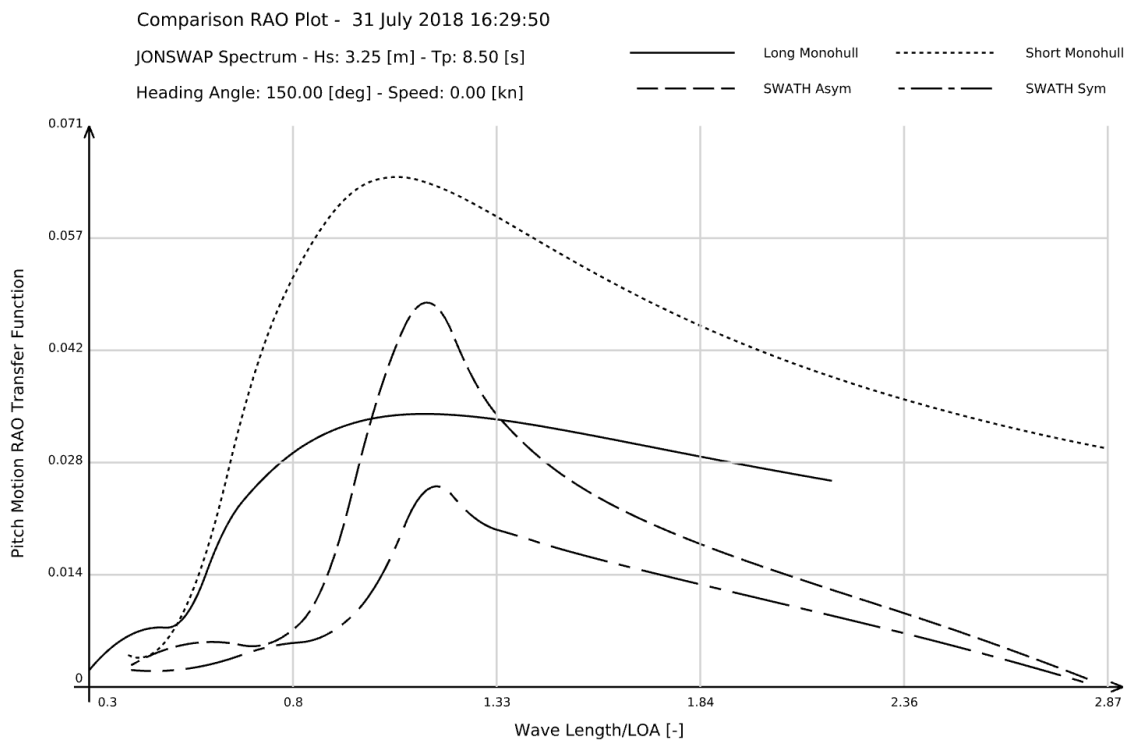


Figure 4.8: Pitch RAO transfer function for sea state 7, 150° heading angle and 0kn.

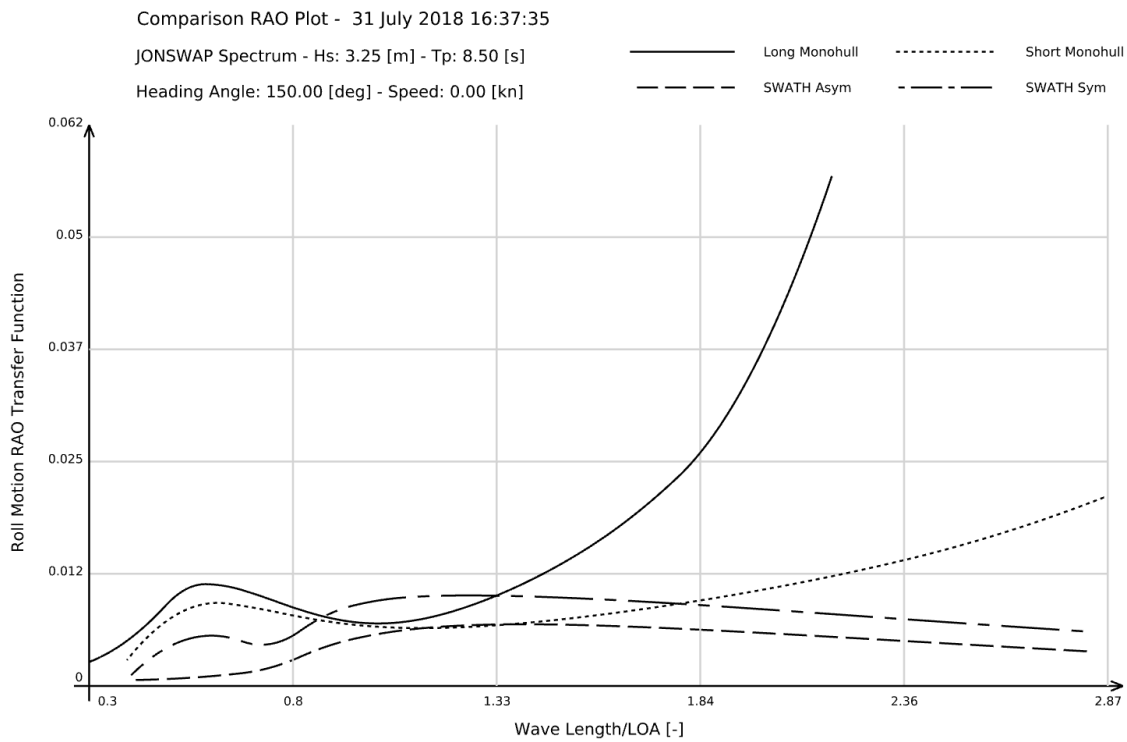


Figure 4.9: Roll RAO transfer function for sea state 7, 150° heading angle and 0kn.

The roll transfer function is now different than zero since the wave direction is now oblique to the vessel bow. The results indicate that for quartering seas, both SWATH vessels have fewer roll motions, especially above $1.33\lambda/LOA$ ratio. This time, the asymmetric SWATH variant has superior performance compared to the symmetric one. What cannot pass unnoticed is the exponential roll response of the long monohull once λ/LOA is higher than 1.5.

Additional RAOs for surge, sway and yaw motions in 150° heading angle, 0kn sailing speed at sea state 7 are presented in Appendix B, Figures A.1, A.2 and A.3, respectively. They indicate that all four vessels have a rather similar behaviour, with somewhat more difference in the yaw RAO. These additional results are responsible for the load on the propulsion system when operating in DP2 mode and are discussed in more detail in Section 4.4 and Chapter 5.

4.4 Body Excitement by Forces and Moments

This section evaluates body excitement, RMS forces and RMS moments, represented in polar plots for different heading angles. The idea is to obtain a more direct connection to the results presented in Section 4.2, and an insight of the power required for dynamic positioning of each vessel.

Firstly, Figures 4.10 and 4.11 presents motions that are directly coupled to the heave RMS motion at the evaluated point, heave, roll and pitch.

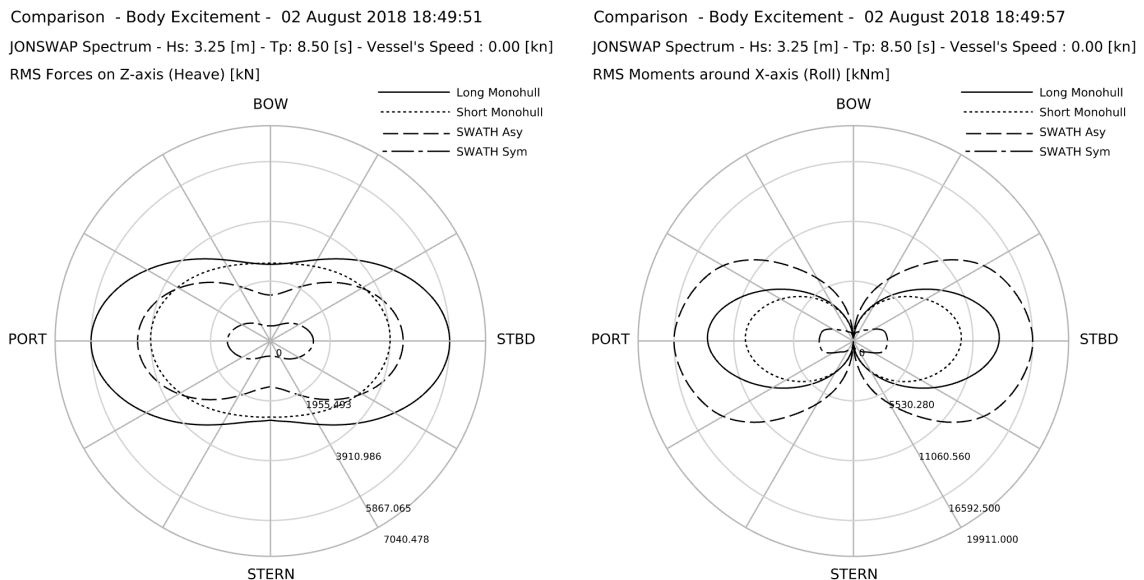


Figure 4.10: Polar plots for heave RMS forces (left) and roll RMS moments (right) for sea state 7 and 0kn sailing speed.

In the left side of Figure 4.10, it can be noticed that the RMS forces in the z axis for the SWATHS are smaller for bow and quartering seas, confirming the results

obtained in Figure 4.3, including that the asymmetric SWATH becomes worse for beam seas.

The right side of Figure 4.10 shows that the RMS moments around x axis (roll motion) are higher for the asymmetric SWATH for all heading angles. This also justifies the results obtained in Figure 4.3, including that the monohull has higher roll motions than the shorter one. What mostly caught the attention is the fact that these moments are much smaller for the symmetric SWATH, indicating that it has significantly less roll motions than all other vessels.

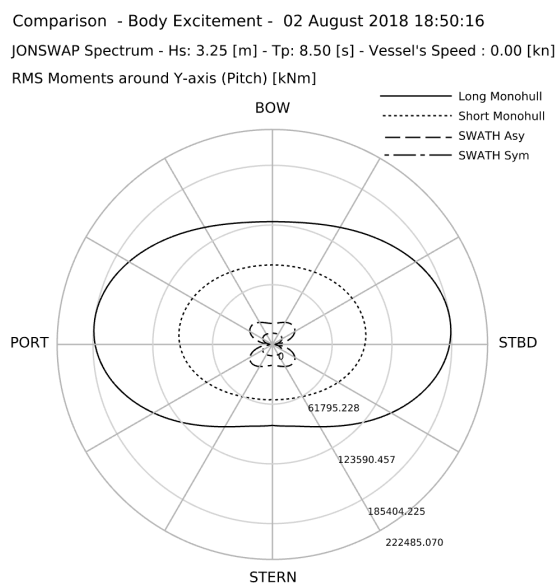


Figure 4.11: Polar plot for RMS moments around y -axis (pitch) for sea state 7 and 0kn sailing speed.

From Figure 4.11, it can clearly be seen that SWATH vessels have extremely smaller moments around the y axis, in other words: less pitch motions. This confirms the results encountered in the pitch RAOs both for 180° and 150° heading angles, Figures 4.6 and 4.8, respectively.

In a second stage of analysis, the power requirement for dynamic positioning system is a good indicator of costs, both for operational and initial investments. One way of comparing it without the propulsion efficiency of both systems is by comparing wave drift forces. As mentioned by Papanikolaou and Zaraphonitis (1987) the longitudinal drift force is identical to the added wave resistance when the vessel is at zero forward speed. Fortunately, one of the outputs of NEWDRIFT+ is the wave added resistance.

The wave drift force can be divided into two force components around the x and y axes, and a resulting moment around the z axis: surge, sway and yaw motions, respectively. These is visualised in Figures 4.12 and 4.13.

By analysing the results in Figure 4.12, it is clear that both SWATH vessels have higher RMS forces in both x and y axes. The combination of these forces can be seen

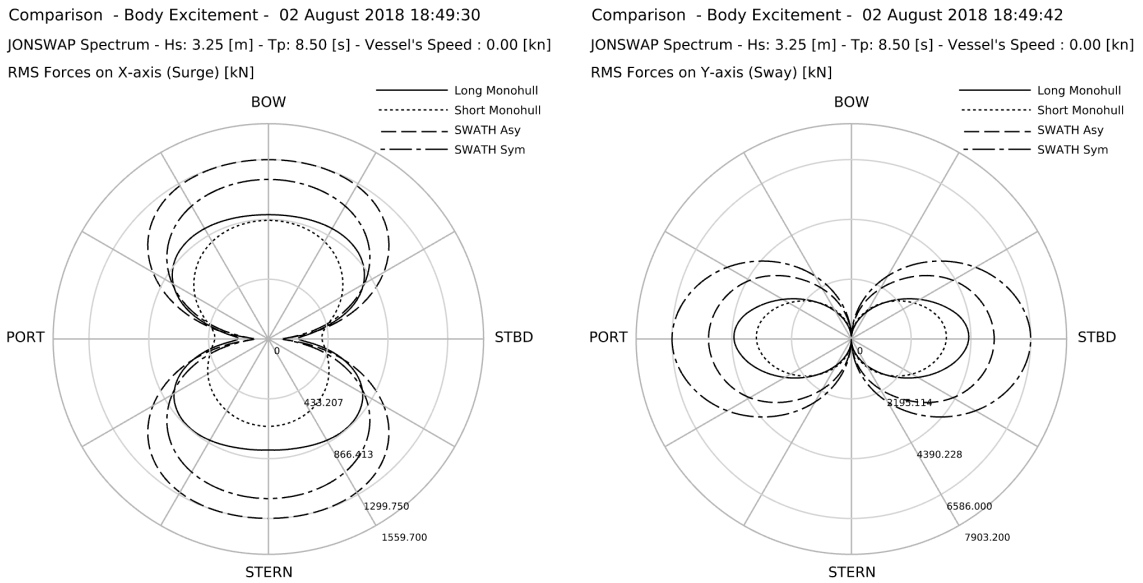


Figure 4.12: Polar plots for surge RMS forces (left) and sway RMS forces (right) for sea state 7 and 0kn sailing speed.

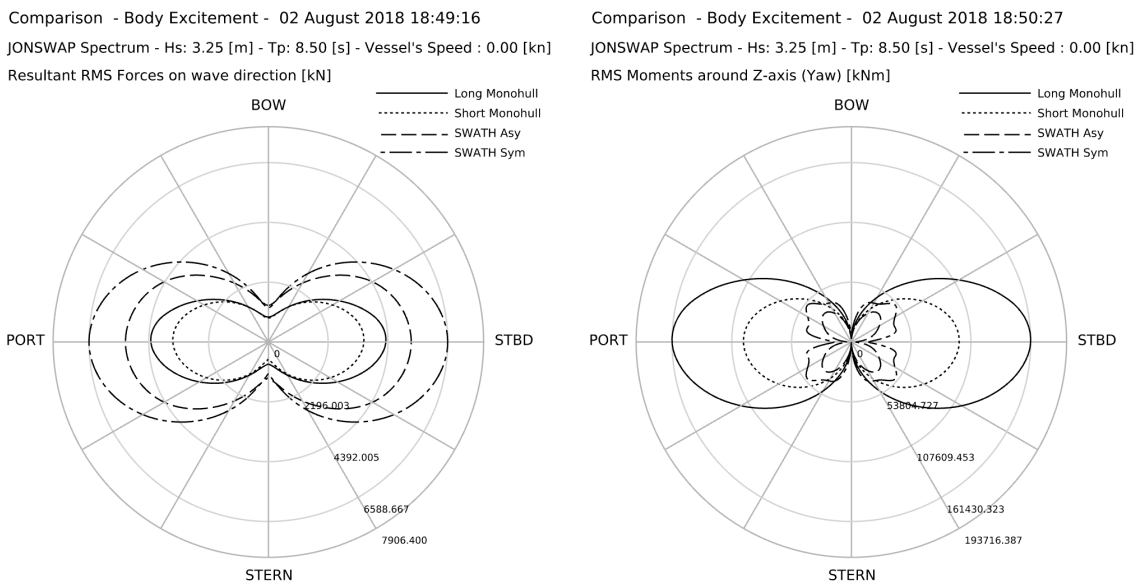


Figure 4.13: Polar plots for resultant RMS forces (left) and yaw RMS moments (right) for sea state 7 and 0kn sailing speed.

in the left side of Figure 4.13, the resultant force vector (not necessarily in the opposite direction of the wave direction).

On the other hand, on the right side of Figure 4.13, the resulting moment around the z axis shows that the SWATHs SOV variants yield significantly less yaw motion. This is a very interesting finding that could counterbalance the effect of drift forces in the SWATHs and, in the end, have a more similar amount of installed power.

4.5 Identified Optimisation Patterns

The whole optimisation process (described in Section 3.8) was handled by the algorithms, without much interference as long as the bounds of the design variables were correct and no errors appeared. But this does not mean that the behaviour of the algorithm could not be identified, on the contrary, CAESES® allows the visualisation of the development of the algorithm, including the chosen values for design variables towards better results.

By carefully analysing the evolution of the design variants, even though the automated design adjustments (presented in Section 3.3.5) camouflaged the results, a few patterns that could and could not be identified were:

- *Displacement position*, as mentioned by Qian et al. (2015) the placement of the displacement far from the waterline was a verified improvement of the seakeeping abilities. The best results were obtained with a rather long parallel midbody, which allows for a lower \overline{KB} . It also became evident that the displacement away from the centreline ($y = 0$) is beneficial. On the other hand, the displacement placement must be balanced with other variables that have the potential to highly interfere with hydrodynamic efficiency;
- *Waterline slope* was very important for both asymmetric and symmetric demi-hulls. The identified pattern for this area was not possible, although the non-existence of the slope is extremely prejudicial. The ideal size and shape of this area was a combination of parameters that could not be identified, but existent;
- *Design waterline*, the shape of the hull on the waterline level was found to be extremely sensitive to the seakeeping performance. Only exact, optimal combinations would yield good results;
- *Inclinations*, for the asymmetric design, the higher the inclination of the upper inner part away from the centreline ($y = 0$), the better.
- *Bilge sizes*, the size of bilges are almost negligible, especially the lower one. It can be assumed constant and optimised in a later and advanced stage of the project.

5 Conclusions

It was, unfortunately, for many reasons, not possible to come to a final clear decision if a SWATH hull is a better alternative for an SOV vessel. Instead, it was possible to pinpoint a variety of positive and negative aspects of the hull form. These are supposed to guide a similar future exploration, assisting to reach the right balance between compromises in geometry, propulsion system and operational capability.

To answer the main research question, the findings of the project are presented in this chapter, grouped in seven topics:

1. Heave Motions

- An asymmetric demi-hull SWATH can be optimised to have similar or even lower requirements for a walk-to-work gangway than a similar sized monohull, especially for head and quartering seas, as indicated in Section 4.2.
- The symmetric demi-hull SWATH variant can have significantly less heave motion than the asymmetric one and the short monohull, with the potential to even be better than operating 80m monohulls SOVs, with larger operational window.
- By varying H_S and T_P , for these particularly optimised vessels, it could be concluded that SWATHs have superior seakeeping performance only for $T_P < 9s$. Further investigation is necessary in order to discover if they can be better in $T_P > 9s$, possibly optimising the hull form for specific sea states.
- With respect to sailing speed (not highly important for SOVs), the SWATHs have significantly less heave motions when increasing the sailing speed.
- Heave motions of SWATHs are highly affected in seas predominated by long swells, as seen in Figures 4.5 and 4.7, indicating that it should be carefully evaluated if it ought to operate in such seas.
- The pitch interference in the heave motions was actually very small as the point analysed was only 5m behind the LCB, although it is important to mention that SWATHs can pitch significantly less than monohulls (Figure 4.6), allowing the positioning of the gangway further aft or forward in the vessel. This gives higher flexibility and could allow a whole new arrangement of the deck space, potentially beneficial.
- As seen in Figure 4.3, the heave performance of the symmetric SWATH is significantly better than the other vessels in quartering seas. This indicates that this SWATH variant could operate in a larger variety of heading angles when in rough seas, increasing the operational window compared to currently operating vessels.

2. Optimisation Process

- The process itself worked as it was supposed to. All design variables that significantly impacted the heave RMS results were included in the Dakota, which worked fine before geometry constraints were imposed (especially the displacement adjustment). With the displacement adjustment, the results became less correlated to the design variables and a surrogate model algorithm might not have been the best choice for the optimisation. A local multi-start optimisation would require more variants, but could possibly yield a better variant. Another option would be to reduce the number of design variables, which could be hard.
- The impact of an inclination of the inner flat of side, yH_{SHIFT} , was clear (about 5% heave motion reduction) and should be considered if proved that it does not totally compromise hydrodynamic performance.
- The shape of the hull on the waterline level was found to be extremely sensitive to computation results. A directly logic optimisation pattern for best results could not be found. Only exact optimal combinations of design variables yield good results, which were found by the optimisation algorithm.
- The slope close to the waterline was found very important for both asymmetric and symmetric demi-hulls. Following intuition, the slope close to the waterline act as a heave damping area, minimising heave motions. During the optimisation process, this was experienced and an optimal size was found by the optimisation algorithm. It was also what inspired the investigation of a symmetric demi-hull SWATH, that with a "damping slope" in both sides of the demi-hull proved to be a promising solution.
- When varying H_S and T_P , it became evident that optimising for only one sea state is not enough. The vessel will encounter different sea states during its lifetime and the middle ground for a best overall performance should be sought for. The optimisation process should include multiple sea states and heading angles, especially with different peak periods.

3. Optimised SWATH Hull Form

- The wetted surface of the SWATH vessels are very similar, but are 75% higher than the short monohull and 30% higher in comparison to the long monohull. This will definitely impact the calm water resistance, requiring higher propulsion power for similar speed.
- The demi-hull symmetric arrangement violated one of the recommendations suggested by the involved partner: the totally flat external sides. This should be addressed with alternative solutions for docking and daughter craft launching procedures.
- Even though significant effort was given to not worsen the hydrodynamic capabilities of a SWATH vessel, the optimised SWATHs might not be optimal for propulsion and calm water resistance. It is definitely a topic for further

research and its results should impact the bounds of the design variables, requiring a new round of optimisation.

- The arrangement of the demi-hulls, especially when the identified pattern for lower heave motion is a rather slender one, meaning that L_{PM} is close to its upper bound, will certainly impact the propeller performance. Firstly, the wake of the most forward propeller is hitting the hull, possibly causing undesired vibrations and noise. If proven excessive, it might be interesting to consider a propulsion system that is able to impulse the vessel with only the two most aft propellers. Secondly, when operating in DP2 mode, it is likely that the wake of one of the propellers become the inflow of another propeller, the impacts of this need to be investigated. Thirdly, the separation distance between the two demi-hulls might result in undesired flow acceleration, vibrations and higher resistance from vortexes generation. Finally, this distance, combined with the off centre buoyancy might result in structural loads for the demi-hull and one way to minimise this is by connecting the two demi-hulls with a wing section, for example in Figure A.4 in Appendix A. This structural element might be multi-functional, and, by intuition, would reduce even more the vessels motions. This idea was cogitated and test during the project, but NEWDRIFT+ was not able to capture the wings effects.

4. Initial Stability

- The SWATH variants have a very distinct limiting vertical centre of gravity, \overline{KM}_T , compared to each other and the monohull SOVs. The optimised asymmetric variant consists of a wider waterline demi-hull than the symmetric one, which is also moved inwards to accommodate the outer waterline slope. This resulted in a much lower \overline{KM}_T for the optimised symmetric SWATH. Although they have higher draught, allowing for the placement of heavy equipment to be lower than in the monohulls, it might not have enough initial stability. Hence, a detailed study of the weight placement for a SWATH SOV is necessary, including the necessary air-gap and air draft. In the worst case scenario, it might be necessary to widen the waterline area or even the whole vessel, triggering a new hull optimisation process.

5. NEWDRIFT+ Impressions

- The utilised software for seakeeping evaluation proved to be very stable while handling monohulls, very flexible in handling alternative geometries, but rather unstable when exposed to geometry constraints. With small variations in one design variable, as conducted in the first step of the optimisation process (Section 3.8.1), the results followed logic and were stable until limitations for displacement and length existed. Once the displacement and LOA adjustments were introduced NEWDRIFT+ displayed unstable results of heave RMS motion, not necessarily wrong, but that should be investigated.

- NEWDRIFT+ added wave resistance calculation is currently validated for monohulls in head and quartering seas, meaning that the polar plots presenting wave drift forces and moments (presented in Section 4.4), although are logically correct, might not entirely represent the real excitation of SWATH vessels.
- The optimised SWATH variants have an exact combination of design variables that, as a conjunct, yields the lowest heave RMS motion. Very small variations of this combination (as in step 4 of the optimisation process, Section 3.8.4) could totally jeopardise the result, which was rather unexpected and leads to doubts about the accuracy of the calculation tool for these types of hull forms.
- The number of points in the spectrum and the size of the mesh utilised in the calculation of each design variant was rather low (22 and 38x11, respectively) so that the required computational time could be reasonable. When increasing these values, theoretically, the accuracy of the model should increase, but instead, it was found that in some variants, the results varied significantly. Definitely a point for further investigation.

6. Station Keeping Requirements

- The results of the polar plots clearly indicated that, although the propulsion arrangement of SWATHs eases manoeuvring, the required power for station keeping could be significantly larger, especially if the efficiency of the propulsion system is lower, than of an SOV monohull. This could be an indication that the energy transferred from the waves to the vessel motion is directed to drift forces for SWATHs, while for monohulls is better balanced between heave excitation and wave drift forces.

7. Financial Aspects

- SWATH vessels are not exactly known for being cheap alternatives to monohulls. Thus, it must have very good reasons and advantages to actually be built. The asymmetric demi-hull variant is the one that clearly has less heave motion than the monohull, especially the short one. If the construction cost of a 62.2m SWATH is on the same cost scale as an 82m monohull, it could be a viable option.
- Regarding the propulsion system, even though the SWATHs have higher resultant drift forces, the configuration of 4 thrusters in the extremities of the vessel might turn out to be better for dynamic positioning. A competitive and efficient propulsion system configuration needs to be investigated to lower operational costs.
- With the market trend for smaller SOVs, it might be that the increased deck area of a 60m SWATH, compared to a 60m monohull, is not yet necessary. Therefore, in order to decrease construction costs, investigation of an even smaller SWATH should be considered.

To summarise the outcomes, there is market space and SWATH vessels are a possible alternative to increase the operational window of SOVs, but they require careful planning and an in-depth holistic study of the vessel, including validation between a diversity of calculation methodologies, time domain simulations and basin model tests.

CAESES® proved to be a very powerful tool for parametric 3D modelling and optimisation of complex geometries.

This page was intentionally left blank.

References

- Abt, C., & Harries, S. (2007, apr). A New Approach to Integration of CAD and CFD for Naval Architects. *6th International Conference on Computer Applications and Information Technology in the Maritime Industries (COMPIT2007)*, 467-479.
- Ad Hoc Marine Designs Ltd. (2013). *Ad Hoc SWATH projects*. Retrieved from <http://www.adhocmarinedesigns.co.uk/projects/>
- Aukland, R. (2017, apr). *ANALYSIS: Supply & Demand of Wind Farm Service Vessels*. Retrieved from <https://www.linkedin.com/pulse/analysis-supply-demand-wind-farm-services-vessels-richard-aukland>
- Bergdahl, L. (2009). *Wave-induced loads and ship motions*. Chalmers University of Technology - Department of Civil and Environmental Engineering, Division of Water Environment Technology.
- Brenner, M. (2008, jun). *Integration of CAD and CFD for the Hydrodynamic Design of Appendages in Viscous Flow*. Technical University Berlin [Master Thesis].
- Brizzolara, S., Bovio, M., Federici, A., & Vernengo, G. (2011, sep). Hydrodynamic Design of a Family of Hybrid SWATH Unmanned Surface Vehicles. *11th International Conference on Fast Sea Transportation, FAST 2011 - Proceedings*.
- Brüning, A., & Precht, E. (2014). Statistical analyses of metocean data for offshore wind design in german waters. *Die Küste*, 81, 167-184.
- Compagnie Maritime Chambon. (2014, mar). *Windkeeper - Vessel support and maintenance for offshore wind farms*. Retrieved from <http://www.cmchambon.com/en/2014/03/windkeeper-2>
- Dörrbecker, M. (2018, jun). *Map of offshore wind farms and connecting power cables in the German Bight*. [digital image] Used under Creative Commons Attribution 2.0 Generic. Retrieved from https://commons.wikimedia.org/wiki/File:Karte_Offshore-Windkraftanlagen_in_der_Deutschen_Bucht.png
- EWEA. (2011, nov). *The European Wind Energy Association - Wind in our Sails: The coming of Europe's offshore wind energy industry*.
- Faltinsen, O., Minsaas, K., Liapis, N., & Skjördal, S. (1980). Prediction of resistance and propulsion of a ship in a seaway. In *Proceedings of the 13th symposium on naval hydrodynamics* (p. 505-529). Shipbuilding Research Assoc. of Japan.
- FKAB. (2018, apr). *Milestone: Contract signing for a 50m offshore wind farm service vessel*. Retrieved from <http://www.fkab.com/en/milestone-contract-signing-for-a-50m-offshore-windfarm-service-vessel>
- Foxwell, D., & de Jongh, M. (2017, feb). *Rolls-Royce unveils SOV innovations at Offshore Wind Journal Conference*. Retrieved from http://www.owjonline.com/news/view,rollsroyce-unveils-sov-innovations-at-offshore-wind-journal-conference_46425.htm
- Friendship Systems AG. (2018). *CAESES®*. (Version 4.3.1) [Computer Software].
- Grace, L., & Lee, W.-H. (2017, may). Cost effective offshore concepts - Compact Semi-Submersible - a new concept of windfarm service operations vessel - VARD

- Marine and DNV-GL. *OTC - Offshore Technology Conference, OTC-27772-MS*. [white paper].
- Haggett, C. (2008). Over the Sea and Far Away? A Consideration of the Planning, Politics and Public Perception of Offshore Wind Farms. *Journal of Environmental Policy & Planning*, 10(3), 289-306. doi: 10.1080/15239080802242787
- Harries, S., Abt, C., & Hochkirch, K. (2004, jul). Modeling meets simulation – Process integration to improve design. *Sonderkolloquium zu Ehren der Professoren Hagen, Schlüter und Thiel*.
- Hasselmann, K., P. Barnett, T., Bouws, E., Carlson, H., E. Cartwright, D., Enke, K., ... Walden, H. (1973, jan). Measurements of wind-wave growth and swell decay during the Joint North Sea Wave Project (JONSWAP). *Deut. Hydrogr. Z.*, 8, 1-95.
- Holthuijsen, L. (2007). *Waves in oceanic and coastal waters* (1st ed.). Cambridge University Press.
- Kitano, T., Mase, H., & Kioka, W. (2002, mar). Theory of significant wave period based on spectral integrals. *Fourth International Symposium on Ocean Wave Measurement and Analysis*, 414-423.
- Kuroda, M., Tsujimoto, M., Fujiwara, T., Ohmatsu, S., & Takagi, K. (2008). Investigation on components of added resistance in short waves. *Journal of the Japan Society of Naval Architects and Ocean Engineers*, 8, 171-176. doi: 10.2534/jjasnaoe.8.171
- Lewis, E. (1989). *Principles of Naval Architecture: Motions in waves and controllability*. Society of Naval Architects and Marine Engineers (U.S.).
- Liu, S., & Papanikolaou, A. (2012, jun). On Nonlinear Simulation Methods and Tools for Evaluating the Performance of Ships and Offshore Structures in Waves. *Journal of Applied Mathematics*.
- Liu, S., & Papanikolaou, A. (2015). Practical approach to the added resistance of a ship in short waves. *Proceedings of the Twenty-fifth International Ocean and Polar Engineering Conference*, 11 - 18.
- Liu, S., & Papanikolaou, A. (2016a, jan). Fast approach to the estimation of the added resistance of ships in head waves. *Ocean Engineering*, 112, 211-225.
- Liu, S., & Papanikolaou, A. (2016b, jun). Prediction of the added resistance of ships in oblique seas. *Proceedings of the Twenty-sixth International Ocean and Polar Engineering Conference*, 495 - 502.
- Liu, S., & Papanikolaou, A. (2017, jun). Approximation of the added resistance of ships with small draft or in ballast condition by empirical formula. *Engineering for the Maritime Environment*, 1-14.
- Liu, S., Papanikolaou, A., & Duan, W. (2007). A time domain numerical simulation method for nonlinear ship motions, AsiaLink-EAMARNET. In *Proceedings of the international conference on ship design, production & operation* (p. 177-185). EAMARNET - The Euro-Asia Maritime Network.
- Liu, S., Papanikolaou, A., & Zaraphonitis, G. (2001). Manual of NEWDRIFT+ [Computer software manual]. (Version 7) Ship Design laboratory, National Technical university of Athens.
- Liu, S., Papanikolaou, A., & Zaraphonitis, G. (2011). Prediction of added resistance of ships in waves. *Ocean Engineering*, 38(4), 641 - 650. doi: <https://doi.org/10.1016/j.oceaneng.2010.12.007>

- Liu, S., & Papanikolaou, A. D. (2011). Time-domain hybrid method for simulating large amplitude motions of ships advancing in waves. *International Journal of Naval Architecture and Ocean Engineering*, 3(1), 72 - 79. Retrieved from <http://www.sciencedirect.com/science/article/pii/S2092678216302072> doi: <https://doi.org/10.2478/JNAOE-2013-0047>
- Liu, S., Shang, B. G., Papanikolaou, A., & Bolbot, V. (2016, jun). An improved formula for estimating the added resistance of ships in engineering applications. *Marine Sciences and Application*, 15.
- Lockheed Martin Skunk Works. (2018). *Historical Programs - Sea Shadow*. Retrieved from <https://www.lockheedmartin.com/us/100years/stories/sea-shadow.html>
- MARIN. (2018, apr). CNIM asks MARIN to verify the performance of a new SWATH design. *MARIN's News magazine for the maritime industry - Report*, 123, 20-21. Retrieved from <https://content.yudu.com/web/1r3p1/0A3a046/MRN123/html/index.html?page=20&origin=reader>
- Maruo, H. (1957). The excess resistance of a ship in rough seas. *International Shipbuilding Progress* 4, 35, 337-345.
- NOAA. (2015). *Marine Operations - NOAA Ship Ferdinand R. Hassler*. Retrieved from <http://www.oma.noaa.gov/learn/marine-operations/ships/ferdinand-r-hassler/about>
- Obhrai, C. (2014). *OFF61 - Offshore Wind Turbine Engineering course - University of Stavanger*. [powerpoint slides].
- Papanikolaou, A. (1984, sep). On calculations of nonlinear hydrodynamic effects in ship motion. *Ship Technology Research*.
- Papanikolaou, A., & Schellin, T. (1992, jan). A three-dimensional panel method for motions and loads of ships with forward speed. *Ship Technology Research*, 39, 145.
- Papanikolaou, A., & Zaraphonitis, G. (1987, jan). On an Improved Method for the Evaluation of Second-Order Motions and Loads on 3D Floating Bodies in Waves. *Ship Technology Research*, 34, 170-211.
- Papanikolaou, A., Zaraphonitis, G., & Androulakakis, M. (1991). Preliminary design of a high-speed swath passenger/car ferry. *Marine Technology*, 28(3), 129-141.
- Puisa, R., & Skaro, A. (2018, mar). *New SOV Concept on Horizon with NEXUS Project Launched*. Retrieved from <https://www.offshorewind.biz/2018/03/22/new-sov-concept-on-horizon-with-nexus-project-launched>
- Qian, P., Yi, H., & Li, Y. (2015). Numerical and experimental studies on hydrodynamic performance of a small-waterplane-area-twin-hull (swath) vehicle with inclined struts. *Ocean Engineering*, 96, 181 - 191. doi: <https://doi.org/10.1016/j.oceaneng.2014.12.039>
- Rolls Royce Marine. (2016, may). *Østensjø Rederi orders second Rolls-Royce designed offshore wind farm support vessel*. Retrieved from <https://www.rolls-royce.com/media/our-stories/press-releases/2016/26-05-2016-rolls-royce-designed-offshore-wind-farm-support-vessel.aspx>
- Rolls Royce Marine. (2018, jul). *Marine Products - UT 540 WP Wind Farm Support*. Retrieved from <https://www.rolls-royce.com/products-and-services/marine/ship-design/our-designs/offshore/wind-farm-support/ut-540-wp.aspx#section-vessel-description>

- Salt Ship Design. (2018). *Wind Farm SOV*. Retrieved from <https://saltship.com/references-collection/2017/5/5/wind-farm-sov>
- SAWE. (2009). *Weight Distribution and Moments of Inertia for Marine Vehicles*. International Society of Allied Weight Engineers - Marine Systems Government. Retrieved from https://www.sawe.org/files/SAWE%20RP_Davy_formatted.doc
- Schellenberger, G. (2011). *SWATH technology, advanced SWATH design methods*. Retrieved from <http://mari-tech.org/wp-content/uploads/2011/11/03%20-%20swath%20technology%20small%20waterplane%20area%20twin%20hull.pdf>
- Siemens Gamesa. (2018). *Integrated service logistics to overcome every offshore challenge*. Retrieved from <https://www.siemens.com/content/dam/webassetpool/mam/tag-siemens-com/smdb/wind-power-and-renewables/service-wind/documents/brochures/siemens-gamesa-offshore-wind-service-logistics-infographic-slides.pdf>
- Snieckus, D. (2014, mar). *Recharge News - "IN DEPTH: How gravity can bring down offshore costs."*. Retrieved from http://www.rechargenews.com/wind/europe_africa/868293/in-depth-how-gravity-can-bring-down-offshore-costs
- St. Denis, M. (1974, jun). On the Spectral Technique for Describing the Seaway-Induced Motions of Ships - A Review of Developments over the Past Two Decades and an Outline of Problems Now in Hand. *SNAME T&R Symposium S-3 on Seakeeping*.
- US Department of Energy. (2017, aug). *Office of Energy Efficiency and Renewable Energy - 2016 Offshore Wind Technologies Market Report*. Retrieved from <https://www.energy.gov/sites/prod/files/2017/08/f35/2016%20offshore%20Wind%20Technologies%20Market%20Report.pdf>
- VARD Marine. (2018). *CSS DESIGNS*. Retrieved from <https://vardmarine.com/vessel-design-portfolio/css-design>
- WAMIT. (2016). WAMIT® User Manual by WAMIT, Inc. [Computer software manual]. (Version 7.2) Massachusetts Institute of Technology.
- WINDEA Offshore GmbH & Co. KG. (2017). *Windea fleet*. Retrieved from <http://windea.de/fleet/>
- WindEurope. (2017, sep). *Wind energy in Europe: Outlook to 2020*.
- WindEurope. (2018, feb). *Offshore Wind in Europe, Key trends and statistics 2017*.
- Østensjø Rederi. (2018). *Edda Passat*. Retrieved from <http://ostensjo.no/fleet/eddapassat>

Appendix

A - Additional Figures

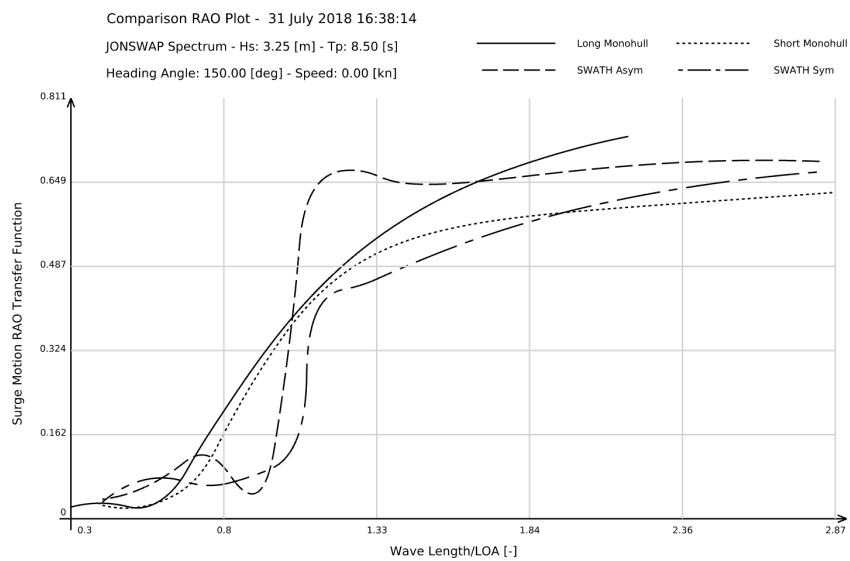


Figure A.1: Surge RAO transfer function for sea state 7, 150° heading angle and 0kn.

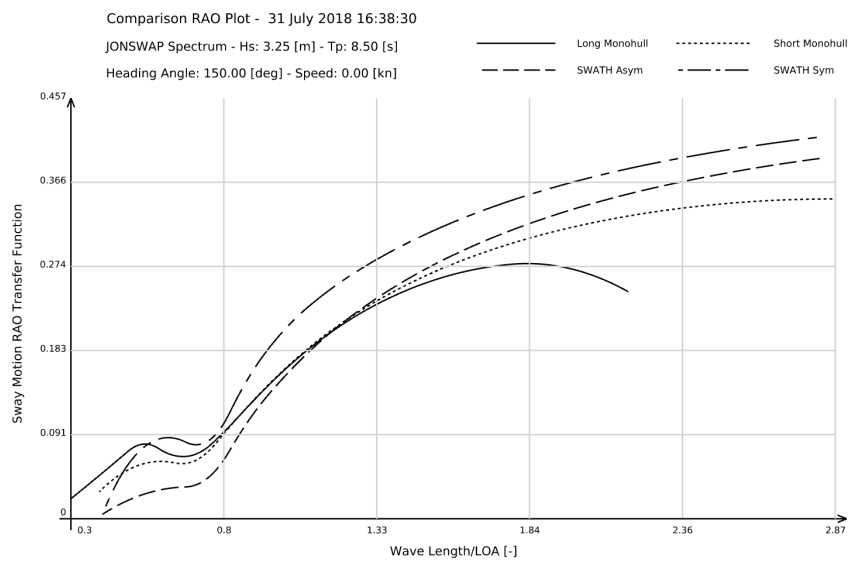


Figure A.2: Sway RAO transfer function for sea state 7, 150° heading angle and 0kn.

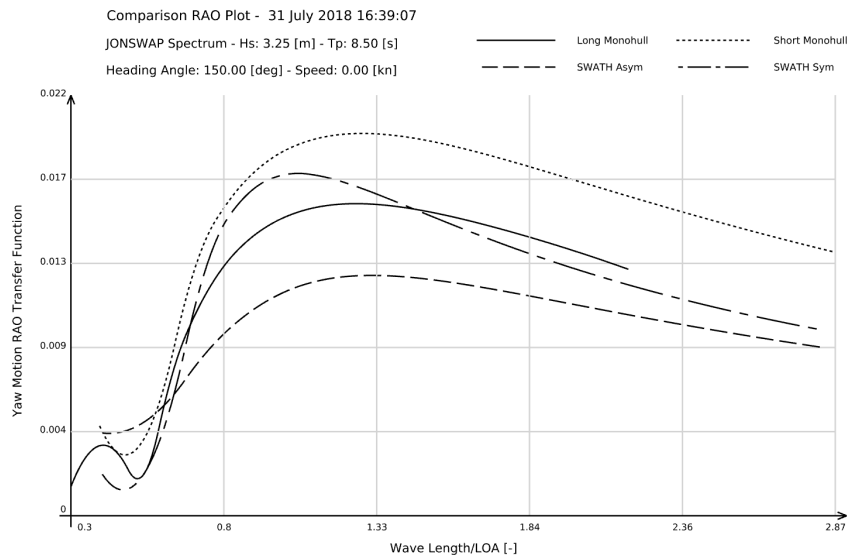


Figure A.3: Yaw RAO transfer function for sea state 7, 150° heading angle and 0kn.

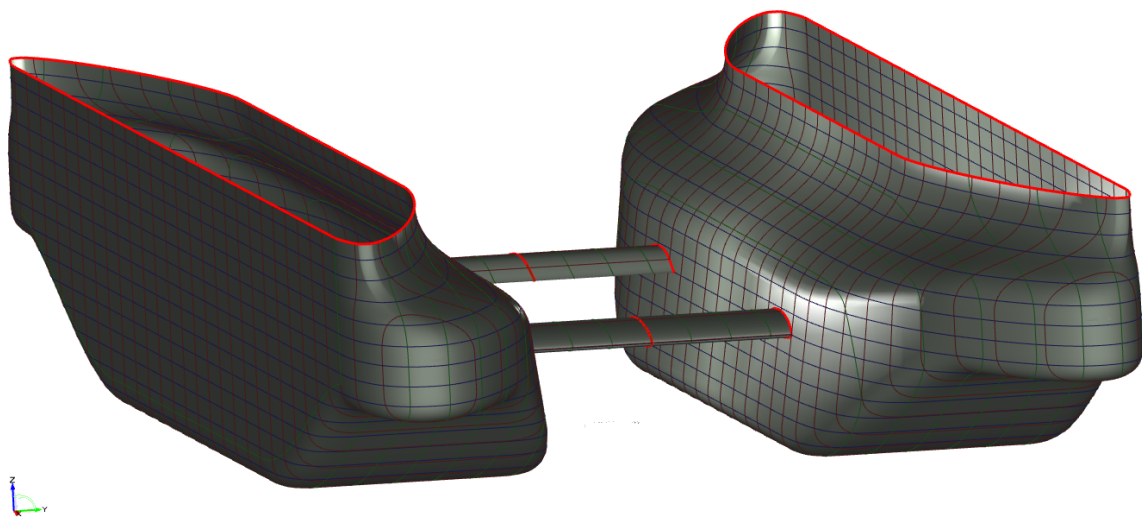


Figure A.4: A concept of the asymmetric SWATH hull with a wing connection between the demi-hulls.

B - Additional Tables

Table B.1: Heave RMS results for different head angles in sea state 7 ($H_S = 3.25\text{m}$ and $T_P = 8.5\text{s}$).

Heading Angle [°]	Heave RMS [m]			
	Long	Short	Asymmetric	Symmetric
	Monohull	Monohull	SWATH	SWATH
90	1.075	0.914	1.331	0.764
100	1.139	0.971	1.304	0.753
110	1.125	0.985	1.174	0.703
120	1.042	0.956	1.052	0.623
130	0.915	0.895	0.917	0.545
140	0.772	0.815	0.751	0.460
150	0.633	0.728	0.682	0.384
160	0.509	0.647	0.605	0.322
170	0.401	0.577	0.454	0.279
180	0.340	0.526	0.423	0.256

Table B.2: Heave RMS results for different speeds in sea state 7 ($H_S = 3.25\text{m}$ and $T_P = 8.5\text{s}$).

Speed [kn]	Heave RMS [m]			
	Long	Short	Asymmetric	Symmetric
	Monohull	Monohull	SWATH	SWATH
0	0.33973	0.52596	0.42335	0.25604
1	0.35336	0.54761	1.10359	0.19343
2	0.37005	0.57601	0.65956	0.35312
3	0.39132	0.61244	0.49139	0.21909
4	0.41802	0.65722	0.47736	0.16703
5	0.44959	0.70997	0.46336	0.13768
6	0.48548	0.76924	0.44109	0.11926
7	0.52331	0.83216	0.41274	0.10637
8	0.56191	0.89671	0.38189	0.09167
9	0.59905	0.95897	0.3516	0.09859
10	0.63378	1.01859	0.3244	0.0898
13	0.71739	1.17348	0.26409	0.08835

Table B.3: Wave scatter diagram - modelled data at OWF Sandbank (German Bight), adapted from Brüning and Precht (2014).

H_s [m] T_P [s]	0-0.5	0.5-1	1-1.5	1.5-2	2-2.5	2.5-3	3-3.5	3.5-4	4-4.5	4.5-5	Total	Acumm
0-1	0.00%	0.00%	0.00%	0.00%	0.00%	0.00%	0.00%	0.00%	0.00%	0.00%	0.00%	0.00%
1-2	0.00%	0.00%	0.00%	0.00%	0.00%	0.00%	0.00%	0.00%	0.00%	0.00%	0.00%	0.00%
2-3	0.16%	0.03%	0.00%	0.00%	0.00%	0.00%	0.00%	0.00%	0.00%	0.00%	0.19%	0.19%
3-4	1.14%	2.75%	0.06%	0.00%	0.00%	0.00%	0.00%	0.00%	0.00%	0.00%	3.95%	4.14%
4-5	1.22%	6.70%	4.24%	0.20%	0.00%	0.00%	0.00%	0.00%	0.00%	0.00%	12.36%	16.50%
5-6	0.39%	4.98%	7.38%	4.57%	0.58%	0.01%	0.00%	0.00%	0.00%	0.00%	17.91%	34.41%
6-7	0.30%	2.60%	6.25%	6.49%	4.37%	1.51%	0.28%	0.01%	0.00%	0.00%	21.81%	56.22%
7-8	0.21%	1.18%	2.57%	3.76%	4.59%	3.43%	1.47%	0.44%	0.11%	0.01%	17.77%	73.99%
8-9	0.20%	0.86%	1.06%	1.05%	1.46%	2.22%	2.60%	1.62%	0.60%	0.19%	11.86%	85.85%
9-10	0.11%	0.52%	0.68%	0.38%	0.37%	0.37%	0.48%	0.91%	1.18%	0.80%	5.80%	91.65%
10-11	0.10%	0.34%	0.57%	0.26%	0.14%	0.10%	0.08%	0.10%	0.18%	0.27%	2.14%	93.79%
11-12	0.08%	0.24%	0.52%	0.28%	0.12%	0.06%	0.05%	0.03%	0.04%	0.02%	1.44%	95.23%
12-13	0.06%	0.20%	0.26%	0.21%	0.06%	0.03%	0.02%	0.01%	0.01%	0.01%	0.87%	96.10%
13-14	0.03%	0.14%	0.12%	0.10%	0.06%	0.03%	0.01%	0.01%	0.00%	0.00%	0.50%	96.60%
14-15	0.01%	0.15%	0.14%	0.07%	0.07%	0.03%	0.01%	0.01%	0.00%	0.00%	0.49%	97.09%
15-16	0.01%	0.12%	0.10%	0.05%	0.03%	0.02%	0.01%	0.00%	0.00%	0.00%	0.34%	97.43%
16-17	0.01%	0.12%	0.07%	0.02%	0.01%	0.01%	0.00%	0.01%	0.00%	0.00%	0.25%	97.68%
17-18	0.00%	0.05%	0.08%	0.01%	0.01%	0.01%	0.01%	0.00%	0.00%	0.00%	0.17%	97.85%
18-19	0.00%	0.03%	0.06%	0.01%	0.01%	0.00%	0.00%	0.00%	0.00%	0.00%	0.11%	97.96%
19-20	0.00%	0.03%	0.04%	0.03%	0.01%	0.00%	0.00%	0.00%	0.00%	0.00%	0.11%	98.07%
Total	4.03%	21.04%	24.20%	17.49%	11.89%	7.83%	5.02%	3.15%	2.12%	1.30%		
Acumm	4.03%	25.07%	49.27%	66.76%	78.65%	86.48%	91.50%	94.65%	96.77%	98.07%		

C - NEWDRIFT+ Input Files

Casedat.dat

```

1
2
3
4
5 ****--<entry>COMMENT</entry>
6   1
7   3 0 0.100
8   0 0
9   1 3
10  0 <entry>ISPEED</entry> 0 0 0
11  <entry>depth</entry> 1
12  3 0
13  <entry>Tp</entry>      <entry>Hs</entry>      <entry>nRAOpoints</entry>      'Wave_length '
14  <entry>Heading</entry> <entry>Heading</entry> <entry>Heading</entry>      'Wave_Headings '
15  1.0000      'Wave_Amplitude '
16  <entry>ShipSpeed</entry>      'Ship_Speed [m/sec] '
17  <entry>xP1</entry> <entry>yP1</entry> <entry>zP1</entry>
18  <entry>xP2</entry> <entry>yP2</entry> <entry>zP2</entry>
19  <entry>xP3</entry> <entry>yP3</entry> <entry>zP3</entry>
20  ***** <entry>COMMENT</entry> *****
21  0

```

InputParameters.dat

```

1  0
2  1
3  <entry> Trim </entry> <entry>Draft</entry> <entry>draftXpos</entry>
4  0.0001
5  <entry>COMMENT</entry>
6  09 32 0.25
7  0 <entry>ILIST</entry> 0 0 0 0
8  <entry>COMMENT</entry>

```

Shipdat.dat

```

1 ****--<entry>COMMENT</entry>----- ***
2  <entry>symmetry</entry>
3  <entry>Length</entry>
4  <entry>Beam</entry>
5  <entry>Draft</entry>
6  <entry>zCC</entry> -999.00000
7  -999.00000 -999.00000 <entry>zCG</entry>
8  -999.00000 -999.00000
9  -1.00000 -1.00000 1.00000 1.00000
10 -999.00000 -999.00000
11 <entry>IXXG</entry>
12 <entry>IYYG</entry>
13 <entry>IZZG</entry>
14  0.00000 0.00000 0.00000

```